STRUCTURAL AND FUNCTIONAL STUDIES OF

BIOTIN-DEPENDENT CARBOXYLASES

Christine Shaoyu Huang

Submitted in partial fulfillment of the

requirements for the degree

of Doctor of Philosophy

in the Graduate School of Arts and Sciences

COLUMBIA UNIVERSITY

2013

ABSTRACT

Structural and Functional Studies of Biotin-Dependent Carboxylases

Christine Shaoyu Huang

A persisting question in biology concerns the exceptional diversity of metabolic enzymes and how they respond to their ligands and dynamic environments with remarkable precision. In humans, the family of biotin-dependent carboxylases holds important roles in intermediary metabolism. Recent years have witnessed significant progress toward understanding these enzymes' roles in homeostatic regulation. However, due to a lack of structural information, their catalytic mechanisms, as well as the macromolecular consequences of their genetic mutations, are still not well understood.

This dissertation describes the characterization of two biotin-dependent carboxylases that catalyze essential metabolic transformations in humans and bacteria, using X-ray crystallography to elucidate their structures and biochemical assays to verify their activities. We engineer a novel chimeric variant of propionyl-CoA carboxylase (PCC) and produce the first crystal structure of its 750-kDa $\alpha_6\beta_6$ holoenzyme. This structure reveals the architecture of PCC's twelve catalytic domains and allows the mapping of its disease-associated gene mutations to predict their effects on enzyme stability and catalysis. We also identify and describe a new domain that is integral to maintaining inter-subunit contacts within PCC. Following this, we extend our studies to

methylcrotonyl-CoA carboxylase (MCC), another 750-kDa $\alpha_6\beta_6$ holoenzyme that differs from PCC primarily in its substrate preference. The crystal structure of MCC assumes a markedly different configuration from PCC despite the high sequence identity between the two. Theorizing that these enzymes may represent unique lineages in the evolution of the biotin-dependent carboxylases, we apply similar approaches to the study of a third biotin-dependent carboxylase. Our efforts have produced the first two holoenzyme structures of CoA-recognizing biotin-dependent carboxylases, and provide valuable insight for understanding the functions of these vital enzymes.

Table of Contents

Chapter III

Structural and biochemical studies of 3-methylcrotonyl-CoA carboxylase

List of Figures and Tables

Chapter I

and ion-pair interactions are indicated with dashed lines. Panels A and C are adapted from Chou *et al.*, 2009, and Panel B is adapted from Shen *et al.*, 2004.

Figure 6. Proposed mechanism of biotin carboxylation in the BC domain of *E. coli* ACC. The reaction schematic is presented in approximately the same view as the active site in Figure 5C. Biotin is considered tethered to BCCP, and the orientation of natural ATP substrate shown in the mechanism is based on the observed binding mode of ADP. Adapted from Chou *et al.*, 2009 and based on the mechanism proposed by Knowles, 1989.

Figure 7. Crystal structures of eukaryotic and prokaryotic carboxyltransferase (CT). (A) The CT domain from yeast ACC in complex with CoA in one monomer and adenine in another monomer (Zhang *et al*, 2003). (B) The CT domain from *Streptomyces coelicolor* PCC (ScPCC), in complex with biotin and propionyl-CoA (Diacovich *et al.*, 2004). (C) Detailed view of the CT active site in ScPCC. The enolate biotin is stabilized by an oxyanion hole (red lines). Green lines separate the Cα of propionyl-CoA and N1' of biotin. (D) A separate oxyanion hole stabilizes the propionyl enolate.

Figure 8. Proposed mechanism of carboxyl group transfer in the CT subunit of *S. coelicolor* PCC. During the carboxyltransferase reaction, the propionyl and biotin enolates are respectively stabilized by the presence of the Gly182/Gly183 and Gly419'/Ala420' oxyanion holes. These oxyanion holes are also present in *S. coelicolor* ACC, and the ' marks indicate residues from a different PCCβ protomer. Adapted from Diacovich *et al.*, 2004.

Figure 9. Sequence alignment of the β subunits of *S. coelicolor* PCC and ACC. The positions of the oxyanion holes are indicated with blue boxes, and the site of the 'molecular switch' is highlighted in orange.

Figure 10. Crystal structure of the C-terminal region of BCCP from *E. coli* ACC. (left) The C-terminal region consists of eight anti-parallel beta-strands, with the biotinylation motif near the middle of the polypeptide sequence. The thumb feature is not present in human ACC. (right)

Detailed view of the biotinylation site and conserved motif. Carboxyl group attachment occurs at N1', indicated in red. Adapted from Athappilly and Hendrickson, 1995.

Figure 11. Two models for biotin translocation in biotin-dependent carboxylases. (a) In the 'swinging-arm' model, biotin translocates between the BC and CT active sites while BCCP remains stationary. Adapted from Tong, 2005. (b) In the 'swinging-domain' model, BCCP-biotin is the mobile unit, as seen in the surface representation of *S. aureus* pyruvate carboxylase (Xiang *et al*, 2008). The active sites of Monomer 1 BC and Monomer 2 CT are separated by 75 Å.

Figure 12. Soraphen A inhibits the biotin carboxylase domain of *S. aureus* ACC. (A) Structure of the *S. aureus* BC domain in complex with soraphen A (green). The active site is indicated with an asterisk. (B) Interactions between soraphen and BC. (Zhang *et al.*, 2003) (C) The conformation of soraphen within the complex with *S. aureus* BC; the numbering scheme of the macrocyclic ring is indicated.

Figure 13. Small-molecule inhibitors of the carboxyltransferase domain of ACC. CP-640186 binds the dimer interface of the CT domain. For the herbicides haloxyfop, tepraloxydim, and pinoxaden, the points of CT anchoring are indicated with the red boxes.

Chapter II

Figure 1. Propionyl-CoA can be fully oxidized to CO_2 through the TCA cycle. The reactions linking PCC activity to the TCA cycle are shown on the right. Following PCC activity, the methylmalonyl-CoA product undergoes racemization and epimerization before transforming into succinyl-CoA, which is a TCA cycle intermediate. These reactions occur within the mitochondrial matrix.

Figure 2. Conserved domains of biotin-dependent carboxylases from bacteria to humans. Colors are assigned based on sequence homology. The CT domain of PC is structurally distinct,

and is colored accordingly. The same domains are present in each enzyme, although the method of assembly presumably varies among different enzymes, forming the basis for structural diversity. The scale bar indicates the number of amino acids. Adapted from Tong, 2007.

Figure 3. Crystal structures of biotin carboxylase (BC), biotin carboxyl carrier protein (BCCP), and carboxyltransferase (CT) from *E. coli* ACC. (A) BC is a dimer, with ADP, biotin, HCO_3^-, and Mg^{2+} bound in the active site of each monomer (Chou *et al*, 2009). (B) BCCP is biotinylated at a conserved Lys. The thumb feature is absent in human ACC (Athappilly and Hendrickson, 1995). (C) CT is a dimer of two stacked monomers, and the CT active sites are located at the monomer interface (Bilder *et al*, 2006). The sequence identities between these structures and their HsPCC homologs are (L-R): 49%, 36%, and 27%.

Figure 4. Crystal structures of the acyl-CoA-recognizing subunits of (a) *P. shermanii* transcarboxylase 12S, (b) *S. coelicolor* PCCβ, and (c) *M. tuberculosis* AccD5. The subunits assemble into a hexamer, and the structures are viewed from the top of each hexamer. Each protomer is colored separately.

Figure 5. Synthesis of the bicistronic expression construct used to express PCC holoenzymes. (A, B) PCC subunits were individually screened for protein overexpression and solubility. (C) PCC holoenzymes were produced by subcloning the PCCα gene and its upstream ribosomal binding site into the PCCβ expression plasmid. Although PCCα is not tagged in the final construct, the formation of the holoenzyme allows the entire complex to be purified using the PCCβ tag, then separated from the PCCβ hexamer based on size.

Figure 6. Crystals of PCC holoenzymes from *H. sapiens, R. pomeroyi*, and a *R. pomeroyi/R. denitrificans* chimera. Crystallization conditions are detailed in the Experimental Procedures. HsPCC crystals were obtained from a modified coexpression construct that omitted 15 residues from the N-terminus of HsPCCβ, while the bacterial crystals contain their respective full-length PCCs. The crystals of HsPCC were obtained by Yang Shen.

Figure 7. Structure of the PCC holoenzyme [39]**.** (A) Looking down the threefold symmetry axis of the RpαRdβ chimera of propionyl-CoA carboxylase (PDB code 3N6R). (B) Looking down the twofold symmetry axis. The gray envelopes in (C) and (D) are cryo-EM reconstructions of human PCC at 15-Å resolution with the crystal structure of the RpαRdβ chimera docked into the envelopes, and are viewed in the same orientations as (A) and (B).

Figure 8. Structures of the (a) BT domain from PCC and (b) the PT domain from *S. aureus* pyruvate carboxylase (SaPC). While BT is encoded as a single domain within the primary sequence of PCCα, the PT sequence is interrupted by the CT domain of SaPC (see Figure 1) at the joint between Helix α1 and the start of the β sheet.

Figure 9. Locations of the active sites and disease-associated gene mutations in the PCC holoenzyme. (A) Molecular surface representation of one α subunit and a β_2 dimer. The bound positions of ADP and bicarbonate in complex with *E. coli* BC (Chou *et al*, 2009) and CoA in complex with transcarboxylase 12S (Hall *et al*, 2003) are shown. The BC and CT active sites are separated by 55 Å. Domains are colored in the same manner as in Figure 7. (B) Cartoon representation of (A), with the locations of propionic acidemia-associated mutations indicated by spheres. The position of CoA binding is indicated with the pink molecule.

Figure 10. Effects of propionic acidemia (PA) gene mutations on PCC holoenzyme stability. The *E. coli* cell pellet fraction is indicated with 'P' and the soluble supernatant fraction is indicated with 'S'. Three combinations of PA mutations were assessed, and the abbreviations are, from left to right: LA+MA (L649A/M640A), LA+LA+MA (L646A/L649A/M650A), and RA+RA+LA+MA (R539A/R540A/L649A/M650A). Control lanes of wild-type RpPCC are in the lanes labeled 'PCC'.

Figure 11. The CT active site. (left) Molecular surface representation of the CT binding pocket. The modeled binding mode of CoA with the 12S subunit of transcarboxylase is shown. (right) Detailed view of the CT active site. Biotinylation occurs on Lys694, which is found within a conserved sequence motif (M<u>K</u>M) of BCCP.

Figure 12. Schematic illustration of the ATP hydrolysis assay. Because none of the reactants or products in the PCC-catalyzed reaction (shown in the purple box) can be tracked spetrophotometrically, a coupled-enzyme system featuring pyruvate kinase (PK) and lactate dehydrogenase (LDH) links the production of ADP to the disappearance of NADH. The reaction is monitored by tracking the decrease in A_{340} over time.

Figure 13. Illustration of shared sequence identities between the α and β subunits of PCC and MCC from humans and *Pseudomonas aeruginosa*. The sites of carboxylation on propionyl-CoA and methylcrotonyl-CoA are indicated with red asterisks.

Table 1. Crystallographic data and refinement statistics
Table 2. Kinetic data for the substrate preferences of wild-type PCC and its mutants
Table 3. Kinetic data for the substrate preferences of various RpPCC D440 mutants
Table 4. Kinetic data demonstrating K^+ activation of PCC

Chapter III

Figure 1. Leucine metabolism in humans. A set of six reactions converts L-leucine into either energy metabolites (acetoacetate and acetyl-CoA) or mevalonate, which is a steroid precursor. The substances indicated in brackets on the right-hand side are metabolites that can accumulate when there is a deficiency in the function of their associated enzymes. Such accumulation can lead to their toxic buildup and subsequent consequences to human health. Adapted from University of Florida, Division of Genetics and Metabolism.

Figure 2. Crystals of the β subunit and holoenzymes of MCC from *Pseudomonas aeruginosa*. (A) Crystals of full-length MCCβ free enzyme. (B) Crystals of full-length MCC

complexed with CoA. (C) Crystals of full-length MCC free enzyme. The crystals in (C) were obtained from the same conditions as (B), but required substantially more time to grow.

Figure 3. Crystal structures of the β subunits of *P. aeruginosa* MCC (left) and *Roseobacter denitrificans* PCC (right). Both subunits assemble as hexamers, and the structures are viewed from the top face of each hexamer. The N domain of each β subunit is colored in cyan, and the C domain is colored in yellow. The arrows designate the direction (N'→C') of the linker that connects the two domains within each enzyme. For clarity, the protomer in the bottom layer under each arrow has been omitted from view.

Figure 4. A flexible 25-residue linker connects the N and C domains of β subunits from acyl-CoA carboxylases. Omit F_o-F_c electron density map at 1.5-Å resolution for the domain linker of PaMCCβ, contoured at 3σ.

Figure 5. Sequence alignment of various carboxyltransferase (CT) domains. The sequences of β subunits from various acyl-CoA carboxylases and the α subunit of glutaconyl-CoA decarboxylase (GCDα), which also recognizes an acyl-CoA substrate, are shown. The linker region is not well conserved among the enzymes.

Figure 6. Schematic representations of β$_2$ dimers from MCC (left) and PCC (right). The MCC β$_2$ dimer is shown with the bound positions of crotonyl-CoA in complex with the α subunit of glutaconyl-CoA decarboxylase (GCDα) (Kress *et al*, 2009), and the PCC β$_2$ dimer is shown in complex with the modeled positions of CoA in complex with transcarboxylase 12S (Hall *et al*, 2003).

Figure 7. Structure of the MCC holoenzyme. (A) A view looking down the threefold symmetry axis of *P. aeruginosa* 3-methylcrotonyl-CoA carboxylase. (B) A view looking down the twofold symmetry axis. The gray envelopes in (C) and (D) are cryo-EM reconstructions of PaMCC contoured at 12-Å resolution, with the crystal structure of the holoenzyme docked within, and the views are presented in the same orientations as (A) and (B).

Figure 8. CoA binding induces minor conformational changes in the structure of the MCC holoenzyme. The holoenzyme structures of the MCC free enzyme (gray) and CoA complex (color) are superimposed at the level of the β_6 hexamer. Differences in the two structures are evident in the positions of the B domain of BC, the α6/α6A helices in the β subunit, as well as the absence of BCCP in the free-enzyme structure.

Figure 9. Comparing the MCC and PCC holoenzymes. The crystal structures of the MCC and PCC holoenzymes are rendered as molecular surfaces, and equivalent domains are colored in similar tones. Only one BCCP was identified in the structure of PaMCC. Although the two enzymes are very similar in terms of sequence conservation, domain organization, and function, their three-dimensional structures are distinct from each other.

Figure 10. The BT domain. (A) Location of the BT domain within the MCC holoenzyme. The sites of four 'hook' residues proposed to contribute to holoenzyme integrity are indicated with spheres. (B) Schematic representation of the BT domain from MCC. (C) Schematic representation of the BT domain from PCC.

Figure 11. Mutations in the BT hook structure can destabilize the MCC holoenzyme. Lane headings indicate P for the *E. coli* cell pellet, S for the supernatant fraction, and E for the eluted protein that was isolated using nickel-charged affinity beads.

Figure 12. The BC and CT active sites of MCC. Stereo view of one α subunit and the β_6 hexamer. The BCCP domain (in blue) must translocate a considerable distance to access the two active sites. The hexamer is viewed from the side, in the same manner as Figure 6.

Figure 13. The CT active site. (left) The substrate-binding pocket is buried deep in the groove formed by the N and C domains of different β subunits. The overlaying portions of the C domain are rendered partially transparent to reveal the positions of biotin and 3-methylcrotonyl-CoA (MCoA). (right) Detailed view of the CT binding site. Helix α6 is rendered partially transparent

to show the MCoA. Although CoA was observed in the MCC holoenzyme structure, the additional acyl groups were modeled using the binding mode of crotonyl-CoA in complex with GCDα (Kress *et al.*, 2009).

Figure 14. Locations of the BC and CT active sites and disease-associated gene mutations in the MCC holoenzyme. (A) Schematic representation of one α subunit and a β_2 dimer with the bound positions of ADP from *E. coli* ACC (Chou *et al*, 2009) and CoA. The locations of missense mutations associated with the human disease methylcrotonylglycinuria are indicated with spheres. Panels (B) and (C) depict the consequences of the E134K mutation in the BC domain, and (D) and (E) indicate likewise for the V375F mutation in the CT domain.

Figure 15. Kinetic assay of wild-type MCC and BCCP eviction mutants. An ATP hydrolysis assay was used to compare the catalytic activities of three MCCβ mutants against wild-type MCC. Each curve represents the average of three separate trials. The activity of wild-type MCC was arbitrarily set to 1.0, and the activities of the mutants are calculated in comparison to this value.

Figure 16. Crystals of BCCP eviction mutants from PaMCC. Mutations were introduced in the MCCβ subunit, with the intention of destabilizing BCCP-biotin interactions. Crystallization conditions are summarized in the Experimental Procedures.

cheerfulness and moving across the country so we could keep the lab's population of UCSD grads constant; Yun Bai for being the older and smarter sister I always wished I had; Dazhi Tan for being the source of all good in the lab, Kehui Xiang for being a very tolerant and extremely helpful baymate; and Tim Tran for many hours of 2 AM discussions in lab ... sometimes about science, but mostly not.

And for my friends outside the lab: Miki Hayano, Regina Lutz, Nam Nguyen, Denise Kwong, Kat Chan, Daniel Luu, Laura Brozek, and Renée Trochet – for putting up with me, encouraging me to push beyond my comfort zone, and for being the best partners in crime ever.

There is also a special collection of people who are unlikely to ever read this dissertation, but were nonetheless instrumental in helping me to develop a love for science and critical thinking, and by default, have helped me reach this day. I would like to thank Katherine Roy, Kim Sharon, Susan Campbell, John Crowell, Christina Johnson, Alex Hoffmann, Shannon Werner, Ciarán Cronin, Oleg Brodsky, and David Molina for being outstanding educators and mentors.

And finally, much love and appreciation to Melissa, Clifford, Mom, Dad, and my grandparents Tuchu and Kim-Kuk Huang – for their love and support throughout everything.

Vita and Publications

2006   Bachelor of Science, University of California, San Diego

2007   Master of Science, University of California, San Diego

2008   Master of Arts, Columbia University

2010   Master of Philosophy, Columbia University

2013   Doctor of Philosophy, Columbia University

Huang, C.S., Ge, P., Zhou, Z.H., Tong, L. (2012) An unanticipated architecture of the 750-kDa $\alpha_6\beta_6$ holoenzyme of 3-methylcrotonyl-CoA carboxylase. *Nature*, 481, 219-23

Huang, C.S.*, Sadre-Bazzaz, K.*, Shen, Y., Deng, B., Zhou, Z.H., Tong, L. (2010) Crystal structure of the $\alpha_6\beta_6$ holoenzyme of propionyl-coenzyme A carboxylase. *Nature*, 466, 1001-5 (*–equal first authorship)

For Milo

Chapter I

Biotin-dependent carboxylases are essential metabolic enzymes

1.1 Introduction to the biotin-dependent carboxylases

1.1.1 Biotin is a mobile prosthetic group
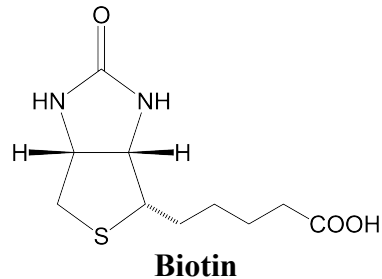
Biotin

Biotin, which is also known as Vitamin H, is a water-soluble vitamin with a backbone structure consisting of two fused 5-member rings and an attached valeric acid side chain. Biotin is essential to many metabolic processes, including fatty acid biosynthesis and oxidation, aerobic respiration, and gluconeogenesis. Although biotin can be synthesized from a pimeloyl-CoA precursor in plants, fungi, and bacteria, higher organisms are incapable of this biosynthesis and must acquire biotin either through their diets, or through the contributions of their intestinal fauna (gut bacteria) [1].

There are three families of biotin-dependent enzymes (carboxylases, decarboxylases, transcarboxylases) and these enzymes are responsible for catalyzing a wide variety of metabolic reactions. The biotin-dependent enzymes are noted for their two-part catalytic mechanisms, with biotin as a participant in both reactions. In each biotin-dependent enzyme, biotin is incorporated as a prosthetic group that is covalently bound to a domain known as the biotin carboxyl carrier protein (BCCP; Figure 1). The covalent linkage occurs through the generation of an amide bond between the terminal carboxyl group of biotin and the ammonium group of a conserved lysine

residue on BCCP. This biotinylated lysine is also referred to as a biocytin group. This addition reaction is catalyzed by a biotin protein ligase (BPL), which has both prokaryotic and eukaryotic variants [2]. Once the biotin is attached to BCCP, it is considered to sit on a 16-Å 'swinging arm' that permits the unit to access the dual active sites of the biotin-dependent enzymes (Figure 1). However, in at least one enzyme (pyruvate carboxylase), the range of this 'swinging arm' is insufficient to reach both active sites. As a result, the biocytin group of pyruvate carboxylase is considered to be situated on a 'swinging domain' of BCCP, where its maximum reach is considerably enhanced [3].
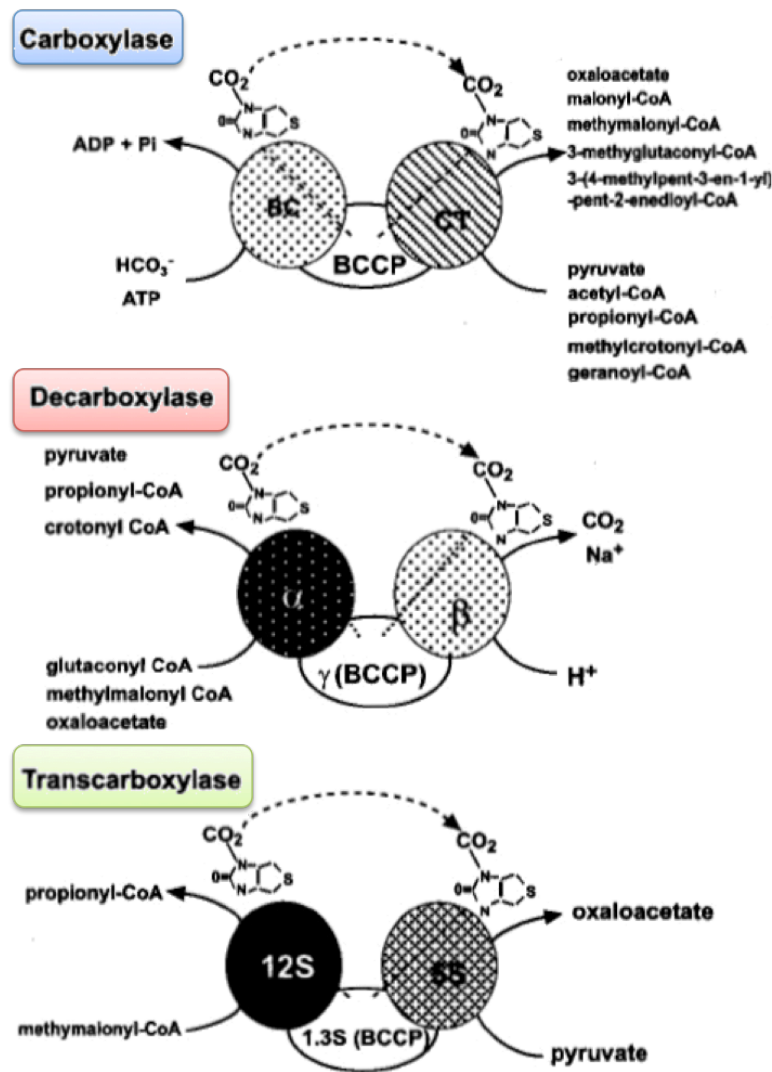
Figure 1. Three classes of biotin-dependent enzymes. Each class of enzymes features a translocating biotin/carboxybiotin system that links the activities of the two active sites. Adapted from Jitrapakee and Wallace, 2003 [4].

The biotin-dependent carboxylases require ATP for their activity, and they catalyze the carboxylation of several metabolites associated with carbohydrate, lipid, and protein metabolism. The first active site (within the BC domain; Figure 1) catalyzes the carboxylation of biotin, which is followed by the resulting carboxybiotin entering the second active site (within the CT domain) to transfer its carboxyl group onto the acceptor molecule [5].

The family of biotin-dependent <u>de</u>carboxylases is also known as the sodium ion transport decarboxylases, and these enzymes essentially work in the reverse manner as the carboxylases. The first active site (on the α subunit) binds the carboxylated CoA molecule, catalyzes its decarboxylation, and the carboxybiotin group translocates into the β subunit, where CO_2 is released from the enzyme. The energy harnessed from decarboxylation is used to pump Na^+ across the cellular or mitochondrial membrane, after which the resulting electrochemical gradient can be used to synthesize ATP for the cell's energy needs [6].

Lastly, the family of <u>trans</u>carboxylases does not incorporate nor release a freely carboxylated molecule. The carboxyl group is removed from methylmalonyl-CoA in the first (12S) active site and is transferred to pyruvate in the second (5S) active site, generating propionyl-CoA and oxaloacetate [7]. Transcarboxylase consists of a central 12S hexameric core, which surrounded by twelve 5S subunits and linked by twelve 1.3S subunits (BCCP).

The focus of this dissertation will be on the family of biotin-dependent carboxylases and in particular, the five carboxylases that are found in humans (acetyl-CoA carboxylase isoforms 1 and 2, propionyl-CoA carboxylase, methylcrotonyl-CoA carboxylase, and pyruvate carboxylase). However, because there is considerable shared sequence and structural homology between the

domains of all the biotin-dependent enzymes, we will also make occasional references to members of the other families.

1.1.2 Domain organization

All biotin-dependent carboxylases are large macromolecular assemblies that function as holoenzymes. The domain arrangements of six unique carboxylases are shown in Figure 2. The carboxylases include: acetyl-CoA carboxylase (ACC), propionyl-CoA carboxylase (PCC), methylcrotonyl-CoA carboxylase (MCC), pyruvate carboxylase (PC), geranyl-CoA carboxylase (GCC), and urea carboxylase (UC). Within this group of enzymes, the ACCs have commanded the most scientific attention. While bacterial ACC is assembled from individual subunits, mammalian ACC is expressed as a single peptide with multiple domains that assembles into a holoenzyme. In humans, ACC is expressed as two tissue-specific isoforms. ACC1 is found in lipogenic tissues (e.g., liver and fat) while ACC2 is found in the tissues of oxidative tissues (e.g., cardiac and skeletal muscle).
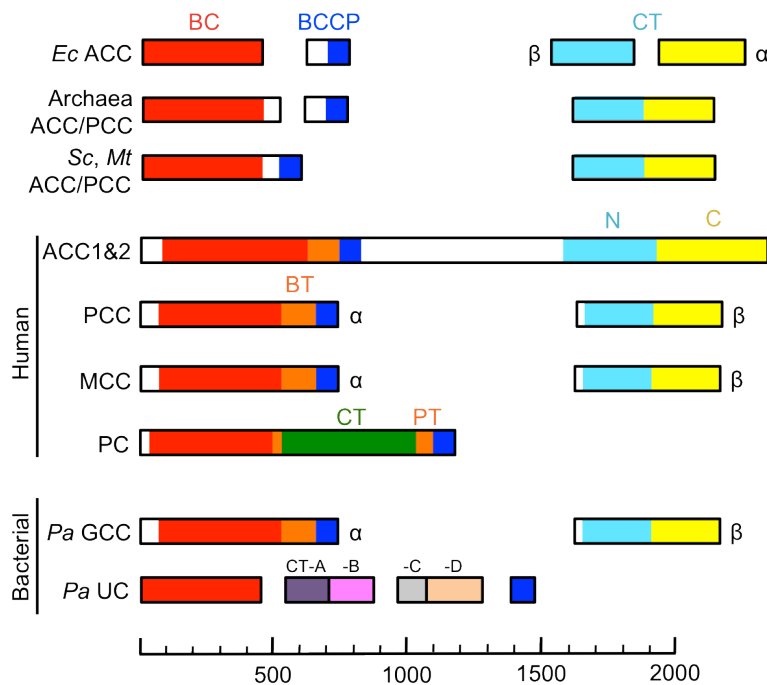
Figure 2. Domain organization of various biotin-dependent carboxylases. Several domains are conserved across species, and are colored accordingly. The CT domains of pyruvate carboxylase (PC) and urea carboxylase (UC) are distinct from those that recognize acyl-CoA substrates. Several species abbreviations are used: *Ec* (*Escherichia coli*), *Sc* (*Streptomyces coelicolor*), *Mt* (*Mycobacterium tuberculosis*), *Pa* (*Pseudomonas aeruginosa*). The scale bar at the bottom indicates the number of amino acids. Adapted from Tong, 2012 [8].

There are three domains found in all biotin-dependent carboxylases: the biotin carboxylase (BC) domain and the carboxyltransferase (CT) domain, which contain catalytic centers; and the biotin carboxyl carrier protein (BCCP), which 'shuttles' reaction intermediates between BC and CT by way of its prosthetic biotin group. The CT domains of PC and UC are unique from those of ACC/PCC/MCC, which recognize acyl-CoA substrates. This difference may have additional implications for the structures of the PC and UC holoenzymes as well.

1.1.3 Human biotin-dependent carboxylases
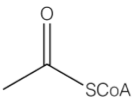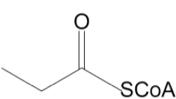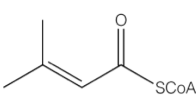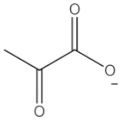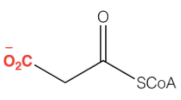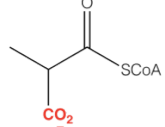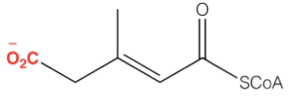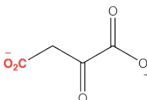
	ACC1 (lipogenic) ACC2 (oxidative)	PCC	MCC	PC
Size	500 kDa (possible oligomers)	750 kDa	750 kDa	500 kDa
Substrate	Acetyl-CoA	Propionyl-CoA	Methylcrotonyl-CoA	Pyruvate
Product	Malonyl-CoA	Methylmalonyl-CoA	Methylglutaconyl-CoA	Oxaloacetate

Figure 3. The five biotin-dependent carboxylases found in humans. The sizes of the holoenzyme and the structures of their substrates and products are shown. The sites of carboxylation are highlighted in red. Note that four of the carboxylases process large acyl-CoA substrates, while pyruvate carboxylase (PC) targets a much smaller organic acid.

ACC1 and ACC2 carboxylate the α-carbon of acetyl-CoA and generate malonyl-CoA as a product. The most basic ACC assembly (the full-length polypeptide) is ~250 kDa in size,

although studies of ACCs from wheat grass and rats have indicated that dimerization is required for ACC activity [9, 10]. PCC also targets the α-carbon of its saturated acyl-CoA substrate, propionyl-CoA, and the carboxylated product is known as methylmalonyl-CoA. Methylcrotonyl-CoA carboxylase accepts an α-β unsaturated acyl ester, and carboxylates the γ-carbon to produce methylglutaconyl-CoA. Both the holoenzymes of PCC and MCC are large assemblies of approximately 750 kDa in size. Finally, PC catalyzes the carboxylation of pyruvate to form oxaloacetate, and its holoenzyme assembles a 500 kDa tetramer.

1.2   Biological roles: essential metabolic enzymes

1.2.1   Tissue/Cellular Localization

In humans, the biotin-dependent carboxylases are widely expressed throughout the body, but are the most active in the tissues and organs involved in energy metabolism. Such organs include those of the digestive tract, liver, and adipose tissue [11, 12]. Of the two ACC isoforms, ACC1 contributes to fatty acid biosynthesis, and is accordingly expressed in lipogenic tissues such as the liver and adipose fat [13]. In contrast, ACC2 mediates fatty acid oxidation and is primarily found in oxidative tissues with high energy demands, such as the liver, heart, and skeletal muscle. Although the liver contains both ACC isozymes, the cellular compartmentalization of malonyl-CoA (either within the cytosol or at the mitochondrial surface) ensures a specific cellular response [14]. Interestingly, ACC1 has been implicated in ensuring the survival of breast cancer cells *in vitro*. The siRNA-mediated silencing of ACC1 in tandem with fatty acid synthase (FAS) genes resulted in a decline in fatty acid synthesis, an arrest in cell proliferation, and the induction of apoptotic pathways within the cancer cells. [15]. Therefore,

ACCs and other components of the lipogenic pathway may serve as possible targets for anti-cancer treatments.

In addition to somatic tissues, the biotin-dependent carboxylases of commensal gut bacteria also provide a significant source of carboxylase activity and consequently, carboxylation products. This proves problematic for individuals with propionic acidemia (PCC deficiency), as they are unable to process the short-chain fatty acids and propionic acid secreted by their intestinal fauna. As a result, patients with propionic acidemia are typically put on metronidazole and/or clindamycin regimens to reduce their numbers of endogenous gut bacteria, and in turn, their propionate load [16, 17].
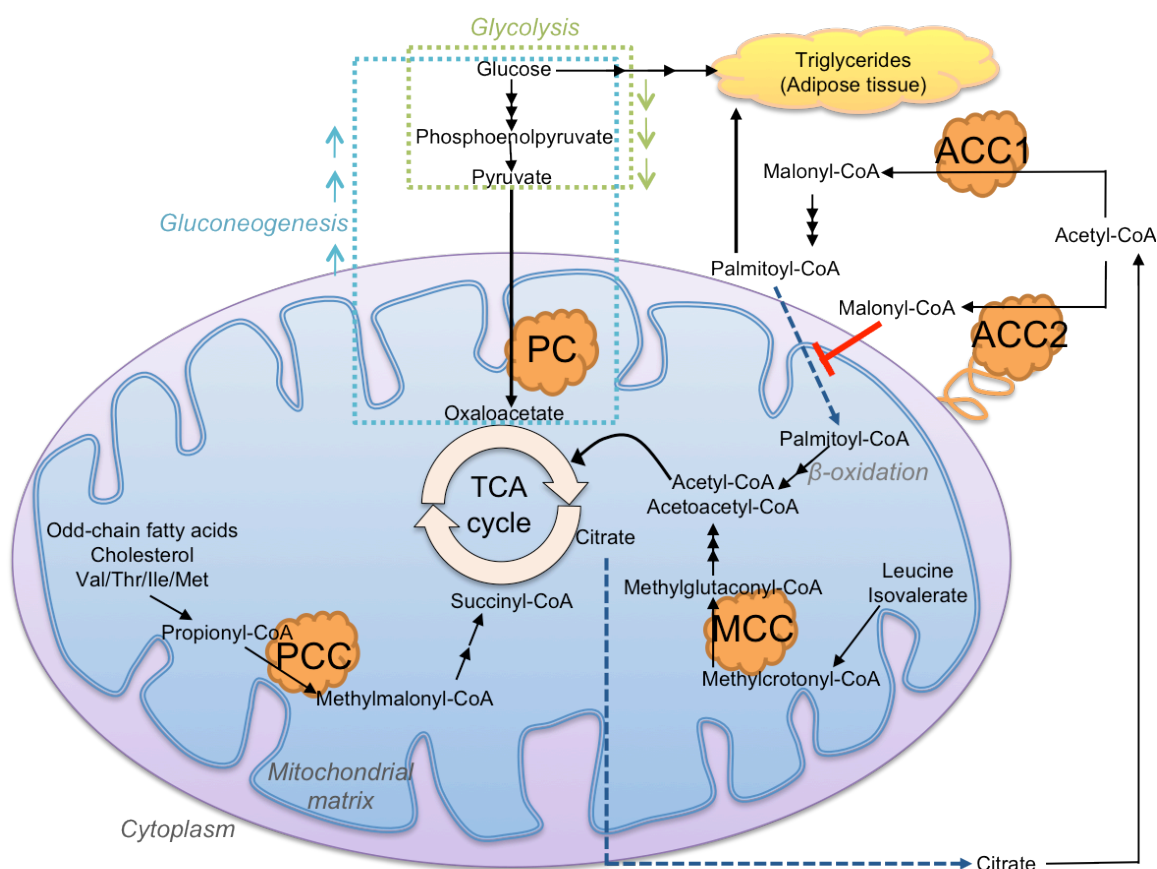
Figure 4. Cellular localization of human biotin-dependent carboxylases. For clarity, only the major metabolic species are shown, and the metabolic pathways are indicated with boxes. The dashed lines indicate the direction of cross-membrane transport across the mitochondrial membranes.

The primary activities and cellular locations of the human biotin-dependent carboxylases are shown in Figure 4. Of the five carboxylases, PCC, MCC, and PC are active within the mitochondrial matrix. Each enzyme is initially synthesized in the cytoplasm with an N-terminal leader peptide that directs their migration to the outer mitochondrial membrane [18-20], and these peptides are proteolytically cleaved during the migration process. At the mitochondrial surface, the enzymes are imported into the organelle in a membrane-potential-dependent manner [19]. In contrast, both ACC isoforms exist as cytoplasmic proteins. ACC1 floats freely in the cytosol, while ACC2 is tethered to the outer mitochondrial membrane, facing the cytoplasm.

1.2.2   Roles in nutrition and energy metabolism

The various substrates of the human biotin-dependent carboxylases are shown in Figure 3, and comprise major metabolites and nutrients that can be found within the human diet. Acetyl-CoA is a key energy 'currency' within the cell, and is produced from the metabolism of all three nutrient groups (lipids, carbohydrates, proteins) primarily through cellular respiration and β-oxidation of fatty acids [21]. Propionyl-CoA is the three-carbon analog of acetyl-CoA, and is also produced from the β-oxidation process. Fatty acids containing an odd number of carbon atoms undergo initial rounds of β-oxidation to remove two-carbon units of acetyl-CoA, until only propionyl-CoA remains. A major source of propionyl-CoA is from the metabolism of several amino acids (Val, Thr, Ile, and Met) as well as cholesterol. Methylcrotonyl-CoA is a product of leucine metabolism. Pyruvate is unlike the other substrates in that it is a small organic acid, lacks the CoA group, and is a major metabolite in several different cellular pathways. The major source of cellular pyruvate results from glycolysis (which produces pyruvate as the end product), although the catabolism of glucogenic amino acids (Ala, Cys, Gly, Ser, Thr) can also

generate pyruvate [22]. Metabolism of cellular pyruvate is achieved through the actions of gluconeogenesis, aerobic/anaerobic respiration, and pyruvate carboxylase (PC).

The compartmentalization of these enzymes within the cell ensures a coordinated and robust response to environmental perturbations. For example, following a large meal, the digested lipids, carbohydrates, and proteins are broken down into TCA cycle intermediates, such as acetyl-CoA. In resting cells, the majority of acetyl-CoA is directed toward fatty acid biosynthesis for long-term energy storage. Because this process takes place in the cytosol, and acetyl-CoA cannot directly pass through the mitochondrial membrane, it is combined with oxaloacetate to form citrate (citrate synthase). Citrate crosses the membrane through the citrate transporter, and is subsequently converted back into oxaloacetate and acetyl-CoA (citrate lyase) [23]. At this point, acetyl-CoA can enter either the lipogenic or oxidative (energy-producing) pathways, depending on the cell's particular energy requirements. When the cell undergoes significant stress and increases its energy demands, the stored energy (in the form of triglycerides) is processed through the fatty acid oxidation pathway and in the mitochondria, where it is released from the TCA cycle in the form of ATP.

The excess cytosolic oxaloacetate, which results from its mitochondrial co-export with acetyl-CoA, needs to be re-imported into the mitochondria to maintain a balanced supply of oxaloacetate across the mitochondrial membrane. In the cytopsol, oxaloacetate is first reduced to malate (malate dehydrogenase), and malate is subsequently oxidized to pyruvate (malic enzyme). Pyruvate crosses the membrane through the pyruvate transporter [24]. Once inside the matrix, the actions of pyruvate carboxylase convert pyruvate back to oxaloacetate, and this species can either enter the TCA cycle for full oxidation to CO_2, or combine with acetyl-CoA to restart the

lipogenic or oxidative pathways. Alternatively, pyruvate can be directly transformed into acetyl-CoA through the pyruvate dehydrogenase complex.

1.3   Catalytic components

Although the existence of the BC and CT reactions has long been known, the finer details of biotin translocation between the BC/CT active sites is still a topic of current research. From a structural perspective, the biotin-carboxylases are remarkably challenging targets. The smallest of the holoenzyme complexes is 500 kDa in size (pyruvate carboxylase), but higher-order oligomers of more than 1 MDa have been reported for mammalian ACCs when bound to the 22-kDa cytosolic protein MIG12 [25]. As such, the elucidation of these holoenzyme structures through classical techniques such as X-ray crystallography and NMR was considered to be an ambitious goal. One modified approach is to first determine the structures of individual domains, and then compile the structural information into a low-resolution electron microscopy (EM) reconstruction of the holoenzyme. The initial studies from this 'divide and conquer' approach are presented in the following sections.

1.3.1   The biotin carboxylase domain

Biotin carboxylase (BC) is a 48-kDa enzyme that catalyzes the ATP-dependent carboxylation of biotin to form carboxybiotin and ADP. The BC domain exists as a monomer in yeast (*Saccharomyces cerevisiae*) and as a 96-kDa homodimer in *E. coli*, although this dimer interface can be disrupted to yield monomeric mutants that still retain some activity *in vitro* [26].

The primary sequences of BC domains from various species are highly conserved. The BC domain of yeast (570 residues) shares 65% sequence identity with the BC domain of human ACC1 (543 residues), while the sequence identity of yeast BC with *E. coli* BC (449 residues) is

slightly lower, at 36%. Generally, there is higher sequence conservation among eukaryotic BCs and among prokaryotic BCs, rather than between eukaryotes and prokaryotes. This discrepancy between eukaryotic and prokaryotic BCs is also thought to result in distinct differences in their three-dimensional structures.

The first crystal structure of biotin carboxylase was determined in 1994 from *E. coli* [27] and was found to feature three distinct domains surrounding a nucleotide-binding site. BC was eventually identified as a member of the ATP-grasp family of enzymes, which primarily catalyze the ATP-dependent conjugation of an amino or thiol group to a carboxylated entity [28, 29]. Family members share a similar overall fold consisting of the A, B, and C sub-domains, and ATP is 'grasped' by the A and C domains. In the structure of *E. coli* BC free enzyme, the B domain assumes an open/extended conformation away from the nucleotide-binding site, and forms a closed lid upon ATP binding. Interestingly, the B-domain of yeast BC maintains a closed conformation, even in the absence of ATP [30].

A search of the Protein Data Base (PDB) reveals that many crystal structures of BC have been determined, from all three branches of life (archaea, bacteria, eukarya). A number of these structures are in complexes with ligands, activators, or inhibitors, and have provided valuable information regarding BC's activity.
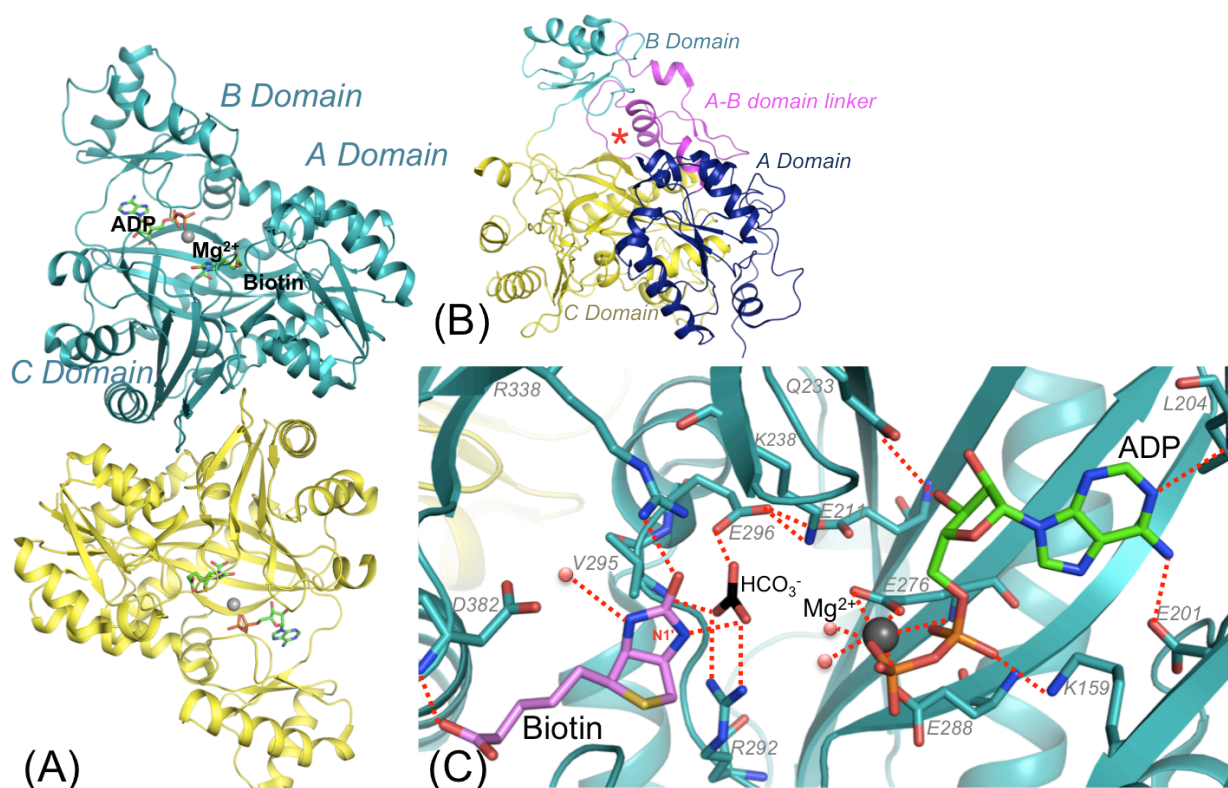
Figure 5. Crystal structures of prokaryotic and eukaryotic biotin carboxylase. (A) Biotin carboxylase from *E. coli* ACC (EcBC), in complex with ADP, bicarbonate, free biotin, and magnesium. (B) Structure of the free-enzyme BC domain from *S. cerevisiae* ACC. The active site is indicated with an asterisk. (C) Detailed view of the EcBC active site. Hydrogen bonding and ion-pair interactions are indicated with dashed lines. Panels A and C are adapted from Chou *et al.*, 2009 [31] and Panel B is adapted from Shen *et al.*, 2004 [32].

E. coli BC (EcBC) forms a homodimer with twofold symmetry, and binding of the ADP nucleotide induces the closed conformation of the B domain (Figure 5A). In comparison, the structure of the BC domain from yeast ACC is a monomer and is shown in Figure 5B. As noted previously, its B domain also maintains a closed conformation over the BC active site, even though ATP is not present.

One explanation for the incongruity in sequence conservation among eukaryotic and prokaryotic BCs is a difference in size; namely, eukaryotic BCs are generally larger than their bacterial counterparts. This phenomenon owes itself to the presence of an elongated A-B domain

linker in eukaryotic BCs, as well as additional insertions within the first two helices of the A domain (Figure 5B) [8, 30].

The structure of EcBC in complex with ADP, bicarbonate, biotin, and magnesium is shown in Figure 5A, and provides valuable information regarding how substrates are recognized within the BC active site. Both ADP and bicarbonate are recognized by a network of interactions formed by the side chains and peptide backbones of nearby residues. Of note, the N1' atom (the site of carboxyl group attachment; see Figure 5) of biotin is located 2.7 Å from bicarbonate, and appears to be poised for catalysis. The divalent magnesium ion is octahedrally coordinated by ADP, Glu276, Glu288, and two water molecules.

It should be noted that, in order to ensure ligand incorporation, the concentrations of the BC ligands in the crystallization conditions are significantly higher than their typical intracellular levels. In addition, the exogenous biotin is not tethered to BCCP as it is found in nature, and thus its binding mode may be slightly different within the context of the ACC holoenzyme. Nevertheless, all the ligands were identified with clearly defined electron density at 2.0-Å resolution, and the observations made within this structure supported the proposal of a mechanism for the BC reaction (Figure 6).
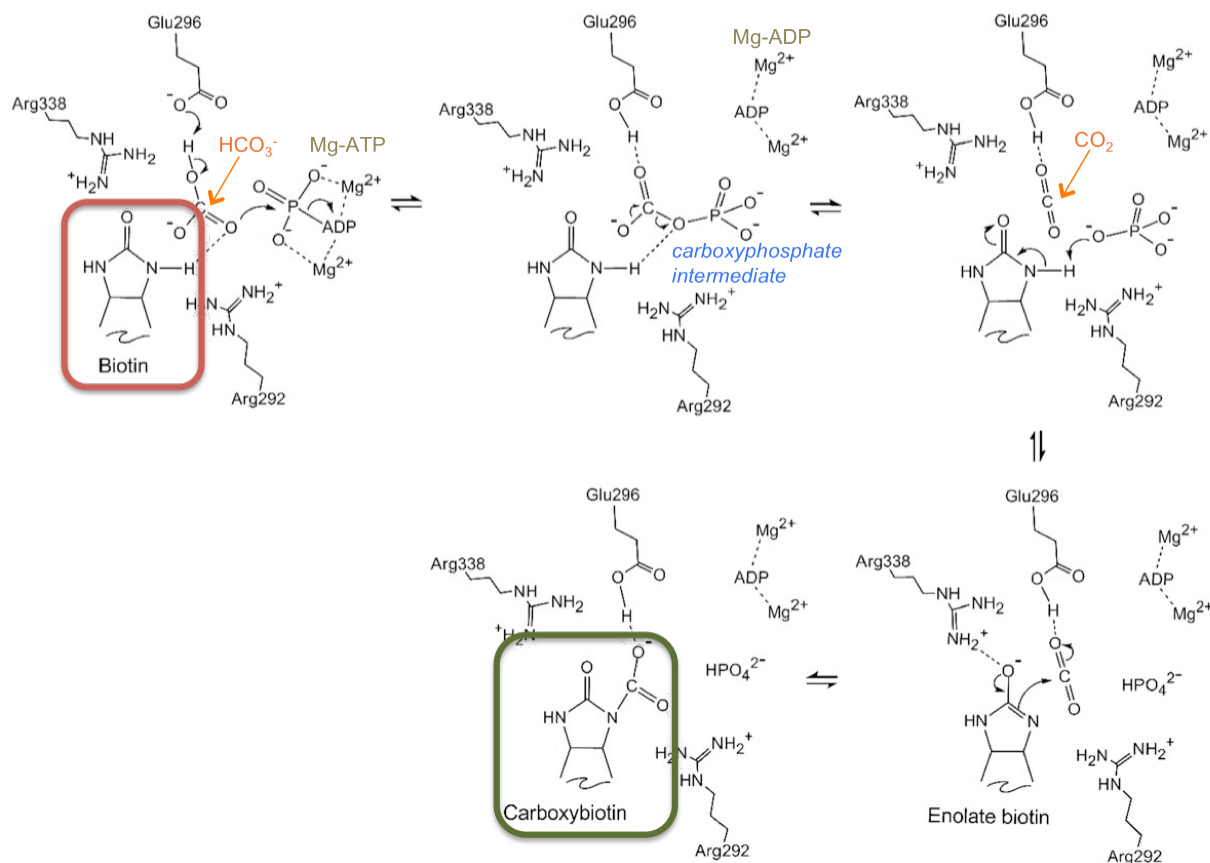
Figure 6. Proposed mechanism of biotin carboxylation in the BC domain of *E. coli* ACC. The reaction schematic is presented in approximately the same view as the active site in Figure 5C. Biotin is considered tethered to BCCP, and the orientation of natural ATP substrate shown in the mechanism is based on the observed binding mode of ADP. Adapted from Chou *et al.*, 2009 [31] and based on the mechanism proposed by Knowles, 1989 [5].

In the proposed mechanism for biotin carboxylation, Glu296 is identified as the general base that initiates catalysis, and its nucleophilicity is likely enhanced by the adjacent Glu211. Although the standard pK_a of a bicarbonate ion is defined as 10.3, it is thought that the acidic residues in the local environment will lower the pK_a and permit its deprotonation. Upon abstraction of the bicarbonate hydrogen, a carboxyphosphate intermediate is formed, and subsequently decomposes into P_i and CO_2. The resulting inorganic phosphate extracts a proton from the N1' atom of biotin, resulting in a biotin enolate that is stabilized by the guanidinium group of Arg338. Lastly, the tautomerization of the biotin enolate into the keto form results in the formation of carboxybiotin, which is a product of the BC reaction. All the key residues

implicated in this mechanism are well conserved among BCs of different species, which likely supports their roles in BC catalysis.

1.3.2 The carboxyltransferase domain

In biotin-dependent carboxylases, the carboxyltransferase (CT) domain catalyzes the carboxylation of the holoenzyme's namesake substrate. Carboxybiotin serves as the carboxyl source and is produced in the preceding BC reaction, whereas the biotin scaffold is permanently tethered to the biotin carboxyl carrier protein (BCCP). The CT reaction does not require additional energy input to proceed. Because the CT domain alone recognizes the carboxylation targets, the CTs that target acyl-CoA substrates are very different than the those that recognize keto acids (such as pyruvate) and carbamides [33]. This dissertation focuses on the enzymes that target acyl-CoA substrates, and all subsequent mentions of CT domains refer to the acyl-CoA enzymes unless otherwise specified.

The primary sequences of CTs from eukaryotic, multi-domain ACCs are highly conserved, but share limited sequence homology with those of prokaryotic, multi-subunit ACCs [4]. This difference is manifested in the unique organization of the eukaryotic and prokaryotic enzymes: eukaryotic CTs consist of two sub-domains (N- and C-terminal domains), while bacterial CTs are assembled from two subunits (α and β). There are no close homologs of CT apart from enzymes associated with acyl-CoA thioester modifications [34], which include the biotin-dependent carboxylases.

The first high-resolution structures of CT were obtained in 2003, featuring the 90-kDa free enzyme from *Saccharomyces cerevisiae* at 2.5-Å resolution and a CoA-bound complex at 2.7-Å resolution [35]. Yeast CT was observed to form a stable homodimer, and the dimer

interface consists of residues that are highly conserved with the CT domains of other ACCs. Each CT protomer contains an internal crotonase fold, which consists of two perpendicular beta-sheets linked by alpha-helices (β-β-α superhelix) [36, 37]. The crotonase motif is only present in the CT domains that accept acyl-CoA substrates.

In the structure of yeast CT, the substrate-binding site was identified at the dimer interface, in a deep groove formed by the N domain from one protomer and the C domain from another protomer. As a consequence, dimerization is required to form the CT active site, and in turn, permit catalysis.

In 2004, the structure of the CT subunit from the bacterium *Streptomyces coelicolor* was reported, and was found to possess many of the same features as its yeast equivalent. One significant difference, however, was that its CT subunits assembled as a ring-shaped hexamer, or a trimer of dimers [38]. This hexameric arrangement has also been witnessed in the CT domains of several bacterial enzymes, including the α subunit of glutaconyl-CoA decarboxylase [39, 40] and the 12S subunit of transcarboxylase [41]. The structure of *S. coelicolor* CT was also obtained in complex with several ligands, lending insight into its catalytic activities. Both the structures of yeast and bacterial CT are presented here, followed by a description of the carboxyltransferase activity.
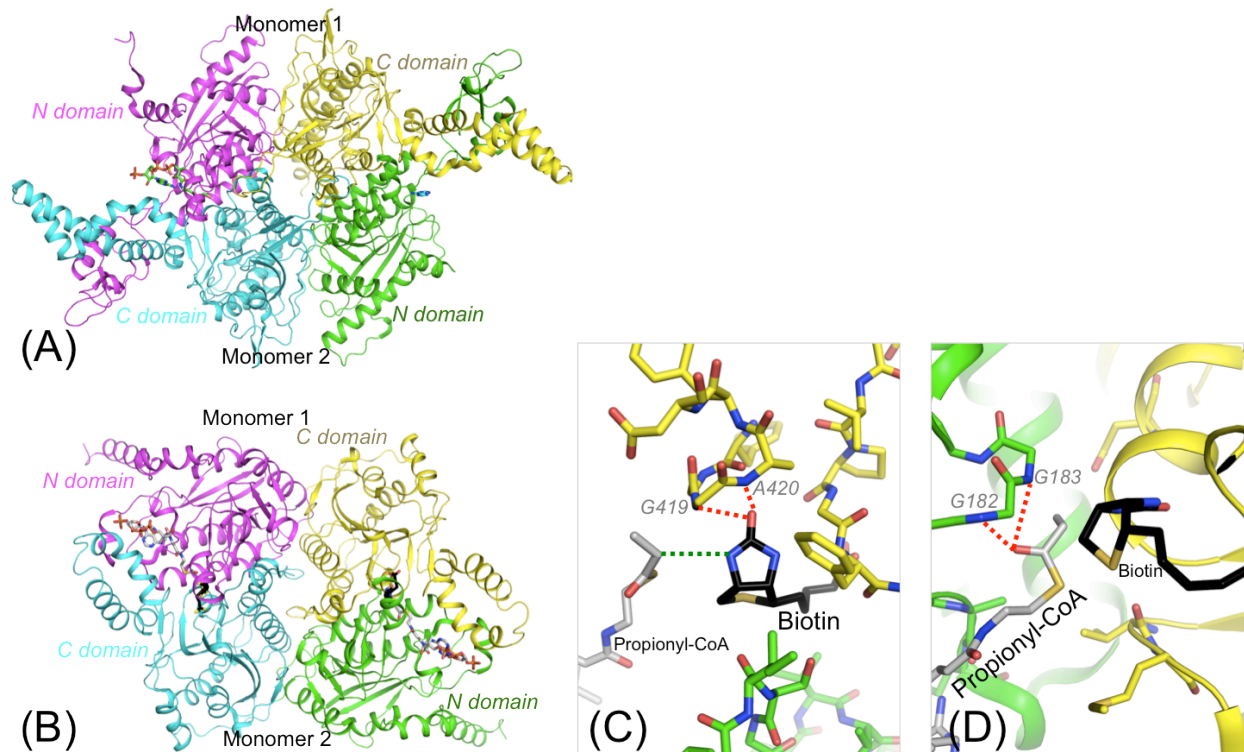
Figure 7. Crystal structures of eukaryotic and prokaryotic carboxyltransferase (CT). (A) The CT domain from yeast ACC in complex with CoA in one monomer and adenine in another monomer [35]. (B) The CT domain from *Streptomyces coelicolor* PCC (ScPCC), in complex with biotin and propionyl-CoA [38]. (C) Detailed view of the CT active site in ScPCC. The enolate biotin is stabilized by an oxyanion hole (red lines). Green lines separate the Cα of propionyl-CoA and N1' of biotin. (D) A separate oxyanion hole stabilizes the propionyl enolate.

Diacovich *et al*. determined the structure of the CT subunit from *S. coelicolor* PCC in complex with biotin and propionyl-CoA, and identified two oxyanion holes (G182/G183 from one β protomer and G419'/A420' from another β protomer) that could be used to stabilize reaction intermediates. In addition, the bound positions of the ligands revealed that the ureido (N1') nitrogen of biotin was appropriately located with respect to the alpha-carbon of propionyl-CoA, thereby facilitating the latter's deprotonation and subsequent enolization.

However, it was not clear which species initiated the carboxyltransfer reaction. Early studies of the CT from *E. coli* ACC suggested that the overall reaction proceeded in a stepwise manner. A series of sulfhydryl-modifying experiments implicated a cysteine residue as the initiating nucleophile [5, 42]. However, an active site cysteine was not found in the structure of

the CT domain from yeast ACC. Moreover, mutations in the vicinity of the active site failed to identify a residue that that was absolutely essential for catalysis. Therefore, the CT mechanism likely features biotin as the active site base – or more specifically, its deprotonated ureido nitrogen [5, 35]. Based on these observations, a detailed mechanism for the CT reaction was described for *S. coelicolor* PCC [38] (Figure 8).
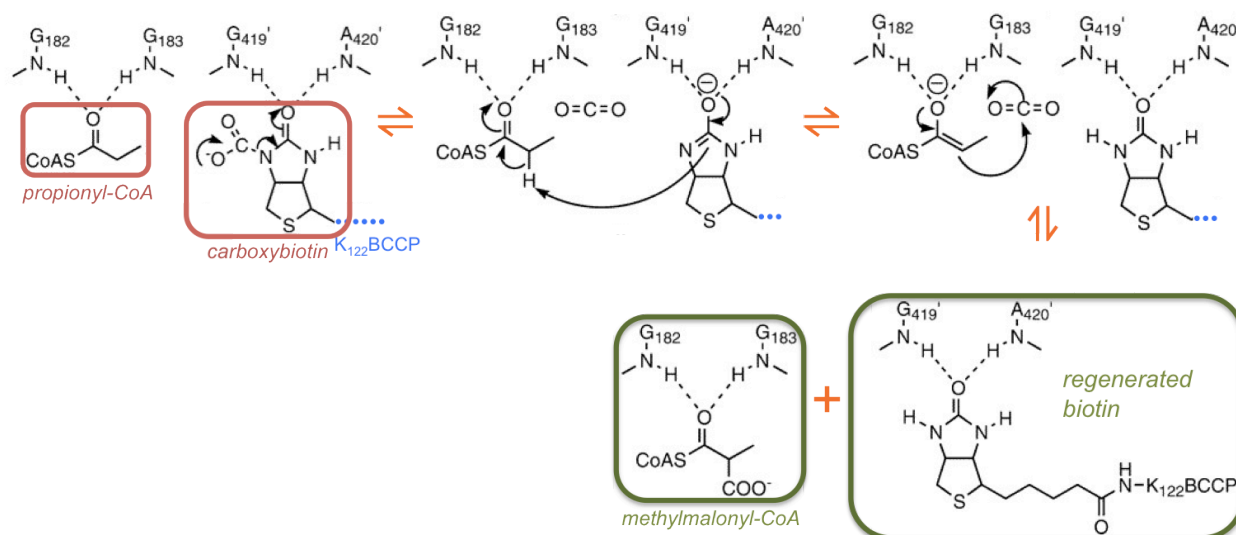
Figure 8. Proposed mechanism of carboxyl group transfer in the CT subunit of *S. coelicolor* PCC. During the carboxyltransferase reaction, the propionyl and biotin enolates are respectively stabilized by the presence of the Gly182/Gly183 and Gly419'/Ala420' oxyanion holes. These oxyanion holes are also present in *S. coelicolor* ACC, and the ' marks indicate residues from a different PCCβ protomer. Adapted from Diacovich *et al.*, 2004 [38].

The proposed mechanism for the CT reaction begins with a conformational change within the enzyme, which bends the planar CO_2-N1'-CO-NH orbitals to destabilize the carboxyl-biotin linkage and liberate CO_2. The resulting biotin enolate is stabilized within the G419'/A420' oxyanion hole before tautomerizing with its keto form, and the ureido nitrogen subsequently abstracts the Cα proton from propionyl-CoA. Biotin is regenerated in this process. The propionyl enolate is stabilized by G182/G183, and its ensuing attack on CO_2 produces methylmalonyl-CoA, which is the overall product of the PCC reaction.

The sequence alignments of various CTs, including *S. coelicolor* ACC as well as the PCCs and ACCs from other organisms, indicate that the G182/G183 and G419'/A420' residue pairs are highly conserved. This suggests that the oxyanion holes are involved in a common catalytic scheme, and emphasizes the usefulness of studying homologous enzymes to better understand the catalytic properties of the entire family of biotin-dependent carboxylases.

One caveat of the mechanism is that the protein-ligand interactions observed in the crystal structure are those of bound propionyl-CoA and biotin, which do not form a productive substrate pair (unlike carboxybiotin/propionyl-CoA or biotin/methylmalonyl-CoA, the latter pair being products of the PCC reaction). However, the location and orientation of the oxyanion holes provide convincing arguments for the proposed catalytic scheme.

Diacovich *et al.* also used the crystal structure of *S. coelicolor* PCCβ to generate a homology model of ACCβ from the same organism. In the process, it was discovered that, with the exception of a single amino acid, nearly every other active site residue was conserved between the two enzymes. This suggested that the recognition of unique acyl group functionalities within the CT domain is limited to a very small subset of amino acids. The variant amino acid was found at position 420 in ACCβ (Ile420) and position 422 in PCCβ (Asp422; see Figure 9). When these residues were exchanged between the enzymes, by generating an I420D mutant in ACC and a D422I mutant in PCC, it was found that the substrate specificity was interconverted as well. In other words, ACCβ-I420D exhibited a preference for propionyl-CoA as a substrate, whereas PCCβ-D422I preferred acetyl-CoA. This 'molecular switch' represents a potential control mechanism for determining catalytic activity in these enzymes, and may be of interest for disease therapies as well. It remains to be seen, however, whether this switch is

present in other biotin-family enzymes as well, and additional structural information is needed to understand its mode of action.

```
ScPCCb_    MSEPEEQQPDIHTTAGKLADLRRRIEEATHAG-SARAVEKQHAKGKLTARERIDLLLDEG 59
ScACCb_    MTVLDEAPGEPTDARGRVAELHG-IRAAALAGPSEKATAAQHAKGKLTARERIELLLDPG 59
           *:   :*    :    : *::*:*:  *. *: ** * :*.  ************:**** *

ScPCCb_    SFVELDEFARHRSTNFGLDANRPYGDGVVTGYGTVDGRPVAVFSQDFTVFGGALGEVYGQ 119
ScACCb_    SFREVEQLRRHRATGFGLEAKKPYTDGVITGWGTVEGRTVFVYAHDFRIFGGALGEAHAT 119
           ** *:::: ***:*.***:*::** ***:**:***:**.* *:::** :*******.:.

ScPCCb_    KIVKVMDFALKTGCPVVGINDSGGARIQEGVASLGAYGEIFRRNTHASGVIPQISLVVGP 179
ScACCb_    KIHKIMDMAIAAGAPLVSLNDGAGARIQEGVSALAGYGGIFQRNTKASGVIPQISVMLGP 179
           ** *:**:*: :*.*:*.:**..*********::*..** **:***:*********::**

ScPCCb_    CAGGAVYSPAITDFTVMVDQTSHMFITGPDVIKTVTGEDVGFEELGGARTHNSTSGVAHH 239
ScACCb_    CAGGAAYSPALTDFVFMVRDTSQMFITGPDVVKAVTGEEITQNGLGGADVHAETSGVCHF 239
           ****:.****:***..** :**:*********:*:****::   : **** .* .****.*.

ScPCCb_    MAGDEKDAVEYVKQLLSYLPSNNLSEPPAFPEEADLAVTDEDAELDTIVPDSANQPYDMH 299
ScACCb_    AYDDEETCLAEVRYLLSLLPQNNRENPPR-AESSDPVDRRSDTLLD-LVPADGNRPYDMT 297
            .**: .:  *: *** **.** .:** .*.:* .  .*: ** :** ..*:****

ScPCCb_    SVIEHVLDDAEFFETQPLFAPNILTGFGRVEGRPVGIVANQPMQFAGCLDITASEKAARF 359
ScACCb_    KVIEELVDEGEYLEVHERWARNIICALARLDGRVVGIVANQPQALAGVLDIEASEKAARF 357
           .***.::*:.*::*.:   :*  **: .:.*:** ********   :** *** ********

ScPCCb_    VRTCDAFNVPVLTFVDVPGFLPGVDQEHDGIIRRGAKLIFAYAEATVPLITVITRKAFGG 419
ScACCb_    VQMCDAFNIPIITLLDVPGFLPGVDQEHGGIIRHGAKLLYAYCNATVPRISLILRKAYGG 417
           *:  *****:*::*::**************.****:****::**.:**** *::* ***:**

ScPCCb_    AYDVMGSKHLGADLNLAWPTAQIAVMGAQGAVNILHRRTIADAGDDAEATRARLIQEYED 479
ScACCb_    AYIVMDSQSIGADLTYAWPTNEIAVMGAEGAANVIFRRQIADA-EDPEAMRARMVKEYKS 476
           **:**.*: :**** .**** :*******:**.*::.** **** :*.** ***:::**:.

ScPCCb_    ALLNPYTAAERGYVDAVIMPSDTRRHIVRGLRQLRTKRESLPPKKHGNIPL 530
ScACCb_    ELMHPYYAAERGLVDDVIDPAETREVLITSLAMLHTKHADLPSRKHGNPPQ 527
            *::** ***** ** ** *::**. :: .*  *:**: .**.:**** *
```

Figure 9. Sequence alignment of the β subunits of *S. coelicolor* PCC and ACC. The positions of the oxyanion holes are indicated with blue boxes, and the site of the 'molecular switch' is highlighted in orange.

1.3.3   The biotin carboxyl carrier protein

In biotin-dependent carboxylases, the BC and CT activities are linked by a carboxybiotin/biotin shuttle, which is covalently tethered to the biotin carboxyl carrier protein (BCCP) at the site of a conserved lysine residue and motif (MKM) [43, 44]. The addition of biotin to BCCP is catalyzed by biotin protein ligase (BPL), which is known as BirA in prokaryotes and as holocarboxylase synthase (HCS) in eukaryotes. This process is remarkably specific, and can target a specific MKM lysine for modification even while tolerating variations in the motif's flanking sequences [45].

While BirA and HCS both share biotin ligase activities, they are not exact orthologs of each other. The length of BirA is 325 residues, while HCS features a DNA-binding domain in its N-terminal half and contains 726 residues in total [46]. The sequence identity of their biotinylation domains is much more similar, and the ~130 amino acids comprising this common region share 60% sequence identity. Both BirA and HCS execute their biotinylation activities in two steps: an addition of ATP to free biotin to form the intermeidate biotinyl-5'-AMP, followed by the transfer of the biotin group to the target protein [47, 48].

An insufficiency in HCS activity in humans leads to holocarboxylase synthetase deficiency, which affects all biotin-dependent enzymes in the body. As a result, affected patients may experience stunted growth and immunodeficiencies [49]. In addition, because HCS is involved in biotinylating several metabolic targets, the levels of biotinylated histone proteins are also reduced as well [50].

E. coli BCCP exists as a single polypeptide and consists of an N-terminal and C-terminal domain. Although BCCP had been isolated in multiple active forms, ranging in size from 45 kDa to 9 kDa, early biochemical techniques occasionally resulted in inadvertent cleavage between the domains, complicating the subsequent data analysis [51]. In 1995, Athappilly and Hendrickson purified recombinant BCCP and treated the product with subtilisin Carlsberg to isolate the 9-kDa C-terminal region, the structure of which is shown:
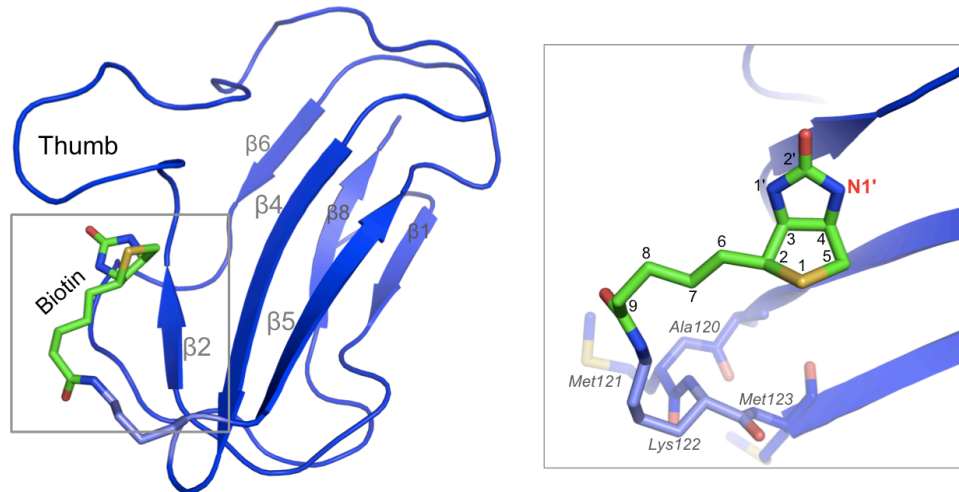
Figure 10. Crystal structure of the C-terminal region of BCCP from *E. coli* ACC [52]. (left) The C-terminal region consists of eight anti-parallel beta-strands, with the biotinylation motif near the middle of the polypeptide sequence. The thumb feature is not present in human ACC. (right) Detailed view of the biotinylation site and conserved motif. Carboxyl group attachment occurs at N1', indicated in red.

The structure of the 9-kDa C-terminal region of *E. coli* BCCP is essentially divided into two halves, and each half consists of four anti-parallel beta-strands (respectively numbered β1-β4 and β5-β8) [52]. The biotinylation site is located at the distal end of a hairpin turn between β4 and β5. The internal residues of BCCP are largely hydrophobic and help to maintain the domain's stability through hydrophobic and van der Waals interactions. These forces are thought to aid in maintaining BCCP's conformation during catalysis, when the carboxybiotin/biotin system translocates repeatedly between the BC and CT domains.

E. coli BCCP was also found to possess a 'protruding thumb' within its C-terminal region, and this 'thumb' interacts with the covalently bound biotin. This feature is not present in human BCCP, and consequently, its bound biotin is more flexible than that of *E. coli* [53]. More impressively, the 'thumb' prevents the human biotin ligase (HCS) from accessing the biotinylation site within BCCP, whereas the bacterial BirA does not experience such interference [54]. This distinction in enzyme-ligand interactions is likely an indication of divergent evolution

in the eukaryotic and prokaryotic biotin-dependent carboxylases over time, and may be an important factor in the development of antibiotics against pathogenic bacteria.

In addition to enzymatic biotinylation, biotin protein ligases have also been shown to possess transcription repressor activity [55, 56]. A recent structural study revealed that *Staphyloccoccus aureus* BPL dimerizes upon binding biotin, and the resulting complex is capable of binding a 44-bp fragment of the *bioO* operon, which controls biotin biosynthesis [57]. Interestingly, the presence of BCCP dissolves the BPL dimer, even in the presence of excess biotin. These findings demonstrate that BCCP is involved in both catalytic and regulatory activities, and provide the first structural data for the DNA-binding family of biotin protein ligases.

1.4   A common mechanism and a translocating factor

The defining attribute of the biotin-dependent carboxylases is the presence of two catalytic activities, linked by the transfer of carboxybiotin/biotin. Although the structures of BC, CT, and BCCP yielded considerable insight into their catalytic potential, there remained many unanswered questions regarding the holoenzymes' overall mechanism. Specifically, very little was known regarding the mode of biotin/carboxybiotin exchange between the BC and CT domains. In addition, several carboxylases were known to comprise higher-order oligomers ($\alpha_4\beta_4$ for PC; $\alpha_6\beta_6$ for PCC and MCC), but it was not certain whether the protomers functioned as independent units, or if they engaged in coordinated catalysis.

The earliest descriptions of biotin-dependent carboxylation gave rise to the 'swinging-arm' model for translocation, in which biotin oscillates between the BC and CT active sites (Figure 11A) [5, 58]. This model was supported by studies of the 1.3S subunit (BCCP) from

Propionibacterium shermanii transcarboxylase, which employed NMR techniques to study the flexibility of the biocytin group [59]. The maximum reach of such a biotin moiety spans approximately 16 Å, which is more than sufficient to cover the 7 Å between the two active sites of *P. shermanii* transcarboxylase [60, 61].
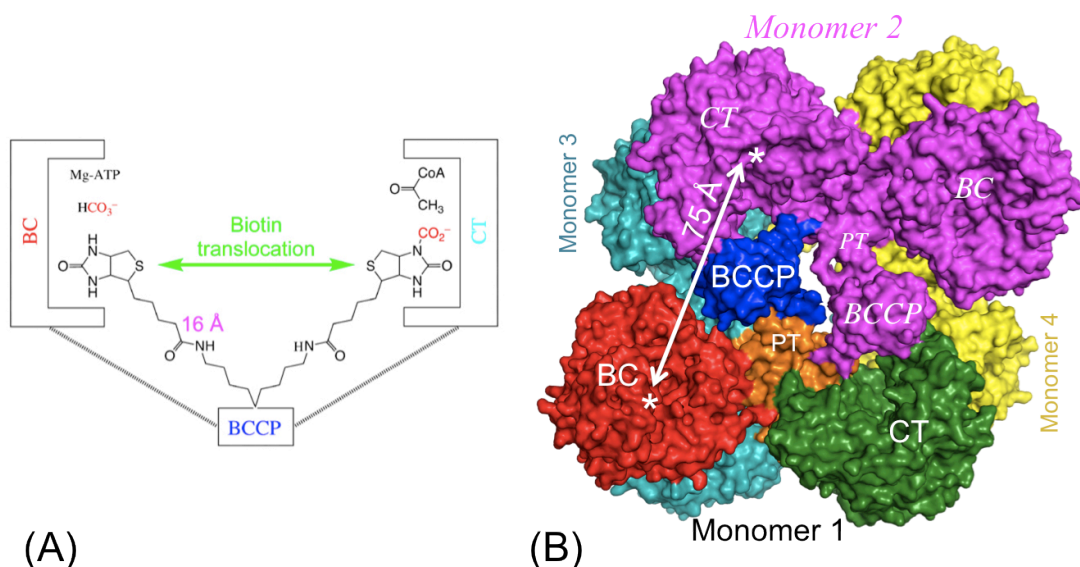
(A)   (B)

Figure 11. Two models for biotin translocation in biotin-dependent carboxylases. (a) In the 'swinging-arm' model, biotin translocates between the BC and CT active sites while BCCP remains stationary. Adapted from Tong, 2005 [62]. (b) In the 'swinging-domain' model, BCCP-biotin is the mobile unit, as seen in the surface representation of *S. aureus* pyruvate carboxylase [3]. The active sites of Monomer 1 BC and Monomer 2 CT are separated by 75 Å.

The biotin 'swinging-arm' was considered the predominant model for translocation until the crystal structures of *Rhizobium etli* and *Staphylococcus aureus* pyruvate carboxylase (PC) were determined. These structures revealed that the BC and CT active sites are separated by 75 Å [3, 63], which is far beyond the range of a fully extended biotin and therefore eliminates the possibility of a biotin swinging-arm for PC catalysis. As a result, a 'swinging-domain' model for BCCP-mediated translocation was proposed. Although the swinging-domain model is strongly supported by the structure of PC, it was uncertain whether the other biotin-dependent carboxylases will also exhibit this feature. Pyruvate is a small organic molecule, and

ACC/PCC/MCC target larger acyl-CoA substrates. In addition, the sequences of the CT domains are vastly different between PC and the acyl-CoA carboxylases.

In addition to pioneering the concept of the swinging domain, the crystal structures of PC revealed that one round of catalysis requires the contribution of *two* different monomers. In Figure 11, the BCCP of Monomer 1 is shown interacting with the CT domain of Monomer 2. This structure provided the first evidence that a biotin-dependent carboxylase could employ different protomers for a single round of catalysis. One implication of such inter-domain coordination is the possibility of allosteric regulation as a control mechanism [64, 65]. However, the relevance of PC's structure for other biotin-dependent carboxylases may be limited due to its unique CT domain. Therefore, a crystal structure of a biotin-dependent *acyl*-CoA carboxylase is of significant importance.

1.5 Potential drug discovery targets

The family of biotin-dependent carboxylases holds many important roles in metabolism and homeostatic regulation, across all walks of life. As such, these enzymes are promising drug targets, and the ability to modulate their expression and activities may hold the key to controlling a number of human diseases, including cancer, diabetes, and pathogenic infections. One particularly enticing target is ACC2, which inhibits fatty acid oxidation in humans (Figure 4). By blocking the activities of ACC2, it is possible to drive continuous fatty acid oxidation. Mice deficient in ACC2 exhibit increased feeding tendencies (hyperphagy) compared to their wild-type counterparts, but display lower body weights [66, 67]. If an inhibitor of human ACC2 is developed and brought to market, it could dramatically enhance the lifestyles of many individuals, particularly those residing in first-world countries and indulging in sedentary habits.

In the past decade, several small molecules have been identified and shown to selectively inhibit the BC and CT domains in a species- and enzyme-specific manner. The differences between these enzymatic orthologs constitute the basis of structure-based drug design for this family of enzymes. While the sequences and structures may be similar across different species, their minute variations are more than sufficient to permit the fine-tuning of an inhibitor's affinity and specificity to target a single enzyme with extreme accuracy. Several examples of specific inhibitors, targeting the BC and CT domains, are discussed in the following sections.

1.5.1   Soraphen A: an inhibitor of biotin carboxylase

Soraphen A is a polyketide natural product that possesses strong fungicide activity and has also been shown to be a highly specific and potent (nanomolar) inhibitor of eukaryotic BCs [68] while exhibiting no effect on bacterial BC [69]. Although the compound was isolated in the early 1990s and its inhibitory activities toward various pathogenic fungal ACCs were well documented [70, 71], it was not until 2003 that a structure of soraphen A, in complex with its enzymatic target, was obtained.
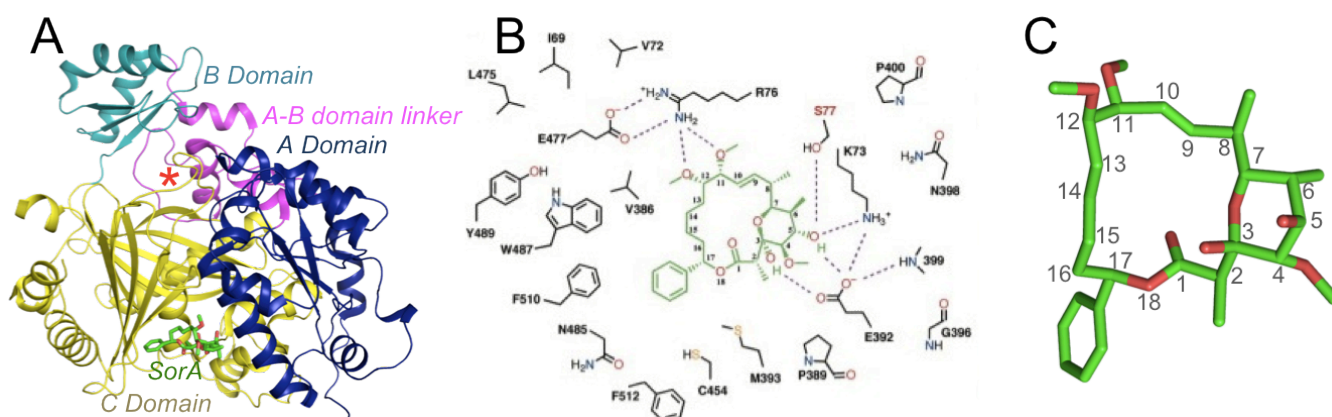
Figure 12.   Soraphen A inhibits the biotin carboxylase domain of *S. aureus* ACC. (A) Structure of the *S. aureus* BC domain in complex with soraphen A (green). The active site is indicated with an asterisk. (B) Interactions between soraphen and BC. [35] (C) The conformation of soraphen within the complex with *S. aureus* BC; the numbering scheme of the macrocyclic ring is indicated.

The crystal structure of soraphen A in complex with the BC domain of *S. aureus* ACC revealed that soraphen is an allosteric inhibitor, and binds approximately 25 Å from the active site, at the interface of the A and C domains (Figure 12A) [35]. There are multiple hydrogen-bonding contacts and van der Waals interactions between the inhibitor and the BC domain, which explains its high binding affinity (Figure 12B). These residues are highly conserved among eukaryotic BCs, and may explain how soraphen is able to preferentially target these BCs over their prokaryotic counterparts. A mutation at any one of these conserved residues has immediate effects on soraphen affinity; in yeast, the K73R mutation confers resistance to the compound [72], while the S77Y mutation is thought to generate steric clashes between the compound and the tyrosine side chain, thereby compromising binding [70]. The high specificity of soraphen for eukaryotic BC domains can also be explained by the architecture of the prokaryotic BC subunit. The structure of *E. coli* BC reveals a 3-Å shift in the position of β19 at the predicted soraphen-binding site; this shift directly clashes with the predicted binding position of soraphen. This finding, coupled with additional rearrangements in the orientation of nearby amino acid side chains, essentially excludes soraphen from binding prokaryotic BC domains. In spite of this wealth of structural and biochemical data, however, the method through which soraphen exerts its inhibitory effects is still not clear.

While soraphen A is still the best-characterized BC inhibitor to date, two recent studies from Pfizer have capitalized on advanced screening techniques to identity new candidate inhibitors against bacterial BC subunits. In the first study, Miller *et al.* employed whole-cell screening to identify a set of antibacterial pyridopyrimidines, and demonstrated their inhibition against *Haemophilus influenzae* BC using *in vitro* and *in vivo* models [73]. A second study by Mochalkin *et al.* used fragment-based screening to assemble a collection of 'building blocks'.

Successive rounds of optimization produced a series of amino-oxazole compounds, and their antibacterial properties were subsequently demonstrated with ACC activity assays and structural data [74]. These new approaches for drug discovery have significant advantages over the classical methods of compound screening, and will likely increase in popularity in the coming years.

1.5.2   Inhibitors of carboxyltransferase

In contrast to the BC domain, a number of inhibitors that target the carboxyltransferase domain have been identified and characterized. Of these, haloxyfop, tepraloxydim, and pinoxaden each comprise their own herbicide class. A fourth compound, CP-640186, is a synthetic inhibitor developed by Pfizer, and was initially identified by high-throughput screening for its activities against mammalian ACCs [14, 75].
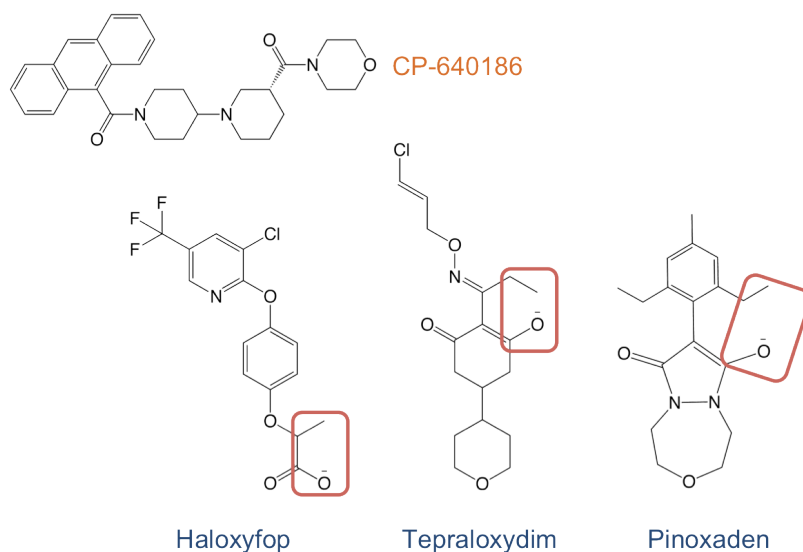
Figure 13. Small-molecule inhibitors of the carboxyltransferase domain of ACC. CP-640186 binds the dimer interface of the CT domain. For the herbicides haloxyfop, tepraloxydim, and pinoxaden, the points of CT anchoring are indicated with the red boxes.

Although the herbicides haloxyfop, tepraloxydim, and pinoxaden are widely used in commercial agriculture, and are commonly used as herbicides to target the plastid ACCs of

invasive weed species, the only available structural data are of each herbicide in complex with the CT domain of yeast ACC [75-77]. These herbicides target the CT active site by outcompeting acetyl-CoA for the substrate-binding site. Although their overall chemical structures are quite diverse, they make two similar points of contact with the CT domain. Figure 13 indicates the points of attachment to the enzyme, which is revealed to be an oxyanion hole located adjacent to a small methyl group. This conservation in the structures of the herbicides suggests that acetyl-CoA takes on a similar conformation at some point during catalysis.

1.6   Conclusion

In humans, the family of biotin-dependent carboxylases consists of five enzymes (ACC1, ACC2, PCC, MCC, and PC) with essential roles in energy metabolism and homeostasis. All five enzymes assemble as holoenzyme complexes and share a common two-part mechanism: an initial ATP-dependent carboxylation of a prosthetic biotin group, followed by the transfer of the carboxyl group to an acceptor molecule. The metabolic significance of the carboxylases is evident from the severe physiological consequences that result when there is a deficiency in the enzymatic activities of ACC1, PCC, MCC, or PC. While many disease-associated mutations have been identified for these enzymes, the absence of structural data on their holoenzymes has precluded further studies on the molecular consequences of the mutations. Before I began my dissertation research, the only holoenzyme structure of a biotin-dependent carboxylase was that of pyruvate carboxylase (PC). However, PC recognizes a structurally distinct substrate compared to ACC1/ACC2/PCC/MCC, which recognize acyl-CoA esters. Therefore, a primary goal of my graduate research was to investigate the holoenzyme assembly of an *acyl-CoA* carboxylase.

In this dissertation, I present the major findings from my research on this family of enzymes. **Chapter 2** chronicles the elucidation of the PCC crystal structure, which reveals several novel findings, including a novel domain that is essential for the holoenzyme architecture, the binding mode of BCCP-biotin to the CT active site, and the mapping of disease mutations onto the structure to predict their effects on enzymatic stability and activity. To investigate the determinants of substrate preference between PCC and MCC, I next focus on the structure of MCC, described in **Chapter 3**. From the MCC structure, I observe a surprising CT domain rearrangement compared to PCC, which is an unanticipated finding considering the high sequence identity between the two enzymes. I also observe significant differences in the overall structure of the MCC holoenzyme. The results of my dissertation work have produced the first two holoenzyme structures of CoA-recognizing biotin-dependent carboxylases, and have paved the way for further understanding of the activity of these vital enzymes.

1.7   References

1.   Streit, W.R. and Entcheva, P. *Biotin in microbes, the genes involved in its biosynthesis, its biochemical role and perspectives for biotechnological production.* Applied microbiology and biotechnology, 2003. **61**(1): p. 21-31.

2.   Bagautdinov, B., Matsuura, Y., Bagautdinova, S. and Kunishima, N. *Protein biotinylation visualized by a complex structure of biotin protein ligase with a substrate.* Journal of Biological Chemistry, 2008. **283**(21): p. 14739-50.

3.   Xiang, S. and Tong, L. *Crystal structures of human and Staphylococcus aureus pyruvate carboxylase and molecular insights into the carboxyltransfer reaction.* Nature Structural & Molecular Biology, 2008. **15**(3): p. 295-302.

4.   Jitrapakdee, S. and Wallace, J.C. *The biotin enzyme family: conserved structural motifs and domain rearrangements.* Current Protein and Peptide Science, 2003. **4**(3): p. 217-29.

5.   Knowles, J.R. *The mechanism of biotin-dependent enzymes.* Annual Review of Biochemistry, 1989. **58**(1): p. 195-221.

6.   Dimroth, P. *Sodium ion transport decarboxylases and other aspects of sodium ion cycling in bacteria.* Microbiological reviews, 1987. **51**(3): p. 320.

7.   Northrop, D.B. *Transcarboxylase VI. Kinetic analysis of the reaction mechanism.* Journal of Biological Chemistry, 1969. **244**(21): p. 5808-19.

8.   Tong, L. *Structure and function of biotin-dependent carboxylases.* Cell Mol Life Sci, 2013. **70**(5): p. 863-91.

9.   Gornicki, P. and Haselkorn, R. *Wheat acetyl-CoA carboxylase.* Plant molecular biology, 1993. **22**(3): p. 547-52.

10.   Davies, S.P., Sim, A.T.R. and Hardie, D.G. *Location and function of three sites phosphorylated on rat acetyl-CoA carboxylase by the AMP-activated protein kinase.* European Journal of Biochemistry, 1990. **187**(1): p. 183-90.

11.   Hynie, I. and Hahn, P. *Changes in the activity of acetyl CoA carboxylase in the intestinal mucosa of the rat during development.* The Journal of Nutrition, 1972. **102**(10): p. 1311-14.

12.   Mao, J., DeMayo, F.J., Li, H., Abu-Elheiga, L., Gu, Z., Shaikenov, T.E., Kordari, P., Chirala, S.S., Heird, W.C., and Wakil, S.J. *Liver-specific deletion of acetyl-CoA carboxylase 1 reduces hepatic triglyceride accumulation without affecting glucose homeostasis.* Proceedings of the National Academy of Sciences, 2006. **103**(22): p. 8552-57.

13.   Diraison, F.d.r., Yankah, V., Letexier, D., Dusserre, E., Jones, P. and Beylot, M. *Differences in the regulation of adipose tissue and liver lipogenesis by carbohydrates in humans.* Journal of lipid research, 2003. **44**(4): p. 846-53.

14.   Tong, L. and Harwood, H.J. *Acetyl-coenzyme A carboxylases: Versatile targets for drug discovery.* Journal of Cellular Biochemistry, 2006. **99**(6): p. 1476-88.

15.   Chajes, V., Cambot, M., Moreau, K., Lenoir, G.M. and Joulin, V. *Acetyl-CoA carboxylase is essential to breast cancer cell survival.* Cancer research, 2006. **66**(10): p. 5287-94.

16.   North, K.N., Korson, M.S., Gopal, Y.R., Rohr, F.J., Brazelton, T.B., Waisbren, S.E. and Warman, M.L. *Neonatal-onset propionic acidemia: neurologic and developmental*

profiles, and implications for management. The Journal of pediatrics, 1995. **126**(6): p. 916-22.

17. Thompson, G.N., Walter, J.H., Bresson, J.L., Ford, G.C., Lyonnet, S.L., Chalmers, R.A., Saudubray, J.M., Leonard, J.V., and Halliday, D. *Sources of propionate in inborn errors of propionate metabolism.* Metabolism, 1990. **39**(11): p. 1133-37.

18. Kraus, J.P., Firgaira, F., Novotn√Ω, J.ô., Kalousek, F.e., Williams, K.R., Williamson, C., Ohura, T. and Rosenberg, L.E. *Coding sequence of the precursor of the beta subunit of rat propionyl-CoA carboxylase.* Proceedings of the National Academy of Sciences, 1986. **83**(21): p. 8049-53.

19. Stadler, S.C., Polanetz, R., Meier, S., Mayerhofer, P.U., Herrmann, J.M., Anslinger, K., Roscher, A.A., R√∂schinger, W., and Holzinger, A. *Mitochondrial targeting signals and mature peptides of 3-methylcrotonyl-CoA carboxylase.* Biochemical and biophysical research communications, 2005. **334**(3): p. 939-46.

20. Wexler, I.D., Du, Y., Lisgaris, M.V., Mandal, S.K., Freytag, S.O., Yang, B.-S., Liu, T.-C., Kwon, M., Patel, M.S., and Kerr, D.S. *Primary amino acid sequence and structure of human pyruvate carboxylase.* Biochimica et Biophysica Acta (BBA)-Molecular Basis of Disease, 1994. **1227**(1): p. 46-52.

21. Russell, M.J. and Martin, W. *The rocky roots of the acetyl-CoA pathway.* Trends in biochemical sciences, 2004. **29**(7): p. 358-63.

22. Williamson, D.H., Lopes-Vieira, O. and Walker, B. *Concentrations of free glucogenic amino acids in livers of rats subjected to various metabolic stresses.* Biochemical Journal, 1967. **104**(2): p. 497.

23. Voet, D., Voet, J.G. and Pratt, C.W. *Fundamentals of Biochemistry: Life at the Molecular Level.* John Wiley & Sons, NewYork, 2006.

24. Sugden, M.C. and Holness, M.J. *Trials, tribulations and finally, a transporter: the identification of the mitochondrial pyruvate transporter.* Biochemical Journal, 2003. **374**(Pt 3): p. e1.

25. Kim, C.-W., Moon, Y.-A., Park, S.W., Cheng, D., Kwon, H.J. and Horton, J.D. *Induced polymerization of mammalian acetyl-CoA carboxylase by MIG12 provides a tertiary level of regulation of fatty acid synthesis.* Proceedings of the National Academy of Sciences, 2010. **107**(21): p. 9626-31.

26. Shen, Y., Chou, C.-Y., Chang, G.-G. and Tong, L. *Is dimerization required for the catalytic activity of bacterial biotin carboxylase?* Molecular Cell, 2006. **22**(6): p. 807-18.

27. Waldrop, G.L., Rayment, I. and Holden, H.M. *Three-dimensional structure of the biotin carboxylase subunit of acetyl-CoA carboxylase.* Biochemistry, 1994. **33**(34): p. 10249-56.

28. Murzin, A.G. *Structural classification of proteins: new superfamilies.* Current Opinion in Structural Biology, 1996. **6**(3): p. 386-94.

29. Galperin, M.Y. and Koonin, E.V. *A diverse superfamily of enzymes with ATP‚Äêdependent carboxylate‚Äîamine/thiol ligase activity.* Protein Science, 1997. **6**(12): p. 2639-43.

30. Thoden, J.B., Blanchard, C.Z., Holden, H.M. and Waldrop, G.L. *Movement of the biotin carboxylase B-domain as a result of ATP binding.* Journal of Biological Chemistry, 2000. **275**(21): p. 16183-90.

31.   Chou, C.Y., Yu, L.P. and Tong, L. *Crystal structure of biotin carboxylase in complex with substrates and implications for its catalytic mechanism.* J Biol Chem, 2009. **284**(17): p. 11690-7.

32.   Shen, Y., Volrath, S.L., Weatherly, S.C., Elich, T.D. and Tong, L. *A mechanism for the potent inhibition of eukaryotic acetyl-coenzyme A carboxylase by soraphen A, a macrocyclic polyketide natural product.* Molecular Cell, 2004. **16**(6): p. 881-91.

33.   Waldrop, G.L., Holden, H.M. and Maurice, M.S. *The enzymes of biotin dependent CO2 metabolism: What structures reveal about their reaction mechanisms.* Protein Science, 2012. **21**(11): p. 1597-619.

34.   Marchler-Bauer, A., Panchenko, A.R., Shoemaker, B.A., Thiessen, P.A., Geer, L.Y. and Bryant, S.H. *CDD: a database of conserved domain alignments with links to domain three-dimensional structure.* Nucleic Acids Research, 2002. **30**(1): p. 281-83.

35.   Zhang, H., Yang, Z., Shen, Y. and Tong, L. *Crystal structure of the carboxyltransferase domain of acetyl-coenzyme A carboxylase.* Science, 2003. **299**(5615): p. 2064-67.

36.   Holden, H.M., Benning, M.M., Haller, T. and Gerlt, J.A. *The crotonase superfamily: divergently related enzymes that catalyze different reactions involving acyl coenzyme a thioesters.* Accounts of Chemical Research, 2001. **34**(2): p. 145-57.

37.   Hamed, R.B., Batchelar, E.T., Clifton, I.J. and Schofield, C.J. *Mechanisms and structures of crotonase superfamily enzymes: How nature controls enolate and oxyanion reactivity.* Cellular and Molecular Life Sciences, 2008. **65**(16): p. 2507-27.

38.   Diacovich, L., Mitchell, D.L., Pham, H., Gago, G., Melgar, M.M., Khosla, C., Gramajo, H. and Tsai, S.C. *Crystal structure of the beta-subunit of acyl-CoA carboxylase: structure-based engineering of substrate specificity.* Biochemistry, 2004. **43**(44): p. 14027-36.

39.   Wendt, K.S., Schall, I., Huber, R., Buckel, W. and Jacob, U. *Crystal structure of the carboxyltransferase subunit of the bacterial sodium ion pump glutaconyl-coenzyme A decarboxylase.* The EMBO Journal, 2003. **22**(14): p. 3493-502.

40.   Kress, D., Br√°gel, D., Schall, I., Linder, D., Buckel, W. and Essen, L.-O. *An asymmetric model for Na+-translocating glutaconyl-CoA decarboxylases.* Journal of Biological Chemistry, 2009. **284**(41): p. 28401-09.

41.   Hall, P.R., Wang, Y.-F., Rivera-Hainaj, R.E., Zheng, X., Pustai-Carey, M., Carey, P.R. and Yee, V.C. *Transcarboxylase 12S crystal structure: hexamer assembly and substrate binding to a multienzyme core.* The EMBO Journal, 2003. **22**(10): p. 2334-47.

42.   Blanchard, C.Z. and Waldrop, G.L. *Overexpression and kinetic characterization of the carboxyltransferase component of acetyl-CoA carboxylase.* Journal of Biological Chemistry, 1998. **273**(30): p. 19140-45.

43.   Chapman-Smith, A. and Cronan Jr, J.E. *The enzymatic biotinylation of proteins: a post-translational modification of exceptional specificity.* Trends in biochemical sciences, 1999. **24**(9): p. 359-63.

44.   Schatz, P.J. *Use of peptide libraries to map the substrate specificity of a peptide-modifying enzyme: a 13 residue consensus peptide specifies biotinylation in Escherichia coli.* Nature Biotechnology, 1993. **11**(10): p. 1138-43.

45.   Reche, P., Li, Y.-L., Fuller, C., Eichhorn, K. and Perham, R.N. *Selectivity of post-translational modification in biotinylated proteins: the carboxy carrier protein of the acetyl-CoA carboxylase of Escherichia coli.* Biochemical Journal, 1998. **329**(Pt 3): p. 589.

46. León-Del-Rio, A., Leclerc, D., Akerman, B., Wakamatsu, N. and Gravel, R.A. *Isolation of a cDNA encoding human holocarboxylase synthetase by functional complementation of a biotin auxotroph of Escherichia coli.* Proceedings of the National Academy of Sciences, 1995. **92**(10): p. 4626-30.

47. Pendini, N.R., Bailey, L.M., Booker, G.W., Wilce, M.C., Wallace, J.C. and Polyak, S.W. *Microbial biotin protein ligases aid in understanding holocarboxylase synthetase deficiency.* Biochimica et Biophysica Acta (BBA)-Proteins and Proteomics, 2008. **1784**(7): p. 973-82.

48. Lee, C.-K., Cheong, C. and Jeon, Y.H. *Substrate recognition characteristics of human holocarboxylase synthetase for biotin ligation.* Biochemical and biophysical research communications, 2010. **391**(1): p. 455-60.

49. Hassan, Y.I. and Zempleni, J. *A novel, enigmatic histone modification: biotinylation of histones by holocarboxylase synthetase.* Nutrition reviews, 2008. **66**(12): p. 721-25.

50. Narang, M.A., Dumas, R., Ayer, L.M. and Gravel, R.A. *Reduced histone biotinylation in multiple carboxylase deficiency patients: a nuclear role for holocarboxylase synthetase.* Human molecular genetics, 2004. **13**(1): p. 15-23.

51. Fall, R.R. and Vagelos, P.R. *Acetyl Coenzyme A Carboxylase: Proteolytic Modification of Biotin Carboxyl Carrier Protein* Journal of Biological Chemistry, 1973. **248**(6): p. 2078-88.

52. Athappilly, F.K. and Hendrickson, W.A. *Structure of the biotinyl domain of acetyl-coenzyme A carboxylase determined by MAD phasing.* Structure, 1995. **3**(12): p. 1407-19.

53. Lee, C.Ä., Cheong, H.Ä., Ryu, K.Ä., Lee, J.I., Lee, W., Jeon, Y.H. and Cheong, C. *Biotinoyl domain of human acetyl‚ÄêCoA carboxylase: Structural insights into the carboxyl transfer mechanism.* Proteins: Structure, Function, and Bioinformatics, 2008. **72**(2): p. 613-24.

54. Healy, S., McDonald, M.K., Wu, X., Yue, W.W., Kochan, G., Oppermann, U. and Gravel, R.A. *Structural impact of human and Escherichia coli biotin carboxyl carrier proteins on biotin attachment.* Biochemistry, 2010. **49**(22): p. 4687-94.

55. Eisenberg, M.A., Prakash, O. and Hsiung, S.-C. *Purification and properties of the biotin repressor. A bifunctional protein.* Journal of Biological Chemistry, 1982. **257**(24): p. 15167-73.

56. Wilson, K.P., Shewchuk, L.M., Brennan, R.G., Otsuka, A.J. and Matthews, B.W. *Escherichia coli biotin holoenzyme synthetase/bio repressor crystal structure delineates the biotin-and DNA-binding domains.* Proceedings of the National Academy of Sciences, 1992. **89**(19): p. 9257-61.

57. Pendini, N.R., Yap, M.Y., Polyak, S.W., Cowieson, N.P., Abell, A., Booker, G.W., Wallace, J.C., Wilce, J.A., and Wilce, M.C. *Structural characterisation of Staphylococcus aureus biotin protein ligase and interaction partners: An antibiotic target.* Protein Science, 2013.

58. Perham, R.N. *Swinging arms and swinging domains in multifunctional enzymes: catalytic machines for multistep reactions.* Annual Review of Biochemistry, 2000. **69**(1): p. 961-1004.

59. Reddy, D.V., Shenoy, B.C., Carey, P.R. and S√∂nnichsen, F.D. *Absence of observable biotin-protein interactions in the 1.3 s subunit of transcarboxylase: An NMR study.* Biochemistry, 1997. **36**(48): p. 14676-82.

60. Fung, C.H., Feldmann, R.J. and Mildvan, A.S. *Proton and phosphorus-31 Fourier transform magnetic resonance studies of the conformation of enzyme-bound propionyl coenzyme A on transcarboxylase.* Biochemistry, 1976. **15**(1): p. 75-84.

61. Fung, C.H., Gupta, R.K. and Mildvan, A.S. *Magnetic resonance studies of the proximity and spatial arrangement of propionyl coenzyme A and pyruvate on a biotin-metalloenzyme, transcarboxylase.* Biochemistry, 1976. **15**(1): p. 85-92.

62. Tong, L. *Acetyl-coenzyme A carboxylase: crucial metabolic enzyme and attractive target for drug discovery.* Cell Mol Life Sci, 2005. **62**(16): p. 1784-803.

63. St. Maurice, M., Reinhardt, L., Surinya, K.H., Attwood, P.V., Wallace, J.C., Cleland, W.W. and Rayment, I. *Domain architecture of pyruvate carboxylase, a biotin-dependent multifunctional enzyme.* Science, 2007. **317**(5841): p. 1076-79.

64. Munday, M.R. and Hemingway, C.J. *The regulation of acetyl-CoA carboxylase--a potential target for the action of hypolipidemic agents.* Advances in Enzyme Regulation, 1999. **39**: p. 205.

65. Keech, B. and Barritt, G.J. *Allosteric Activation of Sheep Kidney Pyruvate Carboxylase by the Magnesium Ion (Mg2+) and the Magnesium Adenosine Triphosphate Ion (MgATP2-).* Journal of Biological Chemistry, 1967. **242**(9): p. 1983-87.

66. Abu-Elheiga, L., Oh, W., Kordari, P. and Wakil, S.J. *Acetyl-CoA carboxylase 2 mutant mice are protected against obesity and diabetes induced by high-fat/high-carbohydrate diets.* Proceedings of the National Academy of Sciences, 2003. **100**(18): p. 10207-12.

67. Harwood Jr, H.J. *Acetyl-CoA carboxylase inhibition for the treatment of metabolic syndrome.* Current opinion in investigational drugs (London, England: 2000), 2004. **5**(3): p. 283.

68. Gerth, K., Bedorf, N., Irschik, H., H√∂fle, G. and Reichenbach, H. *The soraphens: a family of novel antifungal compounds from Sorangium cellulosum (Myxobacteria). I. Soraphen A1 alpha: fermentation, isolation, biological properties.* The Journal of Antibiotics, 1994. **47**(1): p. 23.

69. Weatherly, S.C., Volrath, S.L. and Elich, T.D. *Expression and characterization of recombinant fungal acetyl-CoA carboxylase and isolation of a soraphen-binding domain.* Biochem J, 2004. **380**(Pt 1): p. 105.

70. Vahlensieck, H.F., Pridzun, L., Reichenbach, H. and Hinnen, A. *Identification of the yeast ACC1 gene product (acetyl-CoA carboxylase) as the target of the polyketide fungicide soraphen A.* Current genetics, 1994. **25**(2): p. 95-100.

71. Pridzun, L., Sasse, F. and Reichenbach, H. *Inhibition of fungal acetyl-CoA carboxylase: A novel target discovered with the myxobacterial compound soraphen.* Antifungal agents Oxford: BIOS Scientific Publishers Ltd, 1995: p. 99-109.

72. Vahlensieck, H.-F. and Hinnen, A., *Soraphen A resistant fungi and acetyl-CoA carboxylase.* 1997, Google Patents.

73. Miller, J.R., Dunham, S., Mochalkin, I., Banotai, C., Bowman, M., Buist, S., Dunkle, B., Hanna, D., Harwood, H.J., and Huband, M.D. *A class of selective antibacterials derived from a protein kinase inhibitor pharmacophore.* Proceedings of the National Academy of Sciences, 2009. **106**(6): p. 1737-42.

74. Mochalkin, I., Miller, J.R., Narasimhan, L., Thanabal, V., Erdman, P., Cox, P.B., Prasad, J.V.N.V., Lightle, S., Huband, M.D., and Stover, C.K. *Discovery of antibacterial biotin carboxylase inhibitors by virtual screening and fragment-based approaches.* ACS Chemical Biology, 2009. **4**(6): p. 473-83.

75. Zhang, H., Tweel, B., Li, J. and Tong, L. *Crystal structure of the carboxyltransferase domain of acetyl-coenzyme A carboxylase in complex with CP-640186.* Structure, 2004. **12**(9): p. 1683-91.

76. Xiang, S., Callaghan, M.M., Watson, K.G. and Tong, L. *A different mechanism for the inhibition of the carboxyltransferase domain of acetyl-coenzyme A carboxylase by tepraloxydim.* Proceedings of the National Academy of Sciences, 2009. **106**(49): p. 20723-27.

77. Linda, P.C., Kim, Y.S. and Tong, L. *Mechanism for the inhibition of the carboxyltransferase domain of acetyl-coenzyme A carboxylase by pinoxaden.* Proceedings of the National Academy of Sciences, 2010. **107**(51): p. 22072-77.

Chapter II

Structural and biochemical studies of propionyl-CoA carboxylase

Propionyl-CoA carboxylase (PCC; EC 6.4.1.3) is a member of the biotin-dependent carboxylase family and its activities are essential for metabolizing odd-carbon fatty acids, cholesterol, and several amino acids. PCC is highly conserved from bacteria to humans, and exists as a 750-kDa $\alpha_6\beta_6$ holoenzyme in the mitochondrial matrix of animals. Its importance for human health is evident: over a hundred genetic mutations in human PCC have been linked to propionic acidemia, which is an inherited disorder characterized by acute metabolic deficits. Although an abundance of clinical and functional data exists for PCC, along with a small number of structural studies on its constituent domains, there was no published data on the holoenzyme of any PCC prior to our investigations. In order to understand how PCC works, and to gain insight on the functions of other biotin-dependent carboxylases, we set our sights on obtaining a high-resolution structure of the PCC holoenzyme, with additional structural and functional characterizations to investigate its mechanistic details. A retrospective survey of highlights in PCC research is presented first, followed by the details of our achievements in understanding the architecture of this vital macromolecule, as well as a discussion of ongoing questions in the field.

2.1   Introduction to PCC

PCC was first identified in 1957, when the carboxylation of propionyl-CoA to methylmalonyl-CoA in porcine heart extracts was found to be an ATP-dependent process [1, 2]. In particular, two reactions could be catalyzed with the crude enzyme preparation:

$$\text{ATP} + \text{fluoride} \rightarrow \text{ADP} + \text{fluorophosphate} \qquad (1)$$
$$\text{ATP} + \text{CO}_2 + \text{propionyl-CoA} \leftrightarrows \text{ADP} + \text{P}_i + \text{methylmalonyl-CoA} \qquad (2)$$
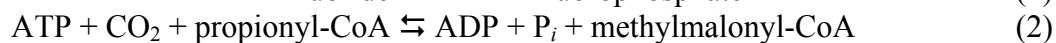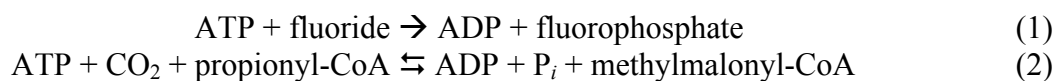
Reaction (2) is the net reaction catalyzed by PCC. However, by recognizing that this enzyme could independently coordinate the removal of orthophosphate from ATP even in the absence of propionyl-CoA [3], Tietz *et al.* identified a hallmark of PCC – its dual catalytic activities housed within a single enzyme – that continues to be studied to this day.

PCC is an essential human enzyme for a number of metabolic transformations. It is directly involved in the catabolism of cholesterol, valine, threonine, isoleucine, and methionine, as well as certain fatty acids. Of all the nutrient groups that are essential for a balanced diet, dietary fats rank the highest in caloric content and contribute significantly to the body's energy reserves. The breakdown of fatty acids involves rounds of β-oxidation for the iterative removal of two-carbon acetyl-CoA units; if the fatty acid contains an odd number of carbon atoms, the oxidation terminates in a three-carbon compound, propionyl-CoA.
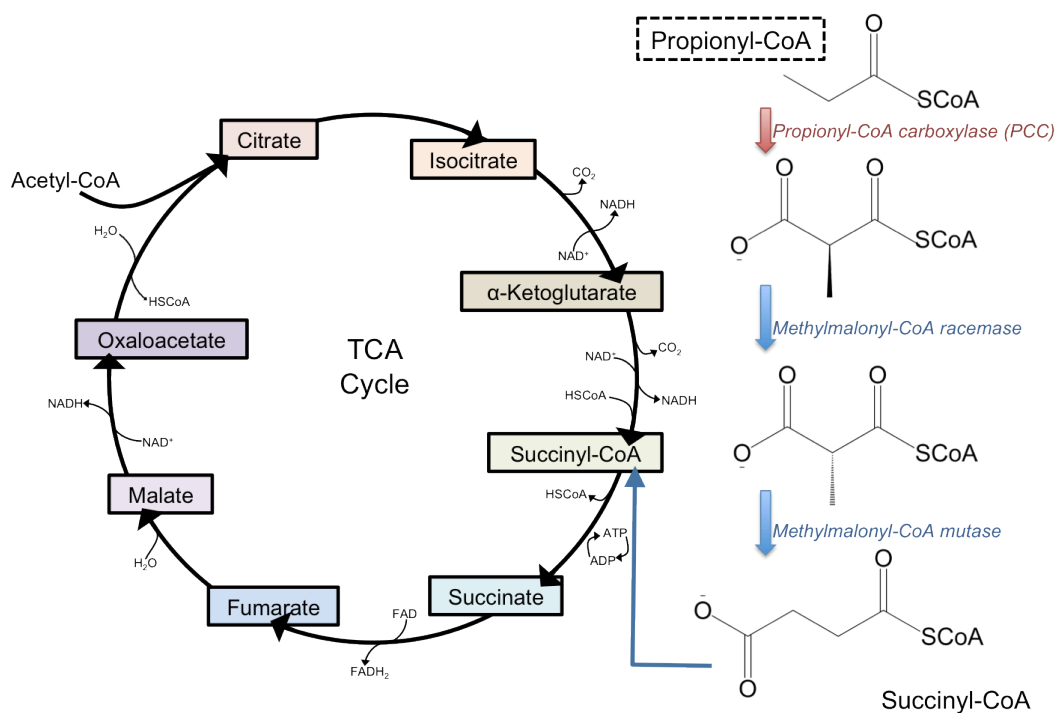
Figure 1. Propionyl-CoA can be fully oxidized to CO_2 through the TCA cycle. The reactions linking PCC activity to the TCA cycle are shown on the right. Following PCC activity, the methylmalonyl-CoA product undergoes racemization and epimerization before transforming into

succinyl-CoA, which is a TCA cycle intermediate. These reactions occur within the mitochondrial matrix.

In healthy individuals, PCC carboxylates the α-carbon of propionyl-CoA to produce D-methylmalonyl-CoA, which undergoes additional epimerization and rearrangement to yield succinyl-CoA for entry into the citric acid cycle (Figure 1). Alternatively, succinyl-CoA can combine with glycine to form δ-aminolevulinic acid, which represents the first committed step for porphyrin (heme) biosynthesis [4]. In individuals with propionic acidemia, a deficiency in PCC activity excludes propionyl-CoA from its usual metabolic fates. Instead, propionyl-CoA is converted to propionic acid and methylcitrate, and their buildup in the bloodstream can lead to the dangerous lowering of blood pH (acidemia) and inhibition of the citric acid cycle, respectively [5, 6]. Additional symptoms may also develop from the accumulation of these toxic metabolites throughout the body. A detailed overview of propionic acidemia, along with its incidence rates, pathophysiology, and current treatment options, will be discussed later.

PCC is classified within the family of biotin-dependent carboxylases, and in humans there are four additional members: two isoforms of acetyl-CoA carboxylase (ACC1 and ACC2), methylcrotonyl-CoA carboxylase (MCC), and pyruvate carboxylase (PC). All five enzymes assemble as holoenzymes, are highly conserved among living organisms, and there is significant structural homology between their functional domains as well. Figure 1 is a schematic representation of the conserved domain structures shared between members of the biotin-dependent carboxylases.
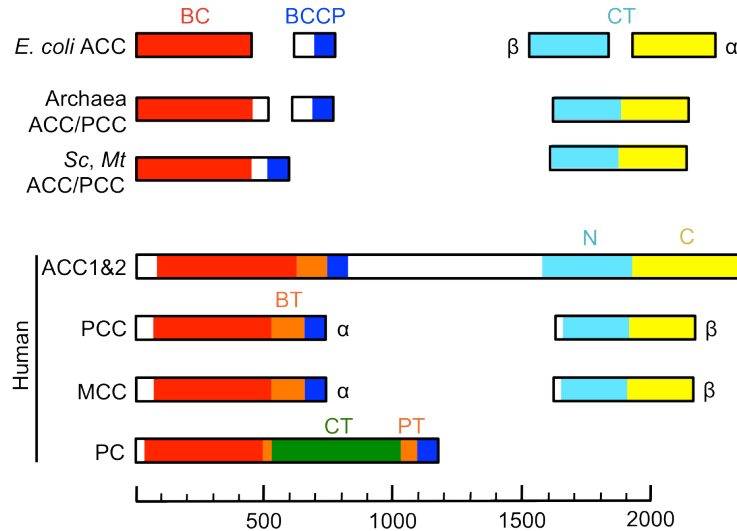
Figure 2. Conserved domains of biotin-dependent carboxylases from bacteria to humans.
Colors are assigned based on sequence homology. The CT domain of PC is structurally distinct, and is colored accordingly. The same domains are present in each enzyme, although the method of assembly presumably varies among different enzymes, forming the basis for structural diversity. The scale bar indicates the number of amino acids. Adapted from [7].

There are three conserved domains found in all family members: the biotin carboxylase (BC) and carboxyltransferase (CT) domains, which mediate catalysis; and the biotin carboxyl carrier protein (BCCP), which employs a prosthetic biotin group to 'shuttle' reaction intermediates between BC and CT. In humans, the BC and BCCP domains are encoded on the *PCCA* gene, and the CT domain is encoded on the *PCCB* gene. PCCα and PCCβ are expressed as separate polypeptide chains, and are targeted to the mitochondria by means of their amino-terminal targeting sequences, which are cleavable localization signals that hone in on the organelles' membrane potential differences [8]. Interestingly, studies in rats have suggested that biotinylation of the BCCP domain may not take place until after PCCα is imported into the mitochondrial matrix [9, 10].

In addition, there are many similarities between the BC, CT, and BCCP domains of different biotin-dependent carboxylases; in spite of this, each enzyme maintains a distinct preference for its particular carboxylation target. These properties, along with the direct

relevance of biotin-dependent carboxylases for human health, have served as major incentives for the structural studies of these enzymes, with PCC as a prime candidate.

From a structural perspective, PCC is a challenging target, due to its size and complexity. A simplified approach is to first obtain high-resolution structures of the individual domains, followed by modeling the structures into low-resolution electron density maps of the holoenzymes. The domain structures would be important accomplishments in their own right, as they are highly conserved between the different carboxylases, contain the catalytic centers, and also serve as targets of enzymatic inhibitors and regulators. The crystal structures of BC, BCCP, and CT from *E. coli* are shown in Figure 2.
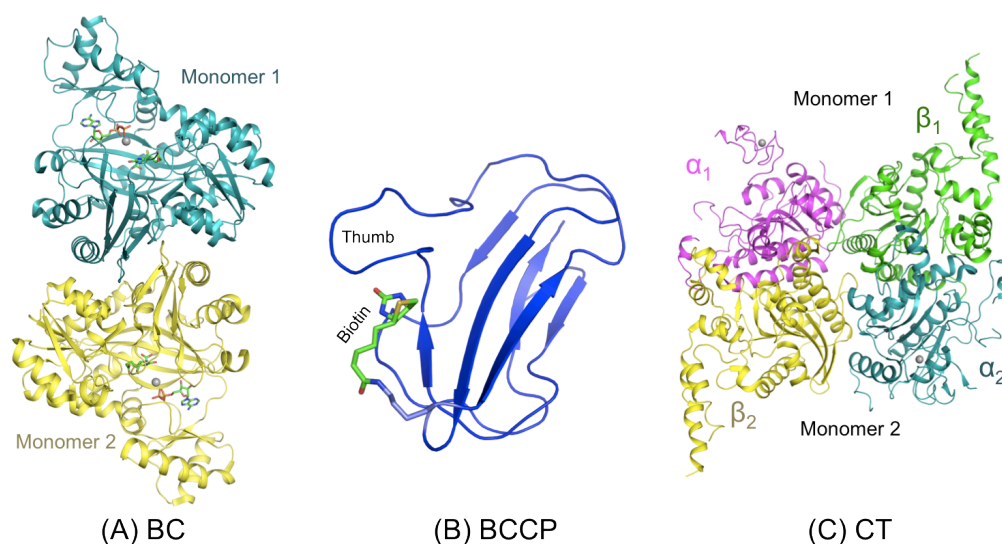
(A) BC   (B) BCCP   (C) CT

Figure 3. Crystal structures of biotin carboxylase (BC), biotin carboxyl carrier protein (BCCP), and carboxyltransferase (CT) from *E. coli* ACC. (A) BC is a dimer, with ADP, biotin, HCO_3^-, and Mg^{2+} bound in the active site of each monomer [11]. (B) BCCP is biotinylated at a conserved Lys. The thumb feature is absent in human ACC [12]. (C) CT is a dimer of two stacked monomers, and the CT active sites are located at the monomer interface [13]. The sequence identities between these structures and their HsPCC homologs are (L-R): 49%, 36%, and 27%.

The structural details will not be addressed here, but a brief review of the major architectural features will facilitate subsequent discussions. *E. coli* biotin carboxylase is a 98-kDa dimer, with each monomer's active site situated 25 Å away from the dimer interface. Upon

ATP binding, the distal ends of the BC domain change conformation to form a 'lid' over the active site [14]. The structure of *E. coli* BCCP (9 kDa, truncated form) was determined to be a 'capped' beta sandwich, with the biotinylated lysine located at the end of a hairpin loop connecting symmetric halves of the molecule [12]. The structure of *E. coli* CT (72 kDa) contains two stacked monomers. Each monomer comprises two subunits (α and β), which are equivalent to the N and C sub-domains in eukaryotic CT. The CT active site is located at the stacking interface, in a deep groove formed by α subunit from one monomer, and the β subunit from another protomer. Therefore, CT <u>must</u> assemble as a $\alpha_2\beta_2$ heterotetramer.

The hallmark mechanism of PCC and other biotin-carboxylases involves the BC and CT domains, and a mobile entity for shuttling biotin/carboxybiotin between their active sites. The original model for communication between the active sites involved a biotin 'swinging-arm' [15]. However, the crystal structures of pyruvate carboxylase (PC) revealed that the distance between BC and CT active sites was beyond the reach of biotin, even in its fully-extended conformation [16, 17]. Instead, the entire BCCP-biotin complex was proposed to translocate between BC and CT, in what is now termed the 'swinging-domain' model (Figure 10, Chapter I).

In the absence of a PCC holoenzyme structure, it is unclear whether PCC adopts the swinging-arm or swinging-domain model. The CT domain of PC is distinct from the other carboxylases, in that they primarily target acyl-CoA substrates, while pyruvate is a much smaller organic molecule. In addition, the primary sequences of the CT domains of PC and acyl-CoA carboxylases are very different. Therefore, efforts toward obtaining a crystal structure of a biotin-dependent *acyl-CoA* carboxylase, such as PCC, were necessary to understand the function of this family of enzymes.

The stoichiometry of the PCC holoenzyme was predicted to be an $\alpha_6\beta_6$ dodecamer as early as 1982 [18], but the exact arrangement of α and β subunits was not known. In 2004, the first crystal structure of PCCβ was determined to be a hexameric ring, which bore a surprising resemblance to the 12S transcarboxylase structure solved the year earlier. In 2005, the structure of *Mycobacterium tuberculosis* AccD5 was also solved and was found to be highly similar to the previous two structures. The crystal structures of all three enzymes are shown in Figure 4.
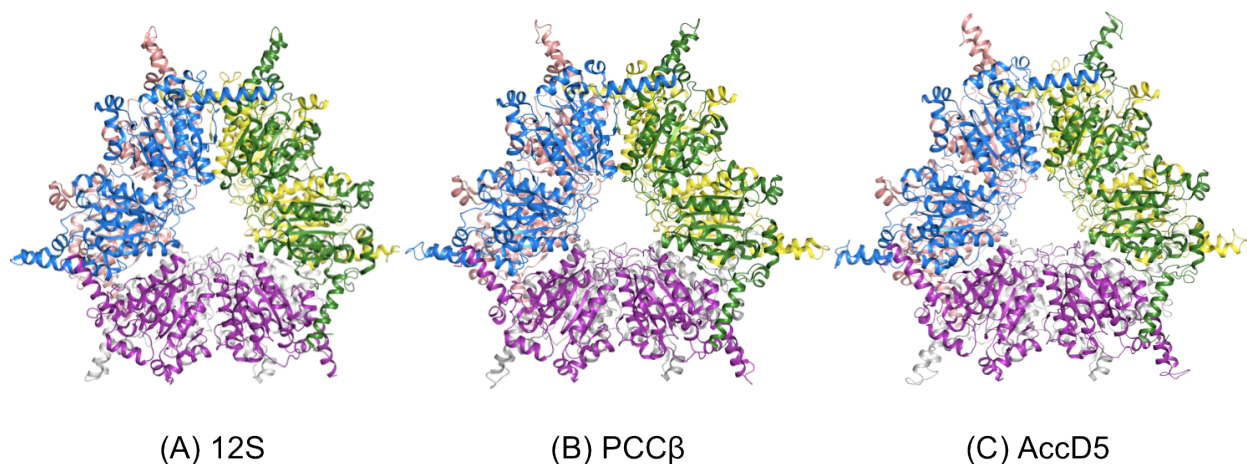
(A) 12S   (B) PCCβ   (C) AccD5

Figure 4. Crystal structures of the acyl-CoA-recognizing subunits of (a) *P. shermanii* transcarboxylase 12S [19], (b) *S. coelicolor* PCCβ [20], and (c) *M. tuberculosis* AccD5 [21]. The subunits assemble into a hexamer, and the structures are viewed from the top of each hexamer. Each protomer is colored separately.

The structures of transcarboxylase 12S, PCCβ, and AccD5 are hexameric rings with 32 symmetry. Each hexamer is a trimeric assembly of dimers, and the dimer is the basic functional unit for catalysis because the active sites are formed at the interface of two protomers. The extensive interactions between protomers help to maintain the structural integrity of the hexamer, and also lend the possibility of cooperativity during catalysis. Although there has been evidence for synergism between the dual active sites of *E. coli* CT (which assembles as an $\alpha_2\beta_2$ dimer) [22], the existence of long-range communication throughout a hexamer has yet to be demonstrated. In addition, because the overall structures of the hexamers are very similar, it is

likely that discrimination between specific acyl-CoA carboxylases is limited to a small region within each hexamer. Therefore, it is possible to observe the binding modes of the various CT substrates and establish a model for substrate selectivity in PCC as well as for the other biotin-dependent carboxylases.

The existence of multifunctional ACC/PCCs with specificity for both acetyl- and propionyl-CoA has been observed for a number of archaeal species, including *Metallosphaera sedula* and *Acidianus brierleyi* [23, 24]. However, the majority of ACCs and PCCs exhibit a clear preference for one substrate. The structure of *S. coelicolor* PCCβ (Figure 4B) was elucidated as a 400-kDa protein complex with bound biotin and propionyl-CoA. By investigating the protein-ligand contacts in the active site binding pocket, Diacovich *et al.* identified a residue (Asp422) whose mutation to Ile converted the specificity of the holoenzyme from propionyl-CoA to acetyl-CoA [20]. This Asp residue appears to be conserved in a number of other PCCs, and its proposed identity as a 'molecular switch' holds the potential for understanding PCC substrate recognition, and possibly for modifying PCC function as well. An obvious implication of the latter is the prospect of restoring PCC function in individuals with deficient PCC activity (propionic acidemia).

PCC is a robust enzyme, and its activity is augmented in the presence of certain activators, including several monovalent cations (NH_4^+, K^+, Cs^+) [25]. While none of these cations are absolutely required for enzyme function, the addition of 8 mM K^+ to porcine heart PCC resulted a 25-fold stimulation in its activity [26]. NH_4^+ and Cs^+ were also found to activate PCC, although to a lesser extent than K^+. The PCC from bovine liver is also activated by K^+, and K^+ may increase the affinity of the enzyme for its substrates. To this end, Georgio *et al.* obtained fluorescence data suggesting that K^+ triggers the closed conformation of biotin carboxylase in

order to bind ADP and initiate catalysis [25]. Potassium may also function as a regulator of PCC activity within cells, due to the correlation between increasing potassium concentration and increased catalytic activity. In the absence of a PCC holoenzyme structure, however, it is difficult to ascertain how potassium interacts with PCC and stimulates its function.

PCC is a crucial enzyme, and PCC$\alpha^{-/-}$ mice die within 36 hours of birth [27]. In humans, propionic acidemia (PA) is an autosomal recessive disorder characterized by the buildup of unprocessed PCC substrates and byproducts, including ketone bodies, ammonia, and propionic acid. If unchecked, the accumulation of toxic metabolites eventually leads to developmental delays, acute and/or chronic neurological deficits, and severe immune deficiencies [28, 29]. There is currently no cure for PA, but symptoms and relapses may be controlled by a strict adherence to a low-protein diet, carnitine supplementation, and metronidazole administration to control the amount of propionic acid produced by intestinal flora [30]. Although there are over a hundred documented mutations within PCC that have been linked to cases of PA, the consequences of these mutations on the structure and function of the enzyme are not clearly defined. In addition, PA spans a wide range of phenotypes, from acute symptoms at birth to late-onset presentations in adults. In the United States, the incidence rate of propionic acidemia is 1 per 35,000 live births, and the disease typically exhibits a progressive pathology. The long-term survival rate for patients exhibiting early-onset PA is 67% [31], which testifies to the importance of PCC research for understanding this disease.

Propionyl-CoA carboxylase is an essential metabolic enzyme with obvious implications for human health, but studies regarding its structure and biochemistry have been limited. A comprehensive knowledge of its activities would also have immense relevance for other members of the biotin-dependent carboxylase family. The absence of a PCC holoenzyme

structure has precluded further studies of the interactions between BC and CT, particularly those governing their association, the basis for biotin (or BCCP-biotin) translocation, the overall catalytic mechanism, and the consequences of gene mutations associated with propionic acidemia. These questions represent the bridging features in our understanding of PCC activity and set the stage for our investigations of the PCC holoenzyme, in hopes of understanding its structure, function, and role in maintaining metabolic vitality.

2.2   Experimental Procedures

Protein purification and mutagenesis

Genomic DNA for *Ruegeria pomeroyi* and *Roseobacter denitrificans* was obtained from ATCC and the full-length PCCs were cloned as bicistronic expression constructs featuring N-terminal hexa-histidine tags in pET-28a (Novagen). To generate the *R. pomeroyi* + *R. denitrificans* chimera (RpαRdβ), the α subunit from *R. pomeroyi* PCC (RpPCCα) was subcloned in place of the α subunit within the *R. denitrificans* PCC (RdPCC) construct, yielding a final sequence of RBS-(His)$_6$-[RdPCCβ]-RBS-[RpPCCα]. Human PCC was similarly prepared, using a cDNA source. "RBS" indicates a ribosomal binding site. The PCCs were over-expressed in *E. coli* BL21 Star (DE3) cells (Invitrogen) in LB media + 1 mM IPTG, supplemented with 20 mg/L biotin, and expressed at 20°C overnight. The resulting cell paste was resuspended in Lysis Buffer (20 mM Tris-HCl (pH 7.5), 250 mM NaCl, 5% (v/v) glycerol, 0.1% (v/v) Triton X-100, and 5 mM dithiothreitol (DTT)) and lysed by sonication. The clarified lysate was incubated with Ni-NTA agarose beads (Qiagen) at 4°C, and the beads were washed with Wash Buffer (20 mM Tris-HCl (pH 7.5), 250 mM NaCl, 10 mM imidazole, and 10 mM β-mercaptoethanol). The eluent was collected in Elution Buffer (Wash Buffer + 250 mM imidazole) and injected onto a Sephacryl S-

300 size-exclusion column (GE Healthcare). The purified protein was concentrated to 15 mg/mL and flash-frozen with liquid nitrogen in Storage Buffer (20 mM Tris-HCl (pH 7.5), 250 mM NaCl, 5 mM DTT, and 5% (v/v) glycerol). Protein samples were stored at -80°C and thawed on ice for subsequent experiments. Biotinylation of the α subunit was confirmed using an avidin gel-shift assay. The N-terminal hexahistidine tags were not removed for crystallization.

All mutants were generated with the QuikChange kit (Agilent) and were sequenced to confirm the presence of mutations. The expression and purification schemes for the mutants were the same as those described for the wild-type enzymes.

Kinetic studies of PCC

The catalytic activity of PCC was measured using a coupled enzyme assay, which links the consumption of ATP by the BC domain to the disappearance of NADH [32]. The reaction buffer contained 100 mM HEPES-KOH (pH 8.0), 0.5 mM ATP, 8 mM MgCl$_2$, 40 mM KHCO$_3$, 0.5 mM propionyl-CoA or acetyl-CoA, 0.2 mM NADH, 0.5 mM phosphoenolpyruvate, 7 U lactate dehydrogenase, 4.2 U pyruvate kinase, and 200 mM KCl. All reagents were obtained from Sigma. The reaction was initiated by adding 2 μg of protein (at 15 mg/mL) to 100 μL of reaction buffer, and the progress was monitored by tracking the absorbance at 340 nm for 5 min.

Crystallization of the PCC holoenzymes

Initial crystallization conditions were identified using commercial sparse-matrix and grid screens (Emerald BioSystems, Hampton Research, Qiagen). Crystals were produced using the microbatch method under paraffin oil (Hampton Research), in a 1:1 drop ratio of protein to precipitant solution. Crystals were cryoprotected via immersion in the precipitant solution

supplemented with glycerol, for a final PEG + glycerol concentration of 35%, and were flash-frozen in liquid nitrogen prior to data collection.

Crystals of the RpαRdβ chimera: the protein samples were at 15 mg/mL and the precipitant solution contained 0.1 M HEPES-KOH (pH 8.0), 0.2 M NaCl, 21% (w/v) PEG-3350, and 16% (v/v) glycerol. After 2 weeks at 4°C, box-shaped crystals of 0.6 mm in length were observed, but most exhibited weak X-ray diffraction.

Crystals of RpPCC: the protein samples were concentrated to 15 mg/mL and the precipitant solution contained 0.2 M succinic acid (pH 6.5), 22% (w/v) PEG-3000, and 2.2% (w/v) benzamidine-HCl. After 5 days at 20°C, small prismatic crystals of 0.25 mm in length appeared. The majority of these crystals also exhibited weak X-ray diffraction, and extensive screening was required to identify crystals suitable for data collection.

Data collection and structure determination

X-ray diffraction data for the chimeric RpαRdβ and RpPCC were collected at 100 K, at the X29A beamline of the National Synchrotron Light Source (NSLS) at Brookhaven National Laboratory. All diffraction images were processed and scaled with *HKL*-2000 [33].

For the RpαRdβ chimera, an X-ray diffraction data set was collected at 3.2-Å resolution, and the crystal belonged to space group $P1$, with cell parameters of $a = 133.9$ Å, $b = 159.2$ Å, $c = 153.7$ Å, $\alpha = 113.9°$, $\beta = 101.0°$, and $\gamma = 109.0°$. The asymmetric unit (and the unit cell) contained a single $\alpha_6\beta_6$ dodecamer. The structure was solved with the molecular replacement program Phaser, using the following as search models: the BC subunit of *E. coli* ACC [11], the CT subunit of *S. coelicolor* ACC [20], and the BCCP domain of *S. aureus* PC [17]. The atomic model was built into the electron density map using O [34], and the structure was refined using CNS [35, 36] and deposited into the Protein Data Bank (accession code: 3N6R).

For RpPCC, an X-ray diffraction data set was collected at 3.2-Å resolution, and the crystal belonged to space group $P3$, with cell parameters of $a = b = 246.3$ Å and $c = 133.5$ Å. Each asymmetric unit contained one $\alpha_2\beta_2$ unit, positioned alongside the crystallographic threefold axis. The crystal exhibited merohedral twinning (twinning fraction of 0.49). The structure was solved with the molecular replacement program COMO [37], using the BC subunit of *E. coli* ACC [11] and the CT subunit of *S. coelicolor* ACC [20] as search models. Twin refinement was executed using CNS. The crystallographic information is summarized in Table 1.

Table 1. *Crystallographic data and refinement statistics*

	RpαRdβ chimera	**RpPCC**
Crystal data		
Space group	*P*1	*P*3
Unit cell dimensions	*a*=133.9Å, *b*=159.2Å, *c*=153.7 Å, α=113.9°, β=101.0°, γ=109.0°	*a*=*b*=246.3 Å, *c*=133.5 Å, α=β=90°, γ=120°
Diffraction data[a]		
Wavelength (Å)	1.075 Å	1.075 Å
Resolution range (Å)	30–3.2	30–3.3
Redundancy	1.9 (1.7)	2.8 (2.0)
Completeness (%)	92 (80)	95 (87)
$<I/\sigma I>$	8.7 (2.0)	7.7 (1.7)
R_{merge} (%)	8.4 (34.2)	10.6 (39.6)
Structure refinement		
No. of reflections used	155,003	125,474
R_{work} / R_{free}[b] (%)	21.2/24.5 (31.9/34.0)	17.0/24.4 (24.9/33.5)
RMSD bond lengths (Å)	0.012	0.010
RMSD bond angles (°)	1.6	1.4

[a]Values in parentheses refer to the highest-resolution shell.
[b]R_{free} = free R factor, based on a random sample of 5% of reflections.

Electron microscopy (EM) studies

All EM studies were performed by our collaborators in the laboratory of Dr. Z. Hong Zhou at the University of California, Los Angeles. Samples of purified *H. sapiens* PCC were diluted to 70 μg/mL in PBS prior to use. For negative stain experiments, 3 μL of diluted sample

was spotted onto a carbon-film-coated, glow-discharged, 300-mesh copper grid, and excess sample was blotted away after 1 min. The sample was twice stained using 2.5% uranyl acetate and air-dried. For cryo-EM experiments, frozen hydrated particles of HsPCC were suspended across Quantifoil carbon grids by plunge-freezing after dilution. Cryo-EM experiments were performed using a JEOL 1200EX electron microscope, and images were recorded on Kodak SO163 films at 50,000X magnification and digitized using a step size of 14 μm/pixel, corresponding to 2.8 Å/pixel on the sample. All EM images were produced with Chimera [38].

2.3   Preliminary studies on PCC

PCC has been a long-sought target in our laboratory. In 2003, the first studies of the α and β subunits from human PCC (HsPCC) were conducted by Yang Shen, a graduate student and subsequent postdoctoral fellow in the lab. Although the α subunit formed an aggregate upon large-scale purification, the β subunit was purified and yielded good-quality crystals that diffracted to 2.4-Å resolution. The structure of HsPCCβ was determined to be a hexamer (not shown), and is very similar to the hexamers shown in Figure 4. In order to investigate the workings of a full-length PCC, structural studies of the human holoenzyme were also pursued. HsPCC was purified to homogeneity and produced crystals that diffracted to 5.5-Å resolution (space group $R3$), but the crystals exhibited near-perfect twinning and could not be improved. Additional efforts to produce a high-resolution holoenzyme structure through truncation mutants and two-species hybrids were not successful.

I assumed responsibility for the PCC project in Spring 2008, and began my investigations by screening through a collection of bacterial PCCs with high sequence identity to the human enzyme. This approach was taken with the assumption that proteins possessing

similar primary sequences are also likely to exhibit similar three-dimensional structures. Each

holoenzyme was generated as a bicistronic expression construct, which places tandem coding

sequences under the control of a single promoter (Figure 5). Although the choice of an N- or C-

terminal histidine tag was arbitrary, it was essential that only one subunit (either PCCα or PCCβ)

carried the tag in the final construct. This modified pull-down approach ensured that the 750-kDa

holoenzyme could be separated from its subunits using nickel-affinity and size-exclusion

chromatography.
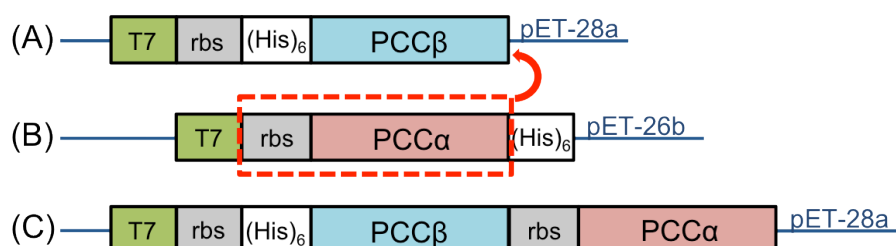
Figure 5. Synthesis of the bicistronic expression construct used to express PCC holoenzymes. (A, B) PCC subunits were individually screened for protein overexpression and solubility. (C) PCC holoenzymes were produced by subcloning the PCCα gene and its upstream ribosomal binding site into the PCCβ expression plasmid. Although PCCα is not tagged in the final construct, the formation of the holoenzyme allows the entire complex to be purified using the PCCβ tag, then separated from the PCCβ hexamer based on size.

The best candidate from this screen of bacterial PCCs was isolated from *Ruegeria*

pomeroyi, a Gram-negative soil bacterium whose PCC shares 60% sequence identity with its

human homolog. RpPCC was purified and produced small prismatic crystals (Figure 6B) that

diffracted to 3.3-Å resolution after extensive screening, which was a significant improvement

over the HsPCC crystals. Although the RpPCC crystals also exhibited perfect twinning (space

group *P*3), the diffraction data were of significantly high resolution to determine the locations of

the BC and CT domains by molecular replacement and produce a model of the PCC holoenzyme.

The structure of RpPCC features the same hexameric arrangement of PCCβ subunits that

was observed in *S. coelicolor* (Figure 4B). Unexpectedly, the BC subunits are situated on the

periphery of the hexamer, with three subunits above the hexameric ring and another three subunits below, thereby forming an $\alpha_3\beta_3\beta_3\alpha_3$ dodecamer complex. As a result, the α subunits are responsible for mediating the packing of RpPCC molecules within the crystal, and presumably, are the cause of the twinning problem.

With the intent of altering the crystal packing, several PCC chimeras were generated by combining α and β subunits from different bacterial species. One particular construct paired the α subunit from *R. pomeroyi* with the β subunit from *Roseobacter denitrificans*, a marine bacterium whose PCCβ subunit shares 88% sequence identity with RpPCCβ. This chimeric PCC was purified and produced block-shaped crystals (Figure 6C).
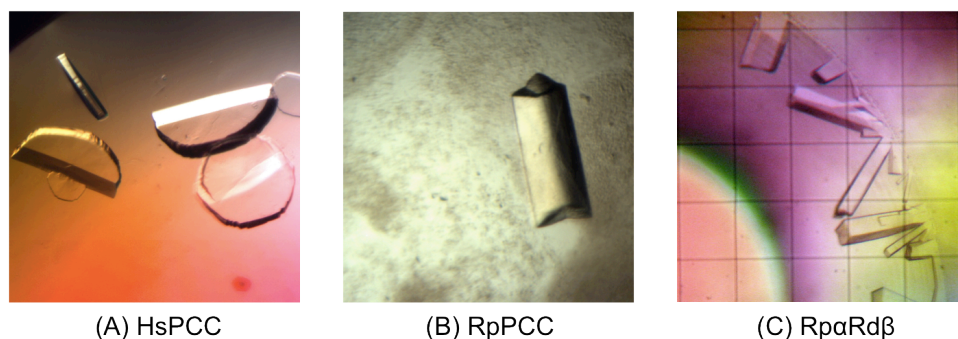
(A) HsPCC (B) RpPCC (C) RpαRdβ

Figure 6. Crystals of PCC holoenzymes from *H. sapiens*, *R. pomeroyi*, and a *R. pomeroyi/R. denitrificans* chimera. Crystallization conditions are detailed in the Experimental Procedures. HsPCC crystals were obtained from a modified coexpression construct that omitted 15 residues from the N-terminus of HsPCCβ, while the bacterial crystals contain their respective full-length PCCs. The crystals of HsPCC were obtained by Yang Shen.

After screening through several hundred candidates, a single crystal produced an X-ray diffraction data set that extended to 3.2-Å resolution. Most importantly, the crystal was not twinned (space group *P*1), and the structure was solved by molecular replacement. The search models consisted of the BC subunit from *E. coli* ACC, the BCCP domain of *S. aureus* pyruvate carboxylase, and the CT subunit from *S. coelicolor* ACC.

This PCC is hereafter referred to as the RpαRdβ chimera, and will serve as the subject of subsequent discussions.

2.4   Structure of the 750-kDa holoenzyme of propionyl-CoA carboxylase

The structure of the RpαRdβ PCC holoenzyme is roughly cylindrical (Figure 7). The β_6 hexamer forms the central core and is composed of two layers, each with three β protomers. This hexamer is very similar to the hexamer structure observed for ScPCCβ (Figure 4B). The six α subunits are monomeric, and are spaced 120° apart on the top and bottom faces of the β_6 hexamer, for a total of three α subunits per face, and the overall structure possesses 32 symmetry.

Although the chimera's bacterial subunits were selected for their similarity to the human PCC enzyme, the extent of their structural similarity was not known based on the sequence comparison alone. In order to address this potential disparity, the laboratory of Z. Hong Zhou (UCLA) succeeded in producing a cryo-electron microscopy (cryo-EM) reconstruction of human PCC at 15-Å resolution, and the resulting model is in excellent agreement with the crystal structure of the chimeric PCC (Figures 7C, 7D). The most significant difference between the two structures is a minor shift in the position of the BCCP domain (Figure 7D). In addition to demonstrating that the structure of HsPCC is highly similar to that of RpαRdβ, the cryo-EM reconstruction also indicates that the PCC holoenzyme maintains the same overall conformation in both the solution state and within the protein crystal.
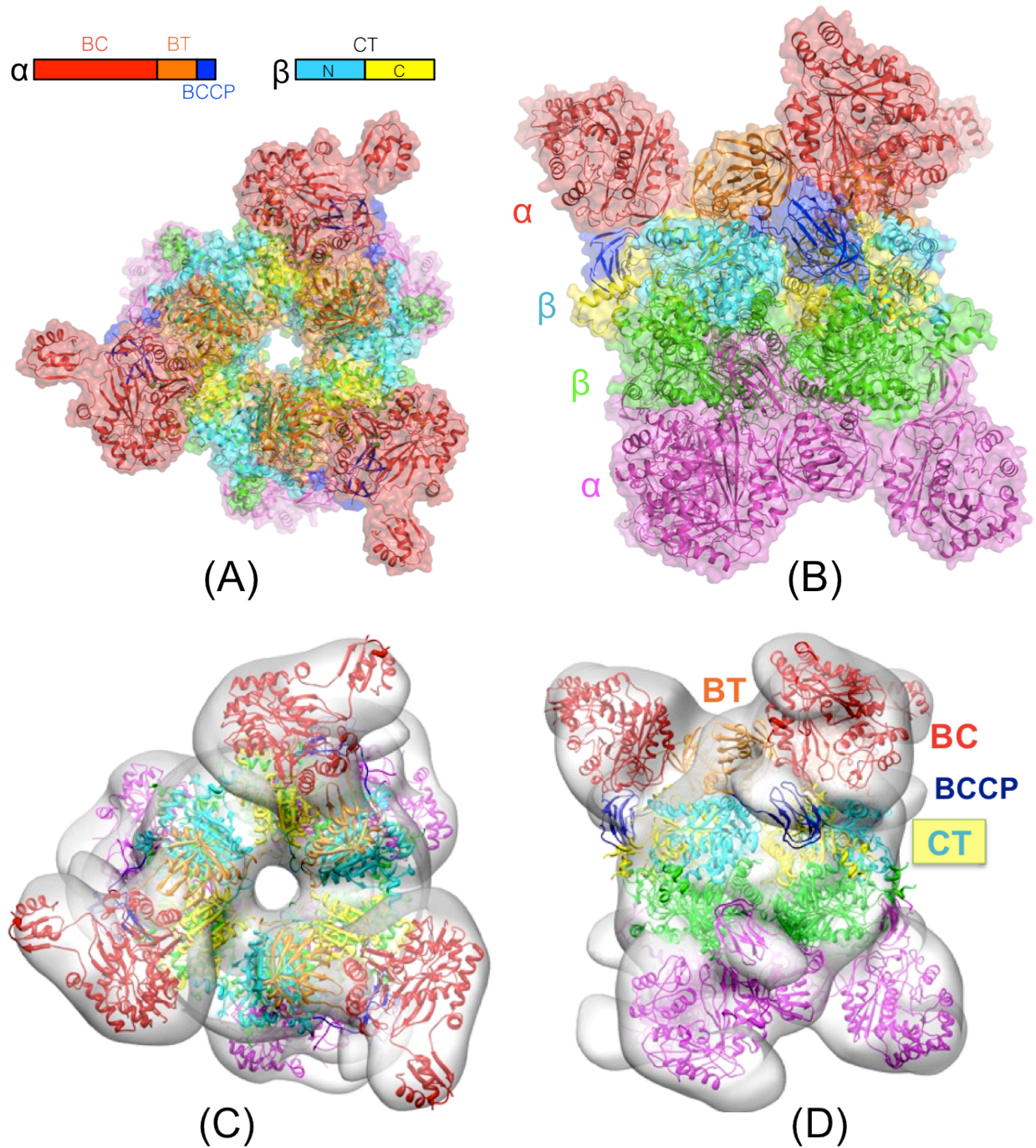
Figure 7. Structure of the PCC holoenzyme [39]. (A) Looking down the threefold symmetry axis of the RpαRdβ chimera of propionyl-CoA carboxylase (PDB code 3N6R). (B) Looking down the twofold symmetry axis. The gray envelopes in (C) and (D) are cryo-EM reconstructions of human PCC at 15-Å resolution with the crystal structure of the RpαRdβ chimera docked into the envelopes, and are viewed in the same orientations as (A) and (B). The crystal structure figures were produced with PyMOL [40], and the cryo-EM figures were generated with Chimera [38].

A primary incentive for obtaining the PCC holoenzyme structure was the possibility of elucidating a decades-old mystery: the connectivity between the BC and CT catalytic domains, and how BCCP mediates catalysis in this 750-kDa holoenzyme. The issue of connectivity is addressed first.

When contemplating the potential domain connections within the PCC holoenzyme, it is plausible to assume that the interaction between the α and β subunits is mediated by the BC and CT domains. Both domains are large and well conserved, and possess ample surface area on which to form inter-domain contacts. However, a close inspection of the RpαRdβ holoenzyme structure reveals that the BC domain actually hovers over the edge of the β_6 hexamer (Figure 7A), and there is very little interaction with the CT domains. Instead, the majority of the α-β subunit interactions are mediated by a new domain, which is colored in orange. As a result of its coordinating the interactions between the **B**C and C**T** domains, this novel domain has been designated the 'BT' domain.

2.4.1 Identification of a novel domain: the BT domain

Prior to the discovery of the BT domain within the PCC holoenzyme structure, its position within the primary sequence of PCCα was considered to be little more than a placeholder between two conserved domains. This 'placeholder' was assumed to be a somewhat flexible linker joining BC and BCCP, and not much attention was paid to it. After all, the BC and CT domains contained the catalytic centers, the BCCP domain mediated the shuttling of reaction intermediates, and each domain that was necessary for PCC catalysis had been accounted for in the preliminary structure of the holoenzyme.

However, after determining the positions of the BC, BCCP, and CT domains within the holoenzyme, there remained a significant portion of unassigned electron density between the

BC/BCCP and CT domains. After building in the missing residues, the structure of the BT domain was revealed, and more importantly, its function as the bridging feature between the α and β subunits was established. The structure of BT is shown in Figure 8, along with the PC tetramerization (PT) domain from *S. aureus* pyruvate carboxylase, with which BT shares weak structural similarity.
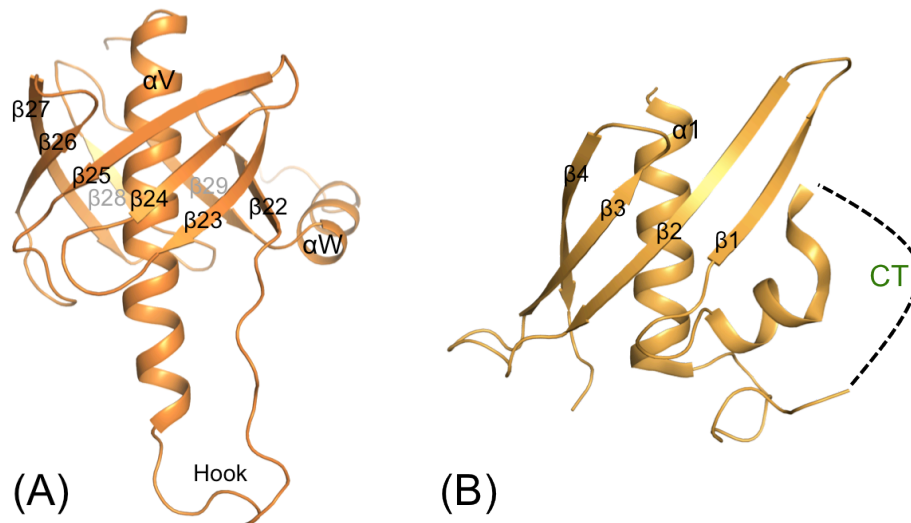
Figure 8. Structures of the (a) BT domain from PCC and (b) the PT domain from *S. aureus* pyruvate carboxylase (SaPC). While BT is encoded as a single domain within the primary sequence of PCCα, the PT sequence is interrupted by the CT domain of SaPC (see Figure 1) at the joint between Helix α1 and the start of the β sheet.

The BT domain is located between the BC and BCCP domains within the primary sequence of PCCα, and its structure consists of an eight-stranded anti-parallel β-barrel with a long helix situated in the center of the barrel. The importance of BT in maintaining the overall architecture of PCC is evidenced by its extensive interactions with the β_6 hexamer (CT subunits): of the 1,950 Å^2 of buried surface area between the α and β subunits, BT accounts for over 70% of the interactions, whereas BC and BCCP account for 10% and 15%, respectively. In particular, the distal loop in the BT domain mediates a majority of the inter-subunit contacts; this makeshift 'hook' (viewed as the bottom-most loop in Figure 8A) forms a number of salt bridges as well as hydrogen bonds with the β subunits. At the C-terminus of BT, helix αW (Figure 8A) also helps

to stabilize the interactions of the α and β subunits, although to a lesser extent than the hook, and the stabilizing forces are largely through hydrophobic contacts.

A retrospective analysis of the PCCα primary sequence using secondary structure prediction did indeed indicate the presence of a long helix with eight accompanying beta strands. However, because the fold of the BT domain was entirely unprecedented, it would have been unlikely that the tertiary structure of BT was correctly predicted by sequence analysis alone. A search for structural homologs of BT in the Protein Data Bank did not return any results. There is, however, a small degree of structural similarity between BT and PT, which is the PC tetramerization domain that mediates tetramer formation in pyruvate carboxylase. PT, however, consists only of a four-stranded anti-parallel β-sheet wrapped around a considerably shorter helix (Figure 8B).

2.4.2 PCC employs a swinging domain for BCCP-biotin translocation

Although the exact role of BCCP in catalysis is not completely answered by the current holoenzyme structure, one conclusion is apparent: the BC and CT active sites of PCC are separated by 55 Å, thus supporting the 'swinging-domain' model for biotin translocation (Figures 4, 9A). The case for BCCP acting as the mobile unit is also assisted by the small change in its position between the cryo-EM structure of HsPCC and the crystal structure of the RpαRdβ PCC chimera. In the crystal structure, BCCP-biotin is observed binding in the CT active site (which also accommodates propionyl-CoA), while the cryo-EM reconstruction places the BCCP domain closer to the BC domain. One possible explanation for the discrepancy is that BCCP-biotin is stabilized with the CT active site in the protein crystal (which contains approximately 50% solvent content), but an aqueous environment may provide alternative stabilizing contributions to lodge the flexible domain in a different conformation.
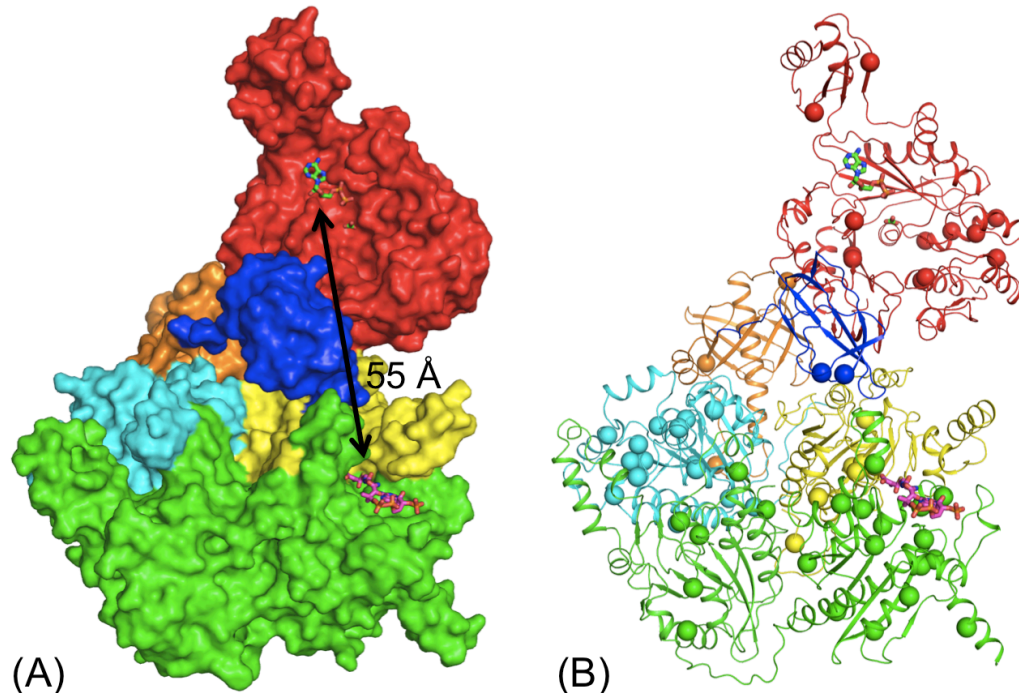
Figure 9. Locations of the active sites and disease-associated gene mutations in the PCC holoenzyme. (A) Molecular surface representation of one α subunit and a β_2 dimer. The bound positions of ADP and bicarbonate in complex with *E. coli* BC [11] and CoA in complex with transcarboxylase 12S [19] are shown. The BC and CT active sites are separated by 55 Å. Domains are colored in the same manner as in Figure 7. (B) Cartoon representation of (A), with the locations of propionic acidemia-associated mutations indicated by spheres. The position of CoA binding is indicated with the pink molecule.

2.4.3   Disease mutations can impair PCC catalysis and/or holoenzyme stability

Propionic acidemia (PA) has been a well known genetic disorder for many decades, due to its acute clinical phenotype and its relatively high incidence rate. Our structural studies of the PCC holoenzyme have provided a valuable tool for understanding the consequences of many PA-associated gene mutations, and may help in the development of disease therapies as well.

Figure 9B indicates the sites of amino acids that are substituted as a result of PA-related mutations. The Cα atoms are indicated as spheres on a foundation of an α subunit and a β_2 dimer, with the latter also indicating the site of propionyl-CoA binding. Several of the mutations are found in the vicinity of the BC and CT active sites, and may impede catalysis. The G631R mutation within the BT domain is located at its interface with the BC domain, and the

substitution of a considerably larger arginine residue is proposed to disrupt the structure. Through thermal shift experiments, it was shown that the G631R mutant is much more susceptible to denaturation than the wild-type enzyme.

To investigate the forces that maintain α-β interactions within the holoenzyme (and therefore contribute to PCC's functionality), we introduced a series of combined mutants at the subunit interface. These experiments took advantage of the fact that within the holoenzyme, only the β subunit of each holoenzyme is His-tagged, allowing for the concurrent pulldown of the untagged α subunit only upon holoenzyme formation. If the α-β interactions are destabilized, α will not be present in the eluent fraction (Figure 10).
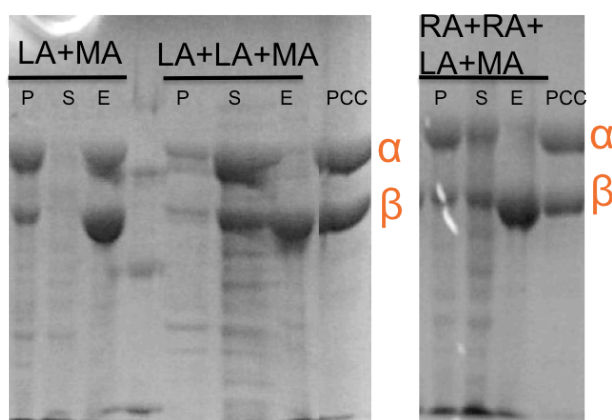
Figure 10. Effects of propionic acidemia (PA) gene mutations on PCC holoenzyme stability. The *E. coli* cell pellet fraction is indicated with 'P' and the soluble supernatant fraction is indicated with 'S'. Three combinations of PA mutations were assessed, and the abbreviations are, from left to right: LA+MA (L649A/M640A), LA+LA+MA (L646A/L649A/M650A), and RA+RA+LA+MA (R539A/R540A/L649A/M650A). Control lanes of wild-type RpPCC are in the lanes labeled 'PCC'.

We determined that PCC is an inherently stable enzyme, and only upon the introduction of three simultaneous mutations were we able to induce dissociation of the α and β subunits. The subunit interface of PCC is therefore proposed to contain an expansive network of interactions that maintain the integrity of the holoenzyme. As such, a single or double PA-associated mutation is unlikely to exert much of an effect on the activity of the holoenzyme.

2.4.4 The carboxyltransferase active site
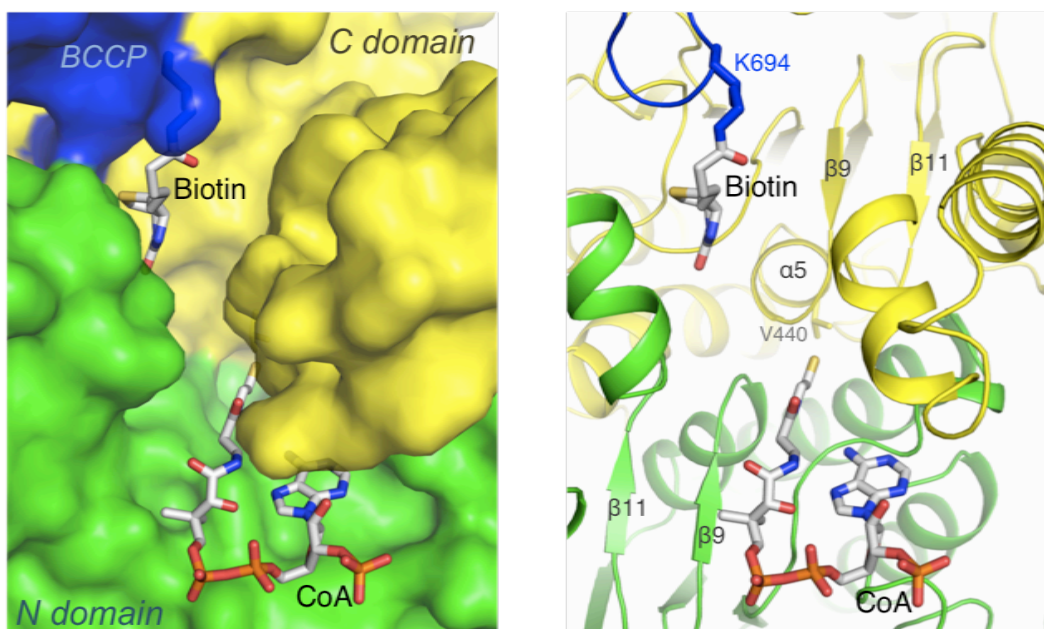
Figure 11. The CT active site. (left) Molecular surface representation of the CT binding pocket. The modeled binding mode of CoA with the 12S subunit of transcarboxylase is shown. (right) Detailed view of the CT active site. Biotinylation occurs on Lys694, which is found within a conserved sequence motif (MKM) of BCCP.

The CT active site is located in a deep groove, formed at the interface of an N domain from one β protomer and a C domain from another β protomer (Figure 11). BCCP-biotin is also observed binding the CT domain. In order to study the potential interactions between propionyl-CoA and the CT active site, the binding mode of CoA in complex with the 12S subunit of transcarboxylase was modeled into the structure. This model reveals that biotin and the CoA ligand occupy different ends of the groove, but the acyl group is expected to come within reach of carboxybiotin to permit catalysis. In our structure of PCC, biotin is held in a catalytically unproductive conformation, but the presence of an actual substrate is likely to extend biotin out farther, in order to permit the transfer of its carboxyl group onto propionyl-CoA.

2.5   Exploring the possibility of a molecular switch for substrate specificity

Several dual-specificity ACC/PCCs have been identified and were found to carboxylate both acetyl-CoA and propionyl-CoA with similar efficiency; however, the majority of ACCs and PCCs are selective for their namesake substrate. The recognition of an acyl-CoA occurs in the CT active site, which is formed only upon the dimerization of two CT protomers. Although the CT domains of acyl-CoA carboxylases are highly conserved across species, and it is unclear how each carboxylase can distinguish its preferred substrate from structurally similar analogs. A possible explanation is that the CT active site fashions a *very* specific environment for its preferred ligand, and accommodates the molecule's size, shape, and electrostatics with extreme accuracy. As such, it it possible to alter the substrate preferences of an enzyme simply by making adjustments to its binding environment.

In 2004, Diacovich *et al.* identified Asp440 of *S. coelicolor* PCCβ as a 'molecular switch.' A D440I mutation was observed to dramatically interconvert the enzyme's substrate preferences from propionyl-CoA to acetyl-CoA [20]. In the structure of RpαRdβ PCC, the position of Asp440 is occupied by a valine (Figure 11). V440 is in the proximity of the CoA substrate's acyl group, and may hold a similar role in determining substrate preference. In order to assess whether this residue truly functions as a 'switch', the Ile mutation was introduced into both RpPCC (which possesses an Asp at residue 440) and the RpαRdβ chimera. The effects on substrate preference and catalysis were monitored using an ATP hydrolysis assay (Figure 12), and the results are presented in Table 2.
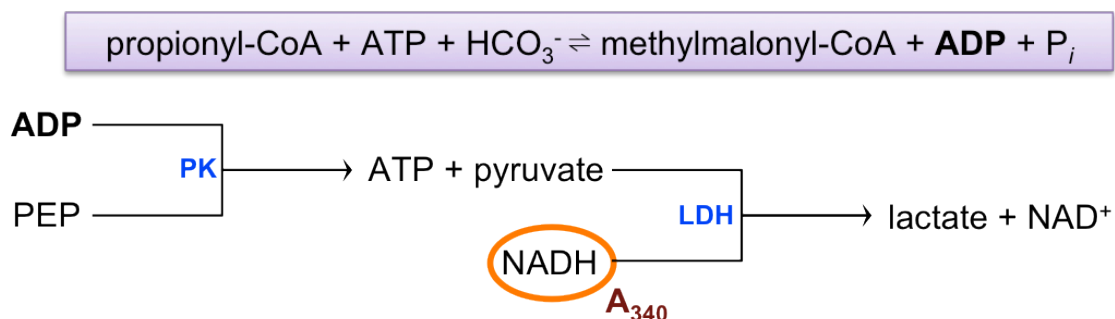
$$\text{propionyl-CoA} + \text{ATP} + \text{HCO}_3^- \rightleftharpoons \text{methylmalonyl-CoA} + \textbf{ADP} + \text{P}_i$$

Figure 12. Schematic illustration of the ATP hydrolysis assay. Because none of the reactants or products in the PCC-catalyzed reaction (shown in the purple box) can be tracked spetrophotometrically, a coupled-enzyme system featuring pyruvate kinase (PK) and lactate dehydrogenase (LDH) links the production of ADP to the disappearance of NADH. The reaction is monitored by tracking the decrease in A_{340} over time.

Table 2. *Kinetic data for the substrate preferences of wild-type PCC and its mutants*

	Relative Activity	
	Propionyl-CoA	**Acetyl-CoA**
RpPCC	1.0 ± 0.1^a	0.27 ± 0.04
RpαRdβ chimera	1.7 ± 0.3	0.15 ± 0.04
RpPCC (D440I)	2.1 ± 0.2	0.24 ± 0.02
RpαRdβ chimera (V440I)	1.6 ± 0.2	0.28 ± 0.05

[a] The activity of wild-type RpPCC against propionyl-CoA was set to 1.0.

In contrast to the results reported by Diacovich *et al*, the D440I and V440I mutations failed to convert the substrate preferences of RpPCC and RpαRdβ to favor acetyl-CoA. It is possible that the chemical environment of RpαRdβ is not similar to that of ScPCCβ, and thus V440 is not an appropriate candidate for controlling substrate discrimination. In order to investigate whether D440 of RpPCC could play a role in determining the fit of substrates within the CT binding pocket, various mutations were introduced to alter the shape, size, and electrostatics of the binding pocket:

Table 3. *Kinetic data for the substrate preferences of various RpPCC D440 mutants*

	Relative Activity	
	Propionyl-CoA	**Acetyl-CoA**
RpPCC	1.0 ± 0.1^{a}	0.22 ± 0.02
D440L	0.12 ± 0.01	0.25 ± 0.05
D440C	1.0 ± 0.1	0.23 ± 0.06
D440A	1.1 ± 0.1	0.43 ± 0.05
D440N	0.29 ± 0.08	0.13 ± 0.06
D440E	0.10 ± 0.08	0.14 ± 0.03

[a] The activity of wild-type RpPCC against propionyl-CoA was set to 1.0.

The kinetic data indicate that the majority of nonconservative mutations failed to alter the substrate preference of RpPCC. Although the D440L and D440E mutants exhibited respective 2- and 1.4-fold higher activities toward acetyl-CoA, the overall activities are dramatically lower than those of wild-type RpPCC. As a result, substrate selectivity may not be determined by a single residue; the maintenance of binding site architecture and/or charge may also be involved in determining substrate preference.

2.6   Preliminary investigations of PCC activation by potassium

Literature reports have demonstrated that the activities of both eukaryotic and prokaryotic PCC can be enhanced with K^{+} and other monovalent ions, with K^{+} being the most effective species. Due to the lack of structural data, the molecular basis of this phenomenon was not clear. Our structure of the PCC holoenzyme provides a valuable foundation on which to study the mechanism of K^{+} activation, and determine how the ion specifically activates PCC while possessing few to no effects on other biotin-dependent carboxylases.

As the effects of potassium on *R. pomeroyi* PCC had not been previously reported, we first sought to characterize its response to K^{+}. In addition, the RpαRpβ PCC chimera was also assayed. This chimera is not a naturally existing species, so while its structural data had indicated

that it was highly similar to the PCCs of other organisms, it remained of interest to determine what kind of catalytic potential a hybrid enzyme could possess. Finally, 3-methylcrotonyl-CoA carboxylase was used as a negative control. This enzyme is another biotin-carboxylase and shares many characteristics with PCC; however, there are no known reports of enhanced MCC activity in response to potassium [41].

These three enzymes were used for an ATP hydrolysis assay (Figure 11) in which the standard reaction components were modified ensure that no exogenous potassium was present in the reaction buffer. To this end, the HEPES buffer was prepared with sodium hydroxide instead of potassium hydroxide, KCl was replaced by NaCl, and $KHCO_3$ was replaced by $NaHCO_3$. In order to titrate increasing amounts of potassium into the reaction, the NaCl was progressively substituted with KCl to maintain a constant ionic strength within the buffer while increasing the concentration of K^+. The results of the titrations are shown in Table 4. Each value represents the average and standard deviation from three separate trials.

Table 4. *Kinetic data demonstrating K^+ activation of PCC*

[K^+] mM	Relative Activity		
	RpPCC	**RpαRdβ chimera**	**Methylcrotonyl-CoA carboxylase (MCC)**[b]
0	1.0 ± 0.08[a]	1.0 ± 0.3	1.0 ± 0.07
3	1.0 ± 0.01	1.7 ± 0.08	1.1 ± 0.01
10	1.1 ± 0.2	1.3 ± 0.1	1.1 ± 0.03
30	1.7 ± 0.1	1.7 ± 0.1	1.0 ± 0.0
100	2.9 ± 0.1	3.3 ± 0.1	0.9 ± 0.1
200	3.9 ± 0.1	3.9 ± 0.04	0.8 ± 0.03

[a] The activity of wild-type RpPCC against propionyl-CoA was set to 1.0.
[b] The MCC reaction substituted 3-methylcrotonyl-CoA in place of propionyl-CoA

The results of the assay demonstrate a clear activation of both PCC species in response to increasing potassium concentration. MCC, as predicted, does not exhibit much variation in response to changing potassium levels. Neither RpPCC nor the chimera appeared to reach its

maximum catalytic efficiency; therefore, it may be worthwhile to increase the upper concentration limit of potassium in order to better understand the extent of its effects. Human PCC, in particular, has been reported to demonstrate a 7-fold increase in activity, in response to K^+ [42].

In order to investigate the structural basis of K^+ activation in PCC, we prepared crystals of the RpαRpβ PCC chimera and soaked them overnight in the presence of the original mother liquor, supplemented with 10-200 mM RbCl and CsCl. Although neither of the cations activate PCC to the extent of potassium, they are significantly larger in size and their electron density within the PCC structure will be more apparent. A preliminary data set was obtained at 4-Å resolution for a crystal soaked with Cs^+, and a fragment of electron density corresponding to the Cs^+ ion was observed near the junction of the BT 'hook' and the adjacent β subunit. As the 'hook' feature of BT has been demonstrated to mediate a substantial portion of α-β interactions within the PCC holoenzyme, it appears possible that the presence of a cation activator at this site may help stabilize the holoenzyme for catalysis. Additional studies are necessary to obtain a higher-resolution model of Cs^+ binding, and the resulting observations can be supplemented with mutation studies to identify the structural components of PCC that are involved in recognizing and responding to the cation activator.

2.7   Structural implications for other acyl-CoA carboxylases

The elucidation of the PCC holoenzyme structure represented a great leap forward in our understanding of biotin-dependent carboxylases. In particular, the structure of a biotin-dependent *acyl-CoA* carboxylase has particular relevance for human health and disease, as four of the

enzymes (including PCC) act upon acyl-CoA esters, which are common intermediary metabolites in the body.

3-methylcrotonyl-CoA carboxylase (MCC) is another biotin-dependent carboxylase that targets an acyl-CoA ester, and is responsible for carboxylating the γ-carbon of 3-methylcrotonyl-CoA to product 3-methylglutaconyl-CoA (Figure 13). MCC is essential for leucine metabolism in humans, and is also involved in terpene metabolism in some bacteria [43]. Like PCC, MCC is also a mitochondrial enzyme in humans, requires ATP and biotin for its function, features the same domain architecture and subunit organization, and its deficiency in humans is also associated with a genetic disease that shares many symptoms with propionic acidemia. PCC and MCC also share significant sequence homology (Figure 13); therefore, it is possible to build a homology model for MCC based on the structure of PCC.
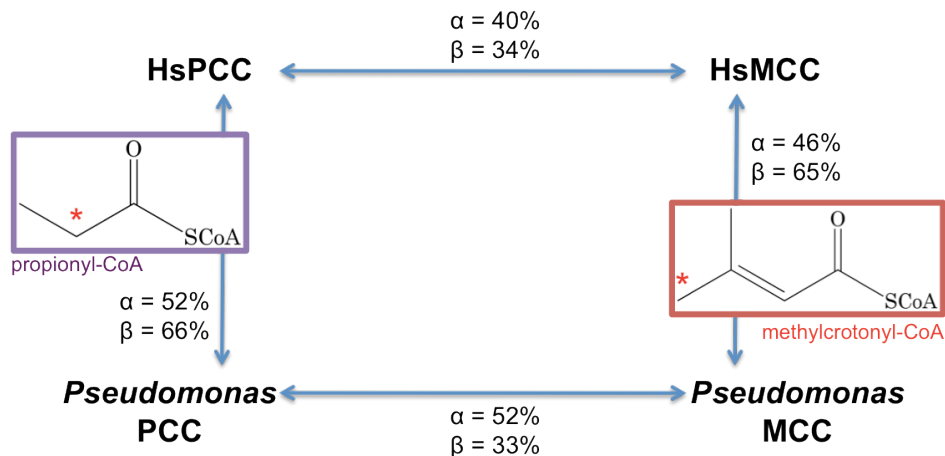
Figure 13. Illustration of shared sequence identities between the α and β subunits of PCC and MCC from humans and *Pseudomonas aeruginosa*. The sites of carboxylation on propionyl-CoA and methylcrotonyl-CoA are indicated with red asterisks.

However, there is one key difference between the two enzymes – their respective choice of substrate. While PCC carboxylates the α-carbon of propionyl-CoA, MCC accommodates a larger substrate and targets its γ-carbon instead (Figure 13). The underlying basis for substrate

selectivity between PCC and MCC is expected to lie in their respective acyl-CoA-recognizing

(β) subunits, and this serves as the motivating factor for our studies of MCC in Chapter III.

2.8   References

1.   Flavin, M. and Ochoa, S. *Metabolism of propionic acid in animal tissues. I. Enzymatic conversion of propionate to succinate.* J Biol Chem, 1957. **229**(2): p. 965-79.

2.   Flavin, M., Castro-Mendoza, H. and Ochoa, S. *Metabolism of propionic acid in animal tissues. II. Propionyl coenzyme a carboxylation system.* J Biol Chem, 1957. **229**(2): p. 981-96.

3.   Tietz, A. and Ochoa, S. *Metabolism of propionic acid in animal tissues. V. Purification and properties of propionyl carboxylase.* J Biol Chem, 1959. **234**(6): p. 1394-400.

4.   Mayer, S.M. and Beale, S.I. *Succinyl-Coenzyme A Synthetase and its Role in delta-Aminolevulinic Acid Biosynthesis in Euglena gracilis.* Plant Physiol, 1992. **99**(2): p. 482-7.

5.   Ando, T., Rasmussen, K., Wright, J.M. and Nyhan, W.L. *Isolation and identification of methylcitrate, a major metabolic product of propionate in patients with propionic acidemia.* Journal of Biological Chemistry, 1972. **247**(7): p. 2200-04.

6.   Cheema-Dhadli, S., Leznoff, C.C. and Halperin, M.L. *Effect of 2-methylcitrate on citrate metabolism: implications for the management of patients with propionic acidemia and methylmalonic aciduria.* Pediatric Research, 1975. **9**(12): p. 905-08.

7.   Tong, L. *Structure and function of biotin-dependent carboxylases.* Cell Mol Life Sci, 2013. **70**(5): p. 863-91.

8.   Browner, M.F., Taroni, F., Sztul, E. and Rosenberg, L.E. *Sequence analysis, biogenesis, and mitochondrial import of the alpha-subunit of rat liver propionyl-CoA carboxylase.* Journal of Biological Chemistry, 1989. **264**(21): p. 12680-85.

9.   Ingaramo, M. and Beckett, D. *Selectivity in Post-translational Biotin Addition to Five Human Carboxylases.* Journal of Biological Chemistry, 2011. **287**(3): p. 1813-22.

10.   Taroni, F. and Rosenberg, L.E. *The precursor of the biotin-binding subunit of mammalian propionyl-CoA carboxylase can be translocated into mitochondria as apo-or holoprotein.* Journal of Biological Chemistry, 1991. **266**(20): p. 13267-71.

11.   Chou, C.Y., Yu, L.P. and Tong, L. *Crystal structure of biotin carboxylase in complex with substrates and implications for its catalytic mechanism.* J Biol Chem, 2009. **284**(17): p. 11690-7.

68

12. Athappilly, F.K. and Hendrickson, W.A. *Structure of the biotinyl domain of acetyl-coenzyme A carboxylase determined by MAD phasing.* Structure, 1995. **3**(12): p. 1407-19.

13. Bilder, P., Lightle, S., Bainbridge, G., Ohren, J., Finzel, B., Sun, F., Holley, S., Al-Kassim, L., Spessard, C., Melnick, M., Newcomer, M., and Waldrop, G.L. *The structure of the carboxyltransferase component of acetyl-coA carboxylase reveals a zinc-binding motif unique to the bacterial enzyme.* Biochemistry, 2006. **45**(6): p. 1712-22.

14. Thoden, J.B., Blanchard, C.Z., Holden, H.M. and Waldrop, G.L. *Movement of the biotin carboxylase B-domain as a result of ATP binding.* Journal of Biological Chemistry, 2000. **275**(21): p. 16183-90.

15. Knowles, J.R. *The mechanism of biotin-dependent enzymes.* Annual Review of Biochemistry, 1989. **58**(1): p. 195-221.

16. St. Maurice, M., Reinhardt, L., Surinya, K.H., Attwood, P.V., Wallace, J.C., Cleland, W.W. and Rayment, I. *Domain architecture of pyruvate carboxylase, a biotin-dependent multifunctional enzyme.* Science, 2007. **317**(5841): p. 1076-79.

17. Xiang, S. and Tong, L. *Crystal structures of human and Staphylococcus aureus pyruvate carboxylase and molecular insights into the carboxyltransfer reaction.* Nature Structural & Molecular Biology, 2008. **15**(3): p. 295-302.

18. Haase, F.C., Henrikson, K.P., Treble, D.H. and Allen, S.H. *The subunit structure and function of the propionyl coenzyme A carboxylase of Mycobacterium smegmatis.* J Biol Chem, 1982. **257**(20): p. 11994-9.

19. Hall, P.R., Wang, Y.-F., Rivera-Hainaj, R.E., Zheng, X., Pustai-Carey, M., Carey, P.R. and Yee, V.C. *Transcarboxylase 12S crystal structure: hexamer assembly and substrate binding to a multienzyme core.* The EMBO Journal, 2003. **22**(10): p. 2334-47.

20. Diacovich, L., Mitchell, D.L., Pham, H., Gago, G., Melgar, M.M., Khosla, C., Gramajo, H. and Tsai, S.C. *Crystal structure of the beta-subunit of acyl-CoA carboxylase: structure-based engineering of substrate specificity.* Biochemistry, 2004. **43**(44): p. 14027-36.

21. Lin, T.-W., Melgar, M.M., Kurth, D., Swamidass, S.J., Purdon, J., Tseng, T., Gago, G., Baldi, P., Gramajo, H., and Tsai, S.-C. *Structure-based inhibitor design of AccD5, an essential acyl-CoA carboxylase carboxyltransferase domain of Mycobacterium tuberculosis.* Proceedings of the National Academy of Sciences, 2006. **103**(9): p. 3072-77.

22. Benson, B.K., Meades Jr, G., Grove, A. and Waldrop, G.L. *DNA inhibits catalysis by the carboxyltransferase subunit of acetyl-CoA carboxylase: Implications for active site communication.* Protein Science, 2008. **17**(1): p. 34-42.

23.   Hugler, M., Krieger, R.S., Jahn, M. and Fuchs, G. *Characterization of acetyl-CoA/propionyl-CoA carboxylase in Metallosphaera sedula. Carboxylating enzyme in the 3-hydroxypropionate cycle for autotrophic carbon fixation.* Eur J Biochem, 2003. **270**(4): p. 736-44.

24.   Ishii, M., Miyake, T., Satoh, T., Sugiyama, H., Oshima, Y., Kodama, T. and Igarashi, Y. *Autotrophic carbon dioxide fixation in Acidianus brierleyi.* Archives of Microbiology, 1997. **166**(6): p. 368-71.

25.   Giorgio, A.J. and Plaut, G.W.E. *The effect of univalent cations of activities catalyzed bovine-liver propionyl-CoA carboxylase.* Biochimica et Biophysica Acta (BBA)-Enzymology, 1967. **139**(2): p. 487-501.

26.   Edwards, J.B. and Keech, D.B. *Activation of pig heart propionyl-CoA carboxylase by potassium ions.* Biochimica et Biophysica Acta (BBA)-Enzymology, 1968. **159**(1): p. 167-75.

27.   Miyazaki, T., Ohura, T., Kobayashi, M., Shigematsu, Y., Yamaguchi, S., Suzuki, Y., Hata, I., Aoki, Y., Yang, X., and Minjares, C. *Fatal propionic acidemia in mice lacking propionyl-CoA carboxylase and its rescue by postnatal, liver-specific supplementation via a transgene.* Journal of Biological Chemistry, 2001. **276**(38): p. 35995-99.

28.   Wolf, B., Hsia, Y.E., Sweetman, L., Gravel, R., Harris, D.J. and Nyhan, W.L. *Propionic acidemia: a clinical update.* Journal of Pediatrics, 1981. **99**(6): p. 835-46.

29.   Ando, T., Rasmussen, K., Nyhan, W.L., Donnell, G.N. and Barnes, N.D. *Propionic acidemia in patients with ketotic hyperglycinemia.* Journal of Pediatrics, 1971. **78**(5): p. 827-32.

30.   Saudubray, J.M., Touati, G., Delonlay, P., Jouvet, P., Schlenzig, J., Narcy, C., Laurent, J., Rabier, D., Kamoun, P., and Jan, D. *Liver Transplantation in Propionic Acidaemia.* European Journal of Pediatrics, 1999. **158**(2): p. S065-S69.

31.   Barshes, N.R., Vanatta, J.M., Patel, A.J., Carter, B.A., O'Mahony, C.A., Karpen, S.J. and Goss, J.A. *Evaluation and management of patients with propionic acidemia undergoing liver transplantation: a comprehensive review.* Pediatric Transplantation, 2006. **10**(7): p. 773-81.

32.   Blanchard, C.Z., Lee, Y.M., Frantom, P.A. and Waldrop, G.L. *Mutations at four active site residues of biotin carboxylase abolish substrate-induced synergism by biotin.* Biochemistry, 1999. **38**(11): p. 3393-400.

33.   Otwinowski, Z. and Minor, W. *Processing of X-ray diffraction data.* Methods in Enzymology, 1997. **276**: p. 307-26.

34.   Jones, T.A., Zou, J.Y., Cowan, S.W. and Kjeldgaard, M. *Improved methods for building protein models in electron density maps and the location of errors in these models.* Acta Crystallographica Section A: Foundations of Crystallography, 1991. **47**(2): p. 110-19.

35.   Brunger, A.T., Adams, P.D., Clore, G.M., DeLano, W.L., Gros, P., Grosse-Kunstleve, R.W., Jiang, J.S., Kuszewski, J., Nilges, M., and Pannu, N.S. *Crystallography & NMR system: A new software suite for macromolecular structure determination.* Acta Crystallographica Section D: Biological Crystallography, 1998. **54**(5): p. 905-21.

36.   Brunger, A.T. *Version 1.2 of the Crystallography and NMR system.* Nature Protocols, 2007. **2**(11): p. 2728-33.

37.   Jogl, G., Tao, X., Xu, Y. and Tong, L. *COMO: a program for combined molecular replacement.* Acta Crystallographica Section D: Biological Crystallography, 2001. **57**(8): p. 1127-34.

38.   Pettersen, E.F., Goddard, T.D., Huang, C.C., Couch, G.S., Greenblatt, D.M., Meng, E.C. and Ferrin, T.E. *UCSF Chimera, A visualization system for exploratory research and analysis.* Journal of Computational Chemistry, 2004. **25**(13): p. 1605-12.

39.   Huang, C.S., Sadre-Bazzaz, K., Shen, Y., Deng, B., Zhou, Z.H. and Tong, L. *Crystal structure of the alpha(6)beta(6) holoenzyme of propionyl-coenzyme A carboxylase.* Nature, 2010. **466**(7309): p. 1001-5.

40.   Schrodinger, LLC, *The PyMOL Molecular Graphics System, Version 1.3r1*. 2010.

41.   Chang, A., Scheer, M., Grote, A., Schomburg, I. and Schomburg, D. *BRENDA, AMENDA and FRENDA the enzyme information system: new content and tools in 2009.* Nucleic acids research, 2009. **37**(suppl 1): p. D588-D92.

42.   Kalousek, F., Darigo, M.D. and Rosenberg, L.E. *Isolation and characterization of propionyl-CoA carboxylase from normal human liver. Evidence for a protomeric tetramer of nonidentical subunits.* Journal of Biological Chemistry, 1980. **255**(1): p. 60-65.

43.   Aguilar, J.A., Diaz-Perez, C., Diaz-Perez, A.L., Rodriguez-Zavala, J.S., Nikolau, B.J. and Campos-Garcia, J. *Substrate specificity of the 3-methylcrotonyl coenzyme A (CoA) and geranyl-CoA carboxylases from Pseudomonas aeruginosa.* Journal of bacteriology, 2008. **190**(14): p. 4888-93.

Chapter III

Structural and biochemical studies of 3-methylcrotonyl-CoA carboxylase

3.1   Introduction to MCC

3-methylcrotonyl-CoA carboxylase (MCC; EC 6.4.1.4) is another member of the biotin-dependent carboxylases, and catalyzes the ATP-dependent carboxylation of 3-methylcrotonyl-CoA to generate 3-methyl-glutaconyl-CoA (Figure 1). MCC is a highly conserved enzyme and is found in all walks of life, from bacteria to man. In humans, MCC is a mitochondrial enzyme and was predicted to be a 500-800-kDa complex, possessing stoichiometrically equivalent amounts of an α subunit, which was determined to contain biotin, and a smaller β subunit [1]. In humans, plants, and bacteria, MCC primarily functions in leucine metabolism (Figure 1).
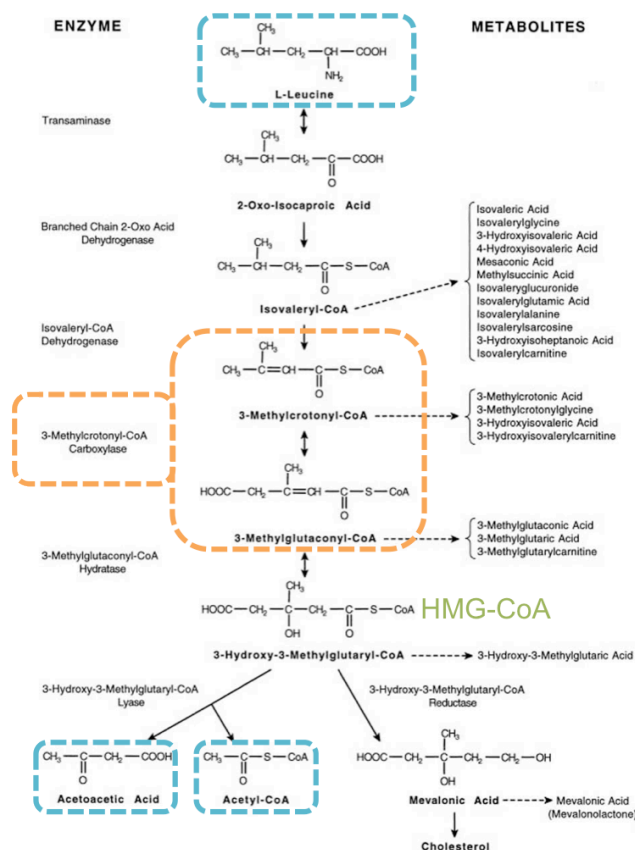
Figure 1. Leucine metabolism in humans. A set of six reactions converts L-leucine into either energy metabolites (acetoacetate and acetyl-CoA) or mevalonate, which is a steroid precursor. The substances indicated in brackets on the right-hand side are metabolites that can accumulate when there is a deficiency in the function of their associated enzymes. Such accumulation can lead to their toxic buildup and subsequent consequences to human health. Adapted from [2].

MCC has been extensively researched for several decades, and its early characterization as a biotin-containing enzyme led to the identification of biotin as a common enzymatic cofactor [3]. MCC's involvement in leucine metabolism was originally studied in *Pseudomonas* organisms, where it was discovered that MCC expression could be induced by growing *Pseudomonas aeruginosa* with leucine as its sole source of carbon and energy [4]. (Before the advent of recombinant cloning technologies, this approach constituted the most reliable method to obtain large amounts of the enzyme for biochemical studies.)

Plant MCCs are also heteromeric complexes consisting of α and β subunits. The genome of *Arabidopsis thaliana* contains two *MCC* genes, each encoding for one subunit. Interestingly, in other plant species, as many as four genes are required to encode for a functional MCC subunit [5].

In humans, deficits in MCC expression or function can result in severe health issues due to the toxic buildup of unprocessed metabolites. Patients with such deficiencies are diagnosed with methylcrotonylglycinuria, and may present with vomiting, lethargy, and in severe cases, may experience seizures and developmental delays [6]. Methylcrotonylglycinuria is very similar to propionic acidemia (Chapter II) in that it is also inherited in an autosomal recessive fashion, has a relatively high incidence rate (1:50,000 individuals worldwide [7]), and spans a wide variety of phenotypes. Some individuals may exhibit acute symptoms at birth, while less-severe forms of the disease may go unnoticed or attributed to other maladies. Because MCC is directly involved in leucine metabolism, the majority of symptoms can be reduced by avoiding this amino acid, usually through a low-protein diet. In some patients, the administration of supplemental biotin has been shown to help as well [8, 9]. A number of mutations in the human *MCCA* and *MCCB* genes (which code for the α and β subunits of MCC, respectively) have been

identified, although additional structural and biochemical data are necessary to understand their consequences on the enzyme itself.

Our interest in MCC stemmed directly from our studies of PCC and other biotin-dependent carboxylases. Throughout our research, one question kept resurfacing: how does each enzyme maintain its particular substrate preferences when its constituent domains are so similar to those of the other enzymes? We decided to approach this question by comparing the β subunits of MCC and PCC, which both recognize acyl-CoA substrates in their CT active sites.

In studying MCCβ, we hypothesized that it would exhibit a very similar structure to the PCCβ hexamer. From our investigations of PCC, coupled with the knowledge that MCC exhibits many similarities to PCC (including high sequence similarity, choice of acyl-CoA substrates, mitochondrial localization, and disease hallmarks), we predicted that "*MCC is a close homolog of PCC … therefore, the PCC structure is directly relevant for MCC*" [10]. Therefore, we focused on the architecture of the CT active site within MCCβ, and we hoped to determine the molecular features that allowed MCC (and not PCC) to (1) recognize a larger substrate and (2) carboxylate a different carbon on the substrate.

3.2   Experimental Procedures

Protein purification and mutagenesis

Samples of *Pseudomonas aeruginosa* PAO1 were donated from Dr. Alice Prince (Columbia University) and the genomic DNA was isolated using established procedures [11]. The α subunit of MCC (PaMCCα) was cloned with a C-terminal hexahistidine tag in pET-26b and the β subunit (PaMCCβ) was cloned with an N-terminal hexahistidine tag in pET-28a. All cloning vectors were obtained from Novagen. The MCC holoenzyme (PaMCC) was generated as

a bicistronic expression construct in pET-28a, and the final sequence of the construct was RBS-(His)$_6$-[PaMCCβ]-RBS-[PaMCCα], with "RBS" indicating a ribosomal binding site. The expression and purification schemes are identical to those described for PCC in Chapter II. All purified protein samples were concentrated to 20 mg/mL, flash-frozen in liquid nitrogen, stored at -80°C and thawed on ice for subsequent experiments. Biotinylation of the α subunit of MCC was confirmed using an avidin gel-shift assay. The N-terminal hexahistidine tags were not removed prior to crystallization.

All point mutations were generated with the QuikChange kit (Agilent) and were sequenced to confirm the presence of mutations. The expression and purification schemes for the mutants were the same as those described for the wild-type enzyme.

Kinetic studies of MCC

The catalytic activity of MCC was measured using a coupled enzyme assay, which links the consumption of ATP by the BC domain to the disappearance of NADH [12]. The reaction buffer contained 100 mM HEPES-KOH (pH 8.0), 0.5 mM ATP, 8 mM MgCl$_2$, 40 mM KHCO$_3$, 0.2 mM NADH, 0.5 mM phosphoenolpyruvate, 7 U lactate dehydrogenase, 4.2 U pyruvate kinase, 200 mM KCl, and 0.5 mM of either methylcrotonyl-CoA, crotonyl-CoA, or propionyl-CoA. All reagents were obtained from Sigma. The reaction was initiated by adding 2 μg of protein to 100 μL of reaction buffer, and the progress was monitored by tracking the UV absorbance at 340 nm for 5 min.

Crystallization of MCC

Prior to setting up crystallization trays, the purified proteins were incubated with 2 mM methylcrotonyl-CoA on ice for 30 minutes. Initial crystallization conditions were identified using commercial sparse-matrix and grid screens (Emerald BioSystems, Hampton Research, Qiagen) and confirmed hits were optimized using the microbatch method under paraffin oil (Hampton Research) at 20°C. Crystals were produced by combining the purified protein (at 20 mg/mL) with precipitant solution in a 1:1 drop ratio. Cryoprotection was ensured by immersing the crystals in their respective precipitant solution, supplemented with glycerol for a final PEG + glycerol concentration of 35%. The cryoprotected crystals were then flash-frozen and stored in liquid nitrogen until data collection.

The precipitant solution for PaMCCβ contained 0.1M MES (pH 6.5) and 1.6M $MgSO_4$. After ten to fourteen days, cubic crystals approximately 0.3 mm^3 in size were obtained (Figure 2A), belonged to the $R32$ space group, and diffracted X-rays strongly (<2.0 Å resolution).

The precipitant solution for the PaMCC holoenzyme contained either 0.2 M Na-malonate or 0.2 M Na_2SO_4, in addition to 20% (w/v) PEG-3350. After approximately two weeks, thin plates approximately 0.45 mm in length were observed (Figure 2B) and belonged to the $P2_1$ space group. The majority of these crystals exhibited weak X-ray diffraction, and extensive screening was required to identify crystals suitable for data collection. CoA was observed in the active site of the β subunit upon elucidation of the final holoenzyme crystal structure.

The conditions for the PaMCC+CoA crystals also produced crystals of the PaMCC free enzyme. After approximately six weeks at 20°C, the drops of protein and precipitant solution were significantly dehydrated, and the thin plates previously observed were replaced by highly birefringent block-shaped crystals, approximately 0.2 mm in length (Figure 2C). These crystals

exhibited significantly stronger X-ray diffraction, belonged to the *R*32 space group, and did not contain bound CoA in the final structure.
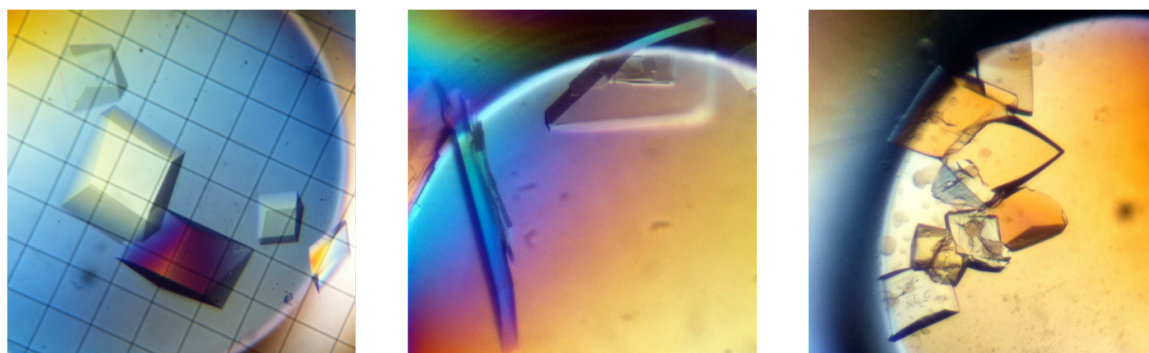
(A) PaMCCβ　　　　　　(B) PaMCC+CoA　　　　　　(C) PaMCC

Figure 2. Crystals of the β subunit and holoenzymes of MCC from *Pseudomonas aeruginosa*. (A) Crystals of full-length MCCβ free enzyme. (B) Crystals of full-length MCC complexed with CoA. (C) Crystals of full-length MCC free enzyme. The crystals in (C) were obtained from the same conditions as (B), but required substantially more time to grow.

In addition, three separate MCC mutants were generated by introducing the following point mutations into the β subunit: V375F, A218T, and a VF/AT double mutant. The crystallization conditions for these three mutants were the same as those for the wild-type MCC holoenzyme, with the exception that the double mutant also required the addition of 3.5% (w/v) benzamidine-HCl to the precipitant solution.

Data collection and structure determination

X-ray diffraction data were collected at 100 K, at the X29A beamline of the National Synchrotron Light Source (NSLS) at Brookhaven National Laboratory. All diffraction images were processed and scaled with *HKL*-2000 [13].

For PaMCCβ, an X-ray diffraction data set was collected at 1.5-Å resolution, and the crystal belonged to the *R*32 space group, with cell parameters of $a = b = 192.4$ Å, $c = 136.8$ Å, $\alpha = \beta = 90.0°$, and $\gamma = 120.0°$. The asymmetric unit contained a single β subunit. The structure was

solved with the molecular replacement program Phaser [14], using the structure of the β subunit of PCC [10] as the search model. The atomic model was built into the electron density map using O [15] and Coot [16], and the structure was refined using CNS [17] and Refmac [18] prior to deposition in the Protein Data Bank (accession code: 3U9R).

For the CoA complex of the PaMCC holoenzyme, an X-ray diffraction data set was collected at 3.5-Å resolution, and the crystal belonged to the $P2_1$ space group, with cell parameters of $a = 131.5$ Å, $b = 255.3$ Å, $c = 152.7$ Å, $\alpha = 90°$, $\beta = 95.7°$, and $\gamma = 90°$. There was one $\alpha_6\beta_6$ dodecamer in the asymmetric unit. The structure was solved using Phaser for molecular replacement, and the structures of PaMCCβ and the BC domain of PCC [10] were used as search models. The BCCP domain of PCC was also used as a search model, but only one copy was found in the PaMCC structure. The structure of the BT domain was built into the electron density after structural refinement with CNS.

For the PaMCC free enzyme, an X-ray diffraction data set was collected at 2.9-Å resolution, and the crystal belonged to the $R32$ space group, with cell parameters of $a = b = 158.9$ Å, $c = 312.0$ Å, $\alpha = \beta = 90.0°$, and $\gamma = 120.0°$. The asymmetric unit contained a single α-β protomer, and the structure was determined by molecular replacement with Phaser, using one α-β protomer from the PaMCC+CoA complex structure as the search model.

The detailed crystallographic data are presented in Table 1.

Table 1. *Crystallographic data and refinement statistics*

	PaMCCβ Free enzyme	PaMCC CoA complex	PaMCC Free enzyme
PDB accession code	3U9R	3U9S	3U9T
Crystal data			
Space group	$R32$	$P2_1$	$R32$
Unit cell dimensions	$a=b=192.4$ Å, $c=136.8$ Å, $\alpha=\beta=90°$, $\gamma=120°$	$a=131.5$ Å, $b=255.3$ Å, $c=152.7$Å, $\alpha=90°, \beta=95.7°$, $\gamma=90°$	$a=b=158.9$ Å, $c=312.0$ Å, $\alpha=\beta=90°, \gamma=120°$
Diffraction data[a]			
Wavelength (Å)	1.075 Å	1.075 Å	1.075 Å
Resolution range (Å)	30–1.5	50–3.5	50-2.9
Redundancy	3.4 (2.6)	3.1 (2.4)	3.6 (3.4)
Completeness (%)	92 (73)	83 (61)	93 (82)
$<I/\sigma I>$	10.8 (2.3)	8.3 (1.7)	16.0 (2.4)
R_{merge} (%)	8.9 (35.9)	12.0 (45.1)	5.8 (38.8)
Structure refinement			
# of reflections used	141,517	104,480	31,522
R_{work} / R_{free}[b] (%)	16.6/18.3 (32.8/31.8)	23.4/29.2 (39.6/42.5)	20.9/26.9 (32.4/35.4)
RMSD bond lengths (Å)	0.017	0.014	0.011
RMSD bond angles (°)	1.7	1.8	1.7

[a]Values in parentheses refer to the highest-resolution shell.
[b]R_{free} = free R factor, based on a random sample of 5% of reflections.

Electron microscopy (EM) studies

All EM studies were performed by our collaborators in the laboratory of Dr. Z. Hong Zhou at the University of California, Los Angeles. Dilutions of the PaMCC holoenzyme were prepared in a buffer containing 25 mM Tris-HCl (pH 7.4) and 250 mM NaCl. For the negative stain experiments, 2.5 µL aliquots of diluted sample were spotted onto carbon-film-coated, glow-discharged, 300-mesh copper grids, and excess sample was blotted away after 1 min. The sample was stained with a solution of 2% uranyl acetate and air-dried. One sample of optimal particle concentration was used for subsequent imaging and three-dimensional reconstruction analysis. The electron micrographs were obtained using a FEI TF20 electron microscope, and the images were recorded on a TVIPS 16MP CCD camera at 70,000X magnification. Approximately 20,500

particles were picked, using manual and automatic methods, during three-dimensional reconstruction. Another 12,000 particles were used for the final reconstruction.

3.3   Initial investigations of MCC

The first investigations of MCC in our laboratory were conducted by Yang Shen, a graduate student and subsequent postdoctoral fellow in the lab. His studies of the α subunit from human MCC were intended to examine catalysis in the BC domain, in comparison to its fungal and bacterial ACC counterparts. However, the α subunits of human MCC were neither soluble nor inducible, and further studies were not performed.

I began examining the molecular basis of substrate recognition in MCC by generating and screening through a collection of full-length bacterial MCCβ subunits with high sequence identity to human MCC (Table 2). The β subunit alone was targeted because the recognition and binding of the acyl-CoA substrate occurs entirely within this subunit, in a manner similar to PCC. In addition, although human MCC would have proven an ideal target, Chu *et al.* described the purification of human MCC holoenzyme as a demanding process, involving baculovirus expression and extremely low yields (36 µg protein per liter of insect cell culture), with the latter aspect being undesirable for crystallization trials [1]. Our success in determining the PCC structure using a bacterial homolog also motivated us to employ a similar approach with MCC.

Table 2. *Bacterial MCCβ constructs*

#	ID	Organism	Vector	% Identity to human
1	Pa	*Pseudomonas aeruginosa* PAO1	pET-28a	65%
2	Pf	*Pseudomonas fluorescens* Pf-5	pET-28a	67%
3	Re	*Rhizobium etli* CFN42	pET-28a	64%
4	Rp[a]	*Rhodopseudomonas palustris* CGA009	pET-28a	63%
5	Rr	*Rhizobium radiobacter* C58	pET-28a	71%
6	Rs	*Rhodobacter sphaeroides* 2.4.1	pET-28a	66%
7	Rp	*Ruegeria pomeroyi* DSS-3	pET-28a	66%
8	Rd	*Roseobacter denitrificans* OCh114	pET-28a	67%

The best candidate from the screen of bacterial MCC β subunits was obtained from *Pseudomonas aeruginosa* PAO1, a Gram-negative bacterium and a well-known opportunistic human pathogen. Its β subunit (PaMCCβ) shares 65% sequence identity with the human homolog. PaMCCβ was purified to homogeneity and produced large rhomboid crystals (Figure 2A) that diffracted to 1.5-Å resolution, and the structure was solved by molecular replacement. With this high-quality crystal structure, we began our investigations of the determinants of substrate preference in MCC.

3.4   Structure of the 360-kDa β_6 hexamer of 3-methylcrotronyl-CoA carboxylase

Upon first glance, the structure of PaMCCβ is remarkably similar to that of PCCβ (Figure 3). Both are hexameric rings approximately 360 kDa in size, and both possess 32 symmetry. Each hexamer is a trimeric assembly of dimers, and the substrate-binding sites are formed at the interface of two protomers, for a total of six active sites in each hexamer.
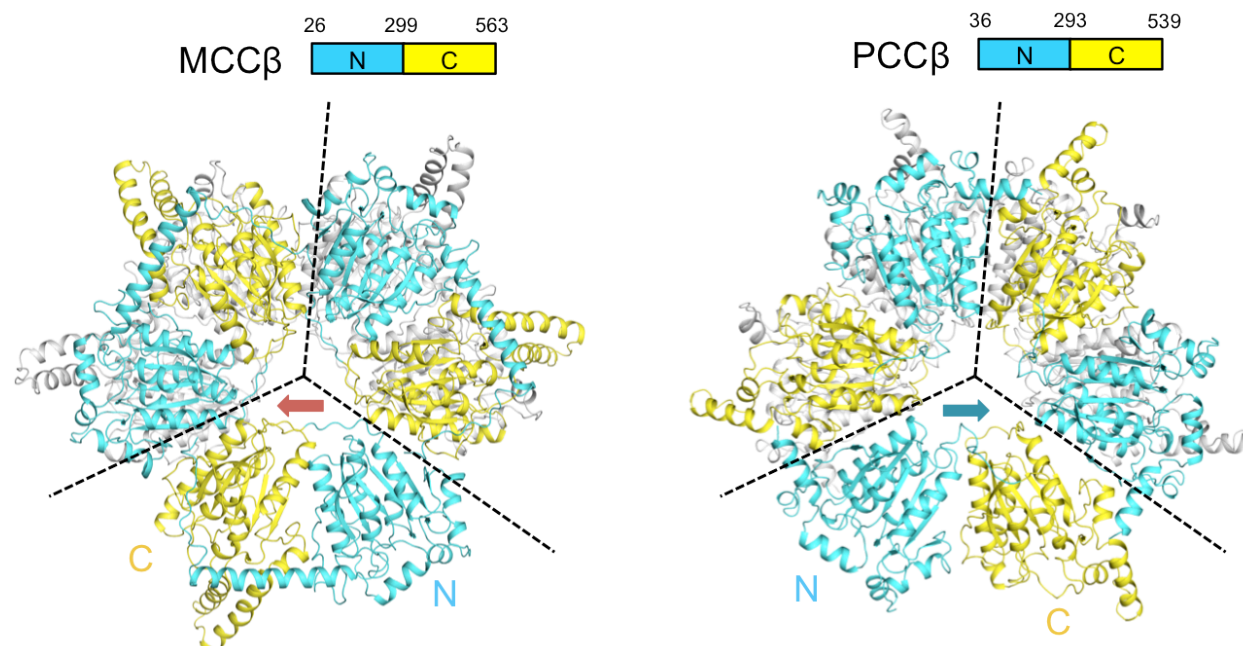
Figure 3. Crystal structures of the β subunits of *P. aeruginosa* MCC (left) and *Roseobacter denitrificans* PCC (right). Both subunits assemble as hexamers, and the structures are viewed from the top face of each hexamer. The N domain of each β subunit is colored in cyan, and the C domain is colored in yellow. The arrows designate the direction (N'→C') of the linker that connects the two domains within each enzyme. For clarity, the protomer in the bottom layer under each arrow has been omitted from view.

However, much to our surprise, the structure of an *individual* β subunit was significantly different between MCC and PCC. The dashed lines in Figure 3 delineate the subunit boundaries within the hexamer, and demonstrate that there is a 'swap' of the N and C domains within each MCCβ subunit as compared to the domain arrangement in PCCβ. This finding was entirely unanticipated and was not predicted from sequence analysis; in fact, there is a shared sequence identity of 33% for the β subunits of MCC and PCC. Given this unexpected result, it was of considerable interest to investigate the origins of the domain swap and its potential consequences on the structure and function of the MCC holoenzyme.

82

3.4.1 A unique domain arrangement for the β subunit of MCC

The N and C domains of the two enzymes are very similar in their overall appearance. Each domain contains a backbone crotonase fold, which consists of two perpendicular beta-sheets linked by alpha-helices [19]. However, this similarity in appearance does not extend to the primary sequences. In other words, the N domain of MCCβ shares a higher sequence identity with the N domain of PCCβ than it does with the C domain of PCCβ. The same logic applies for the corresponding C domains of MCCβ and PCCβ. Therefore, the domain swapping is not a consequence of an internal gene rearrangement within the primary sequences of the β subunits.

Figure 4. A flexible 25-residue linker connects the N and C domains of β subunits from acyl-CoA carboxylases. Omit F_o-F_c electron density map at 1.5-Å resolution for the domain linker of PaMCCβ, contoured at 3σ.

```
PaMCCb_    1  -------------------------MAILHTQINPRSAEFAANAATMLEQVNALRTLL 33GRIHEGGGSAAQARHSARGKLLVRERINRLLDPGSPFLELSALAAHE
RdPCCb_    1  -----------------------------MKDILEQLEDRR 12AAARLGGGQKRIDAQHGRGKLTARERVDLLLDEGS-FEEFDMFVTHR
HsMCCb_    1  MWAVLRLALRPCARASPAGPRAYHGDSVASLGTQPDLGSALYQENYKQMKALVNQLHERV 60EHIKLGGGEKARALHISRGKLLPRERIDNLIDPGSPFLELSQFAGYQ
HsPCCb_    1  ----------------MAAALRVAAVGARLSVLASGLRAAVRSLCSQATSVNERIENKR 43RTALLGGGQRRIDAQHKRGKLTARERISLLLDPGS-FVESDMFVEHR
PaGCCb_    1  -------------------------MPAIQSELDVNGEDFARNREAMLAAVAGFRELE 33QKVLDKA-AEARPKFEKRGQLLPRERLALLLDPGAPFLELSSLAGYK
CmGCCb_    1  -------------------------MITIDTRIDSTSDTFATQRAGMQALTDRLRALE 33QRAVDAS-SRARSSFQKRGALLPRERVACLLDPGAPFLPLATLAGYG
AfGCDa_    1  -----------------MGFYSMPRYFQNMPQVGKPLKKADAANEEQLKKIEEEIHQLI 42KEAQEAG--KADADVNKRGELTALQRIEKLVEPGS-WRPLNTLFNPQ


PaMCCb_   81  VYG-------EEV 86AAAGIVAGIGRVEGVECMIVGNDATVKGGTYYPLTVKKHLRAQAIALENRLPCIYLVDSG 146GANLP-RQDEVFPDREHFGRIFFNQANMSA
RdPCCb_   59  CTDFNMQDQKP-- 69AGDGVVTGWGTINGRVVYVFSQDFTVLGGSVSETHSKKICKIMDMAMQNGAPVIGINDSG 129GARIQEGVDSLAGYG-----EVFQRNIMAS
HsMCCb_   108 LYD------NEEV 114PGGGIITGIGRVSGVECMIIANDATVKGGAYYPVTVKKQLRAQEIAMQNRLPCIYLVDSG 174GAYLP-RQADVFPDRDHFGRTFYNQAIMS
HsPCCb_   90  CADFGMAADKNKF 102PGDSVVTGRGRINGRLVYVFSQDFTVFGGSLSGAHAQKICKIMDQAITVGAPVIGLNDSG 162GARIQEGVESLAGYA-----DIFLRNVTA
PaGCCb_   80  LHD----DKDGTQ 88AGGGIIAGIGYIAGVRCLVSASNSAIKGGTISPTGLKKTLRLQQIAMENKLPVVTLTESG 148GANLN-YAAEIFVEG---ARGFANQARISA
CmGCCb_   80  LDDP---NPDTSI 89PGGSLVAGIGFVCGVRCMVLATDSGIDAGAMTEAGNLKLMRCQDIALENRLPLIHLVESA 149GANLRKYRVEKFVRG---GTIFYNLARLSA
AfGCDa_   87  GNKN--------- 90GSVAIVKGLGRVNGKWCVVVASDNKKLAGAWVPGQAECLLRASDTAKTLHVPLVYVLNCS 150GVKFD-EQEKVYPNRRGGGTPFFRNAELNQ


PaMCCb_   176 RGIPQIAVVMGSCTAGGAYVPAMSDETVMV 205REQATIFLAGPPLVKAATG----------------EVVSAEELGGADVHCKVSGVADHY 248AEDDDHALAIAR
RdPCCb_   155 GVVPQISMIMGPCAGGAVYSPAMTDFIFMV 184KDSSYMFVTGPDVVKTVTN----------------EQVSAEELGGATTHTRKSSVADAA 227FENDVEALAEVR
HsMCCb_   203 SKNIAQIAVVMGSCTAGGAYVPAMADENIIV 233RKQGTIFLAGPPLVKAATG----------------EEVSAEDLGGADLHCRKSGVSDHW 276ALDDHHALHLT
HsPCCb_   187 SGVIPQISLIMGPCAGGAVYSPALTDFTTFMV 217KDTSYLFITGPDVVKSVTN----------------EDVTQEELGGAKTHTTMSGVAHRA 260FENDVDALCNL
PaGCCb_   175 MGIPQVTVVHGSSTAGGAYQPGLSDYVVVV 204RGKAKMFLAGPPLLKAATG----------------EIASDEELGGAELHAQVAGTAEYL 247AENDADGVRLAR
CmGCCb_   177 AGLPVITVVHGSSTAGGAYMPGLSDYVVMV 206RKRARAFLAGPPLLKAATG----------------EIATDEELGGADLHATVSGLAEYL 249AEDDEHAIATAR
AfGCDa_   180 LGIPVIVGIYGTNPAGGGYH-SISPTVIIA 208HEKANMAVGGAGIMGGMNPKGHVDLEYANEIADMVDRTGKTEPPGAVDIHYTETGFMREV 268YASEEGVLEGIK


```
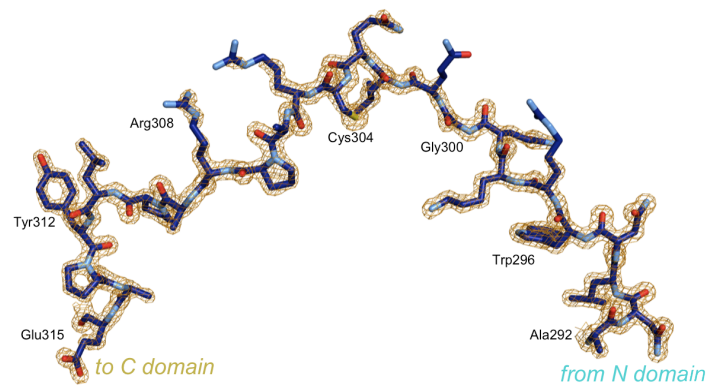
Linker

```
PaMCCb_   261 RCVANLNWRKQGQLQ-CRAPRAPLYPAEELYGVIPADSKQPYDVREVI 307ARLVDGSEFDEFKALFGTTLVCGFAHLHGYPIAILANN-------------------G
RdPCCb_   240 RLVDFLPLNNREKPPVRPFFDDPDRIEPSLDTLVPDNPNTPYDMKELI 287HKLADEGDFYEIQEEFAKNIITGFIRLEGRTVGVVANQP-------------LVLAG
HsMCCb_   288 RKVVRNLNYQKKLDVT-IEPSEEPLFPADELYGIVGANLKRSFDVREVI 335ARIVDGSRFTEFKAFYGDTLVTGFARIFGYPVGIVGNN------------------
HsPCCb_   272 RDFFNYLPLSSQDPAPVRECHDPSDRLVPELDTIVPLESTKAYNMVDII 320HSVVDEREFFEIMPNYAKNIIVGFARMNGRTVGIVGNQP-------------KVAS
PaGCCb_   260 EIVGMLPWNAQLPARPARSWREPLYPVEELGGVVPADPKKPYDVREIV 307ARIADGSEFLDFKNEFDGQTVCGHLRIEGHACGLIGNN-------------------G
CmGCCb_   262 DIVASLDW-PRVDQTPPRPARAPKLPAAELEGVMTLDHKRPVDMREVI 308ARLVDDSAWLPFKPDYGPGTVCGHARIEGHAVGFIANN-------------------G
AfGCDa_   281 KYVGMLPKYDPEFFR-VDDPKAPAFPADDLYSMVPLNDKRAYDIYNVI 327ARLFDNSELHEYKKGYGPEMVTGLAKVNGLLVGVVANVQGLLMNYPEYKAAGSVGIGG


PaMCCb_   347 IL 348FAEAAQKGAHFIELACQRGIPLLFLQNITGFMVGQKYEAGGIAKHGAKLVTAVACARVPK 408FTVLIGGSFGAGNYGMCG--RAYDPRFLWMWPNARIGVMG
RdPCCb_   332 CL 333DIDSSRKAARFVRFCDAFEIPLLTLIDVPGFLPGTSQEYGGVIKHGAKLLYAYGEATVPM 393VTVITRKAYGGAYVVMSS--KHLRADFNYAWPTAEVAVMG
HsMCCb_   374 GVL 376FSESAKKGTHFVQLCCQRNIPLLFLQNITGFMVGREYEAEGIAKDGAKMVAAVACAQVPK 436ITLIIGGSYGAGNYGMCG--RAYSPRFLYIWPNARISVM
HsPCCb_   364 GCL 366DINSSVKGARFVRFCDAFNIPLITFVDVPGFLPGTAQEYGGIRHGAKLLYAFAEATVPK 426VTVITRKAYGGAYDVMSS--KHLCGDTNYAWPTAEIAVM
PaGCCb_   347 PI 348TPQGAAKAAQFIQLCEQSNTPLLFLHNTTGFMVGTESERQGVIKHGSKMIQAVANARVPK 408LTLVVGGSYGAGNYAMCG--RGLDPRFIFAWPNSRTAVMG
CmGCCb_   348 PI 349DPAGATKAAQFIQACNQSGTPIVFLQNTTGFIVGKASEEAGMIKHGSKMIQALSNSTVPH 409VTLYCGASFGAGNFGMCG--RGFHPRFCFSWPNARTAVMG
AfGCDa_   386 KL 387YRQGLVKMNEFVTLCARDRLPIVWIQDTTGIDVGNDAEKAELLGLGQSLIYSIQTSHIPQ 447FEITLRKGTAAAHYVLGGPQGNDTNAFSIGTAATEIAVMN


PaMCCb_   447 GEQAAGVLAQVKREQAERAG 466QQLGVEEEAKIKAPILEQYEHQGHPYYSSARLWDDGVIDPAQTREVLALALSAALNAPIE 526PT---AFGVFRM----------
RdPCCb_   432 AKGATEIIHRGD-------- 443----LGDPEKIAQHTADYEERFANPFVASERGFVDEVIQPRSTRKRVARAFASLRNKSVQ 499PMWKKHDNIPL-----------
HsMCCb_   474 GGEQAANVLATITKDQRAREG 494KQFSSADEAALKEPIIKKFEEEGNPYYSSARVWDDGIIDPADTRLVLGLSFSAALNAPIE 554KT---DFGIFRM---------
HsPCCb_   464 GAKGAVEIIFKG--------- 475------HENVEAAQAEYIEKFANPFPAAVRGFVDDIIQPSSTRARICCDLDVLASKKVQ 528RPWRKHANIPL----------
PaGCCb_   447 GAQAGKVLRIVTEEKHAKEG 466KEADPKMLEMLETVTAQKLDSQSTALYGTASLWDDGLVDPRDSRRLLGYLLDICAEAEAR 526PLKGNSFGVARF----------
CmGCCb_   448 GEQAAMTLEIVARQQAARKG 467VPVDEAALAAQTAEIVANFERQGSAFVTSGLLLDDGVIDPRDTRAVLAFVLATAREAAAR 527TPRAMQFGVARF----------
AfGCDa_   488 GETAATAMYSRRLAKDRKAG 507--KDLQPTIDKMNNLIQAFYTKSRPKVCAELGLVDEIVDMNKIRGYVEAFTEAAYQNPES 565ICPFHQMILPRAIREFETFVKK
```
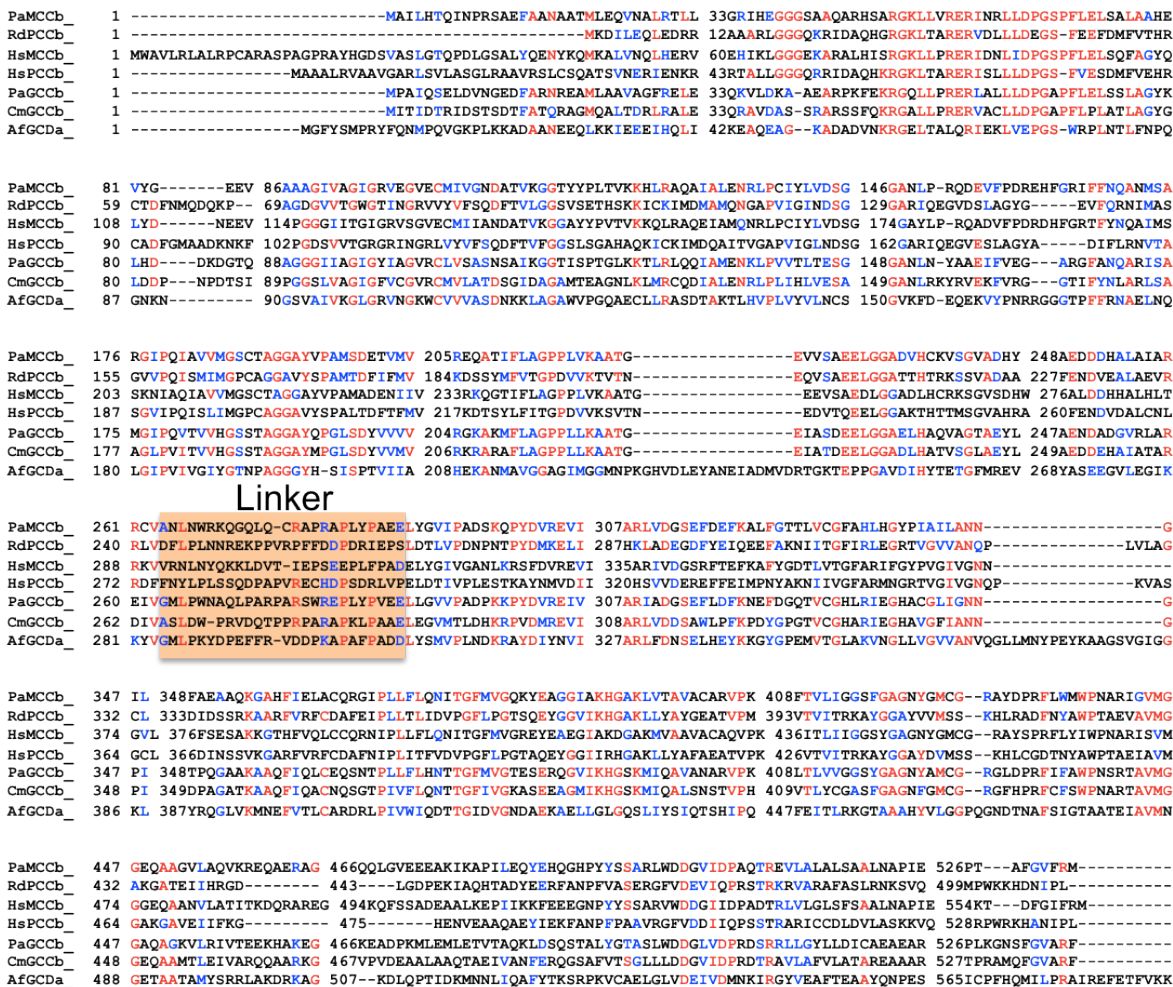
Figure 5. Sequence alignment of various carboxyltransferase (CT) domains. The sequences of β subunits from various acyl-CoA carboxylases and the α subunit of glutaconyl-CoA decarboxylase (GCDα), which also recognizes an acyl-CoA substrate, are shown. The linker region is not well conserved among the enzymes.

Instead, the domain swap is a result of a <u>connectivity difference</u> between the N and C domains. A 60° rotation of either hexamer around its threefold axis places the N and C domains at equivalent positions to those of the other hexamer. However, the connection between the domains runs in opposite directions, and is thusly indicated by the arrows in Figure 3. In our structure, the electron density for the linker in PaMCCβ is clearly defined at 1.5-Å resolution (Figure 4). This linker is present in all the acyl-CoA-recognizing subunits of biotin-dependent carboxylases (Figure 5). Although the length of the linker is essentially constant between the

enzymes, its sequences are not highly conserved. This suggests that the linker is not well-structured and functions as a simple and flexible connection between the two domains.

One explanation for the 'swapped' domains in PaMCCβ is the presence of a long (25-residue) helix at the N-terminal end of the N domain (Figure 3). This helix falls across the outer edge of the corresponding C domain, and may be involved in stabilizing the unique domain connectivity in MCCβ. In our structure of PaMCCβ, there are several points of close contact that can be attributed to hydrophobic and van der Waals interactions. There are no ion pairs observed between the N-terminal helix and the C domain.

One approach to assessing the role of the N-terminal helix is to generate a series of truncation mutants within the motif, and observe the effects of the mutations on the structure of the MCCβ hexamer. If a mutant assumes the domain organization of PCCβ, then the helix can be assumed to possess stabilizing interactions with the C domain. To date, two mutants have been made: the M22 mutant is missing the N-terminal one-third of the helix, and the N27 mutant is missing the N-terminal half. Both mutants were expressed in the insoluble fraction of the *E. coli* cell lysate, preventing further studies. This suggests that while the helix has not yet been implicated in the domain swap, its presence is essential to allow for proper folding and assembly of the PaMCCβ subunits.

3.4.2 Consequences of the domain swap on the CT active site

The initial incentive for studying MCCβ was to identify the molecular basis for substrate recognition, and how the elements governing its substrate preferences compared to those of PCCβ. (For reference, the structures of 3-methylcrotonyl-CoA and propionyl-CoA are shown in Chapter II.) Our efforts to produce a co-crystal of MCCβ in complex with its native substrate

were unsuccessful; therefore, we prepared a model of the PaMCC β₂ dimer with the bound positions of crotonyl-CoA from the alpha subunit of *Clostridium symbiosum* glutaconyl-CoA decarboxylase (GCDα) [20], as shown in Figure 6. GCDα shares 26% sequence identity with PaMCCβ and also features the same domain connectivity. (The binding of glutaconyl-CoA to GCDα is the first step of the decarboxylation reaction, and for this reason it is referred to as the α subunit of the holoenzyme. The biotin-dependent carboxylases bind acyl-CoA substrates during the 2nd reaction, and their β subunits are named accordingly.)
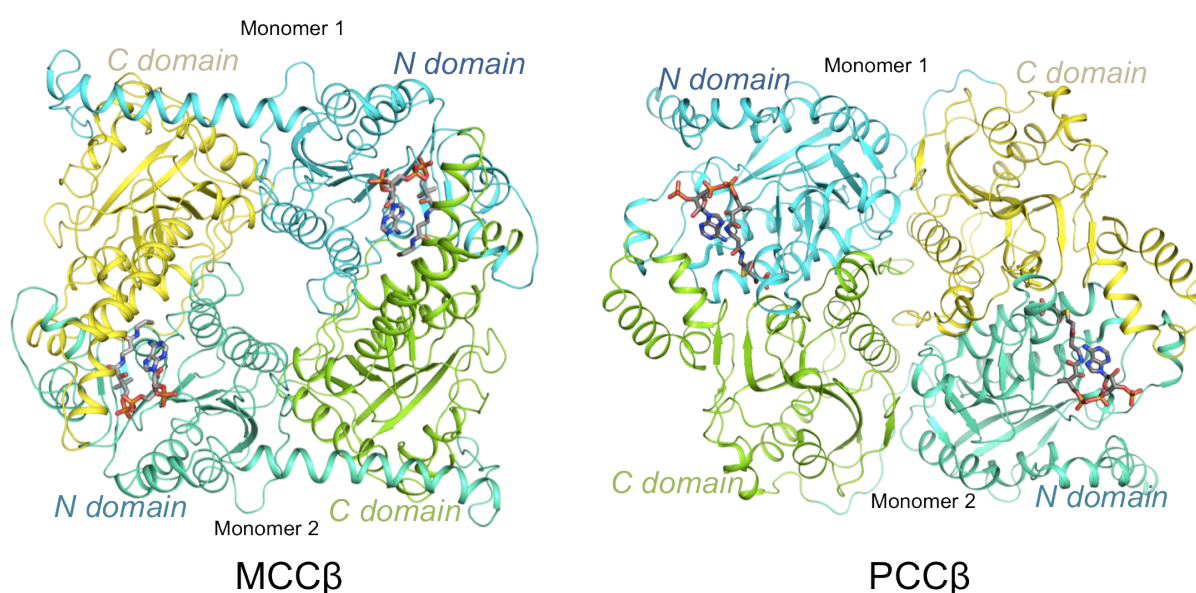
Figure 6. Schematic representations of β₂ dimers from MCC (left) and PCC (right). The MCC β₂ dimer is shown with the bound positions of crotonyl-CoA in complex with the α subunit of glutaconyl-CoA decarboxylase (GCDα) [20], and the PCC β₂ dimer is shown in complex with the modeled positions of CoA in complex with transcarboxylase 12S [21].

The resulting structural model revealed another consequence of the N/C domain swap, which was a swap in the positions of the CoA binding sites between MCCβ and PCCβ. Although the active sites are still formed at the interface of N and C domains from opposing protomers, their overall positions within the hexamer are different. From a biochemical perspective, this active-site rearrangement does not have significant consequences on catalysis, as MCC holds

important roles in intermediary metabolism and its robust activity has been extensively documented in many species. Therefore, MCC's functional activity is not compromised because of its unique β-subunit organization.

From a structural perspective, however, there is a strong possibility that the active-site swap precludes the MCC holoenzyme from possessing the same overall architecture as PCC. The rationale for this lies in the precise architecture of the catalytic components, and their co-evolution over time. In other words, the BCCP domain of PCC has evolved to 'expect' the CT active site at a specific location within the β_6 hexamer. The structure of the PCC holoenzyme shows six BCCP domains, all bound in identical conformations to the CT active site of the nearest PCCβ protomer. If the CT active site is moved to MCC's location (which is related to PCC by a 60° rotation around the ring), the configuration of PCC's BC/BCCP is unlikely to 'find' the new location, unless the positions of the BC/BCCP are moved as well. To investigate this hypothesis, a crystal structure of the MCC holoenzyme was pursued.

3.5 Structure of the 750-kDa $\alpha_6\beta_6$ holoenzyme of 3-methylcrotonyl-CoA carboxylase

The MCC holoenzyme from *Pseudomonas aeruginosa* (PaMCC) was produced as a bicistronic expression construct, similar to the PCC holoenzyme (Chapter II). The enzyme was readily purified and produced thin plate-shaped crystals. One crystal produced a data set diffracting to 3.5-Å resolution, and the resulting structure is shown in Figure 7.
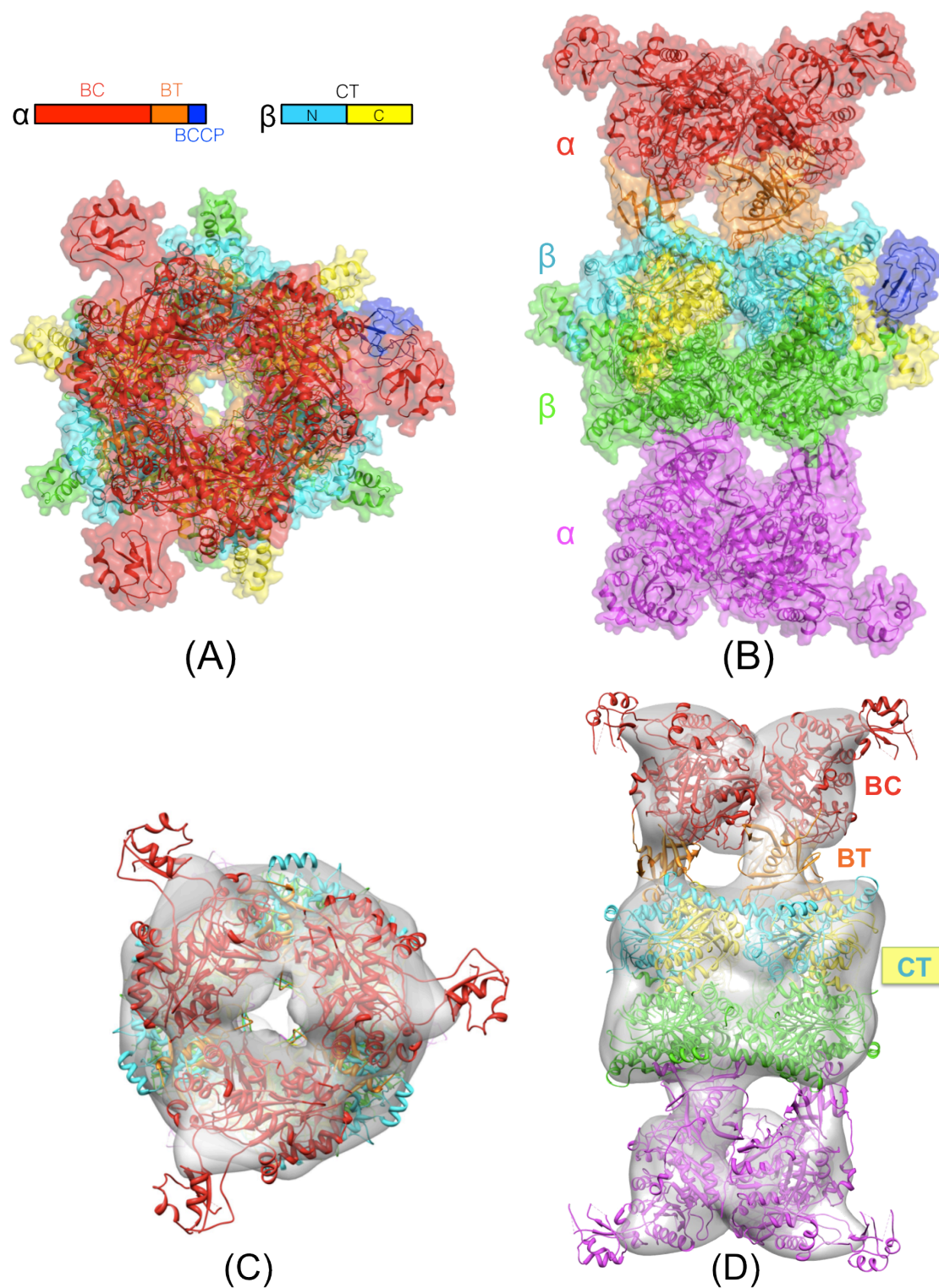
Figure 7. Structure of the MCC holoenzyme. (A) A view looking down the threefold symmetry axis of *P. aeruginosa* 3-methylcrotonyl-CoA carboxylase [22]. (B) A view looking down the twofold symmetry axis. The gray envelopes in (C) and (D) are cryo-EM reconstructions of PaMCC contoured at 12-Å resolution, with the crystal structure of the holoenzyme docked within, and the views are presented in the same orientations as (A) and (B). The crystal structure figures were produced with PyMOL [23] and the cryo-EM figures were generated in Chimera [24].

Like PCC, the structure of the PaMCC holoenzyme is an $\alpha_6\beta_6$ dodecamer, 750 kDa in size, displays 32 symmetry, and also assumes a cylindrical shape. The β_6 hexamer comprises the central core, and the subunit architecture also follows an $\alpha_3\beta_3\beta_3\alpha_3$ arrangement. Only a single ordered BCCP was observed in the structure of PaMCC complexed with CoA, and the domain is disordered in the PaMCC free-enzyme structure.
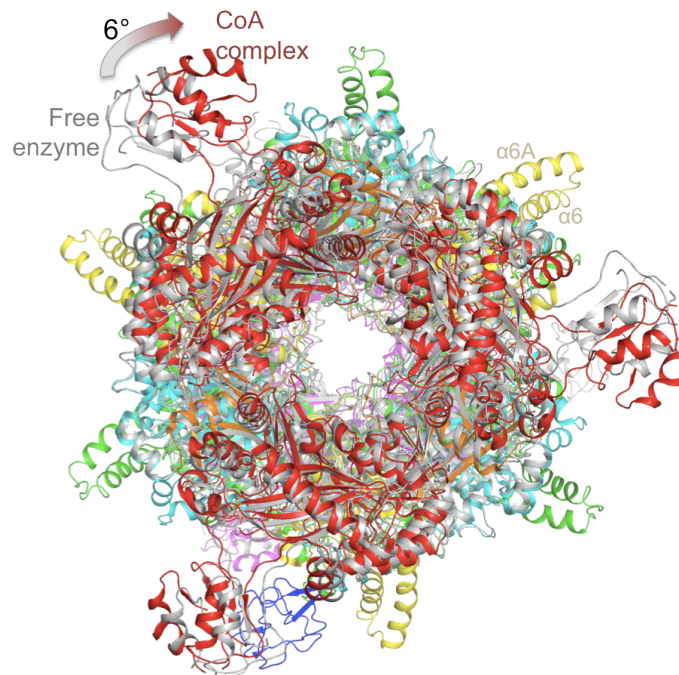

Figure 8. CoA binding induces minor conformational changes in the structure of the MCC holoenzyme. The holoenzyme structures of the MCC free enzyme (gray) and CoA complex (color) are superimposed at the level of the β_6 hexamer. Differences in the two structures are evident in the positions of the B domain of BC, the $\alpha6/\alpha6A$ helices in the β subunit, as well as the absence of BCCP in the free-enzyme structure.

The binding of CoA does not have significant effects on the overall architecture of the MCC holoenzyme. There is, however, a minor ($\sim6°$) rotational difference in the positions of the α subunits with respect to the crystallographic threefold axis, upon CoA binding (Figure 8). In addition, the free-enzyme structure exhibits a few sites with disordered segments, including the $\alpha6$-$\alpha6A$ extensions of the β subunit's C domain (viewed as the yellow and green protrusions from the hexamer) and within the distal B domain of the BC subunit (viewed as the unconnected

red and magenta strands in Figures 7B and 7D). In general, however, the structures of the CoA complex and the free enzyme are very similar, and may represent transitional stages within the overall MCC reaction. The subsequent MCC holoenzyme structures shown in this Chapter are of the CoA complex (3U9S) unless otherwise noted.

Our collaborators in the laboratory of Dr. Z. Hong Zhou (UCLA) also produced a cryo-electron microscopy (cryo-EM) reconstruction of PaMCC at 12-Å resolution, and the crystal structure docks very well into the cryo-EM envelope (Figures 7C and 7D). The cryo-EM structures do not show the BCCP domain, which may be due to the domain's inherent flexibility. The excellent agreement between the structures indicates that MCC maintains the same conformation in both the solution state and within the protein crystal.
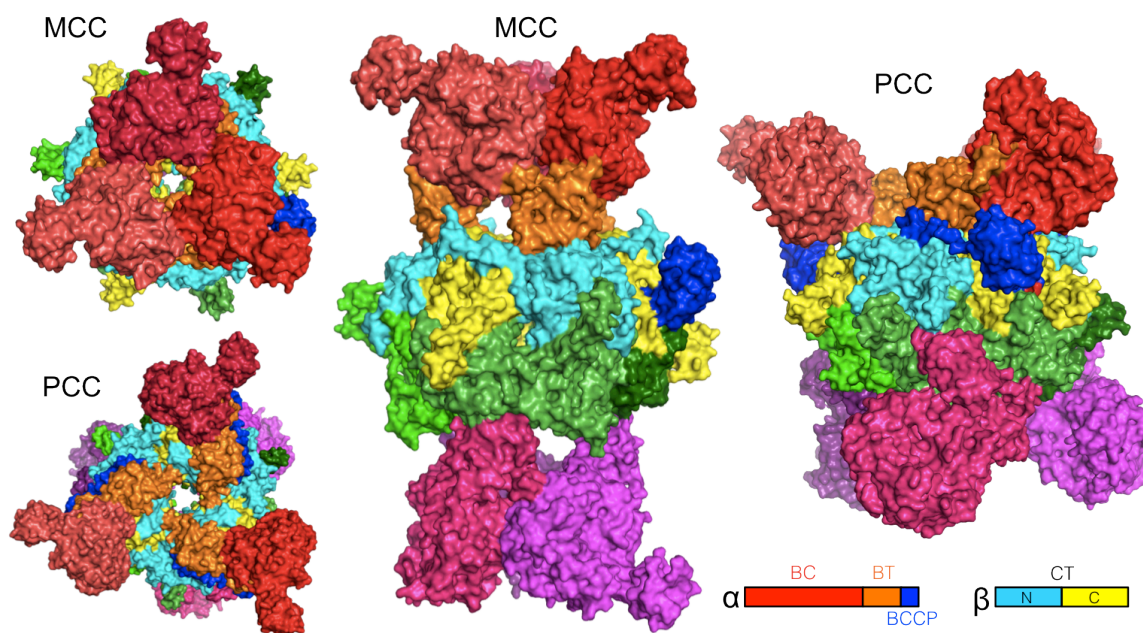

Figure 9. Comparing the MCC and PCC holoenzymes. The crystal structures of the MCC and PCC holoenzymes are rendered as molecular surfaces, and equivalent domains are colored in similar tones. Only one BCCP was identified in the structure of PaMCC. Although the two enzymes are very similar in terms of sequence conservation, domain organization, and function, their three-dimensional structures are distinct from each other.

Although there are a number of structural similarities shared by the MCC and PCC holoenzymes, their overall three-dimensional architectures are very different (Figure 9).

The arrangement of α subunits around the hexameric core is entirely unique between the two enzymes. While the α subunits of PCC are monomeric and are splayed far apart from each other, the α subunits of MCC form a single trimeric unit at the top and bottom of the holoenzyme structure. The forces maintaining the trimeric association are relatively weak in nature; biochemical investigations of MCCα show that it does not form a stable oligomeric complex in solution, and the results of size-exclusion chromatography indicate that the size of the purified protein is equivalent to that of a single α monomer (unpublished studies).

In the MCC holoenzyme structure, the BC/BT domains essentially sit atop the N-domain of the underlying β subunit. A single BCCP domain was observed in the holoenzyme structure, and also binds a CT active site. Interestingly, the binding mode of this BCCP is nearly identical to the one observed in PCC – but because of the swapping of the positions of the N- and C-domains, the BCCP in MCC contacts a *different* β_2 dimer than the one above which its BC/BT domains are located. Therefore, a single round of catalysis in MCC involves one α subunit and two β_2 dimers (one to form the 'foundation' under the BC/BT domains and another to form the CT active site). In PCC, a corresponding round of catalysis involves one α subunit and one β_2 dimer, because this dimer provides both the 'foundation' and CT active site. Therefore, an $\alpha_2\beta_2$ tetramer of PCC is probably catalytically active, while such a version of MCC is not.

The dimensions of the MCC holoenzyme are also elongated with respect to PCC; the formation of the α-subunit trimers extends the length of the MCC holoenzyme to approximately 210 Å, while the vertical dimension of PCC measures approximately 160 Å. The size of the β_6 hexamer is unchanged between the two structures, with a diameter of approximately 140 Å. In addition, although the active sites of MCCβ are located in different positions than those of PCCβ, both holoenzyme structures feature at least one BCCP bound to the CT active site. Finally, the

structure of the MCC holoenzyme also reveals the presence of a BT domain, which was first identified in our structure of PCC (Chapter II).

3.5.1 The BT domain of MCC

MCC also features a BT domain for mediating BC-CT interactions, and its overall fold resembles a short α-helix surrounded by a highly curved, 7-stranded β-sheet (Figures 10A-B). The BT domain of PCC, in contrast, features a long helix surrounded by an 8-stranded β-barrel (Figure 10C). Both BT domains possess a distal 'hook' that anchors the α subunits into the β hexamer, although the conformation of MCC's hook is quite different from that of PCC.
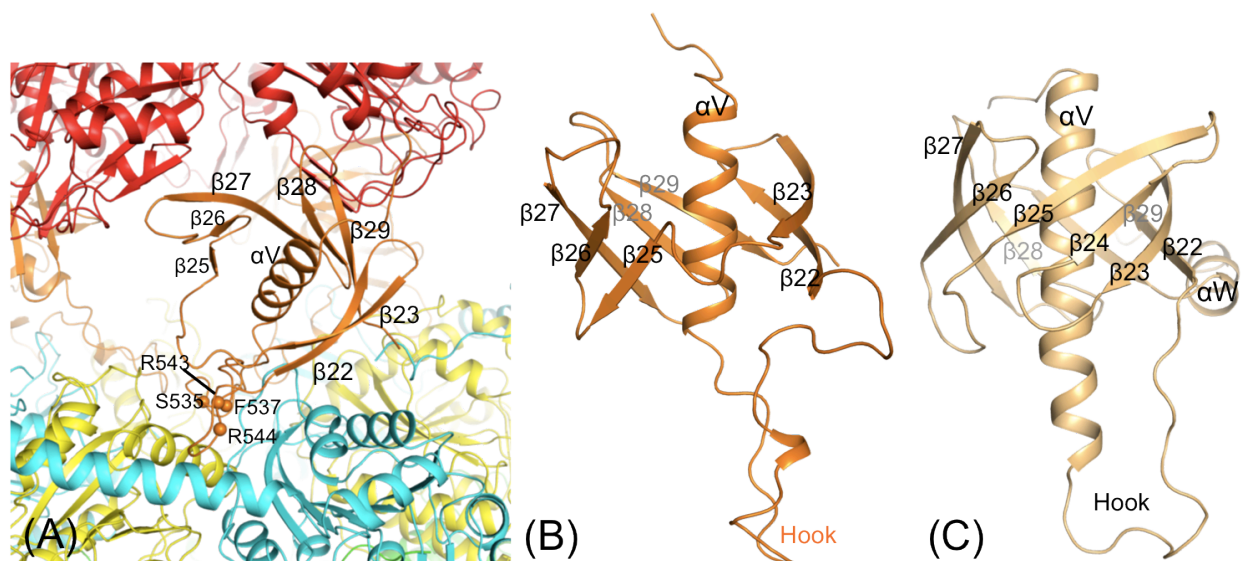
Figure 10. The BT domain. (A) Location of the BT domain within the MCC holoenzyme. The sites of four 'hook' residues proposed to contribute to holoenzyme integrity are indicated with spheres. (B) Schematic representation of the BT domain from MCC. (C) Schematic representation of the BT domain from PCC.

Of the approximately 3,000 Å^2 of buried surface area between each α subunit and the β_6 hexamer, approximately 55% of the interactions are mediated by the BT domain. The BCCP domain, when bound to the active site of the β subunit, contributes approximately 23% of the interactions (as measured by the amount of buried surface area between the two domains). Interestingly, there is no direct contact between the BC domain and the β_6 hexamer in the

structure of the MCC holoenzyme (the two are separated by 18 Å), which is very different from the BC domains in PCC.

The 'hook' feature in BT interacts with both the N and C domains of the β subunit, and the conformations of its component side chains appear to make several ion-pair interactions with the side chains from the β_6 hexamer. In order to understand the contribution of these 'hook' residues to BT's function in maintaining α-β association, a series of non-conservative mutations were generated at the sites of selected residues, and the resulting effects on holoenzyme stability were measured by a pull-down experiment. (In the MCC holoenzyme construct, only the β subunit carries the hexahistidine tag. If the α subunits associate with the β hexamer to form an intact holoenzyme, the entire $\alpha_6\beta_6$ complex can be isolated using the β-His$_6$ tags. If the α subunits fail to bind the β subunits, then only the β subunits alone will be purified by nickel-affinity chromatography.)
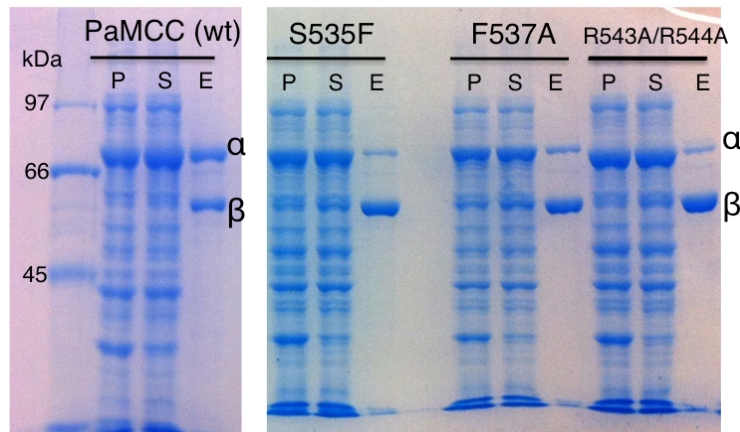

Figure 11. Mutations in the BT hook structure can destabilize the MCC holoenzyme. Lane headings indicate P for the *E. coli* cell pellet, S for the supernatant fraction, and E for the eluted protein that was isolated using nickel-charged affinity beads.

The results of the pull-down experiment implicate Ser535, Phe537, Arg543, and Arg 544 in maintaining the integrity of the MCC holoenzyme. Figure 11 demonstrates that the levels of α-subunits co-eluted with MCCβ are significantly reduced compared to the wild-type levels, which

represent the stoichiometric ratios of α to β subunits in native MCC. From a functional perspective, any of these mutations can severely inhibit MCC holoenzyme integrity, and in turn, MCC's catalytic activity.

3.5.2 The carboxyltransferase active site

The structure of PaMCC lent considerable insight into the consequences of the domain swap on the active site locations, and revealed that the active sites of the α and β subunits are separated by 80 Å, which to date is the largest distance between the two active sites of a biotin-dependent carboxylase. More important, Figure 12 reveals that for a given α subunit, its BT domain primarily contacts the closest β subunit, but its BCCP domain accesses the active site of an *adjacent* β subunit.
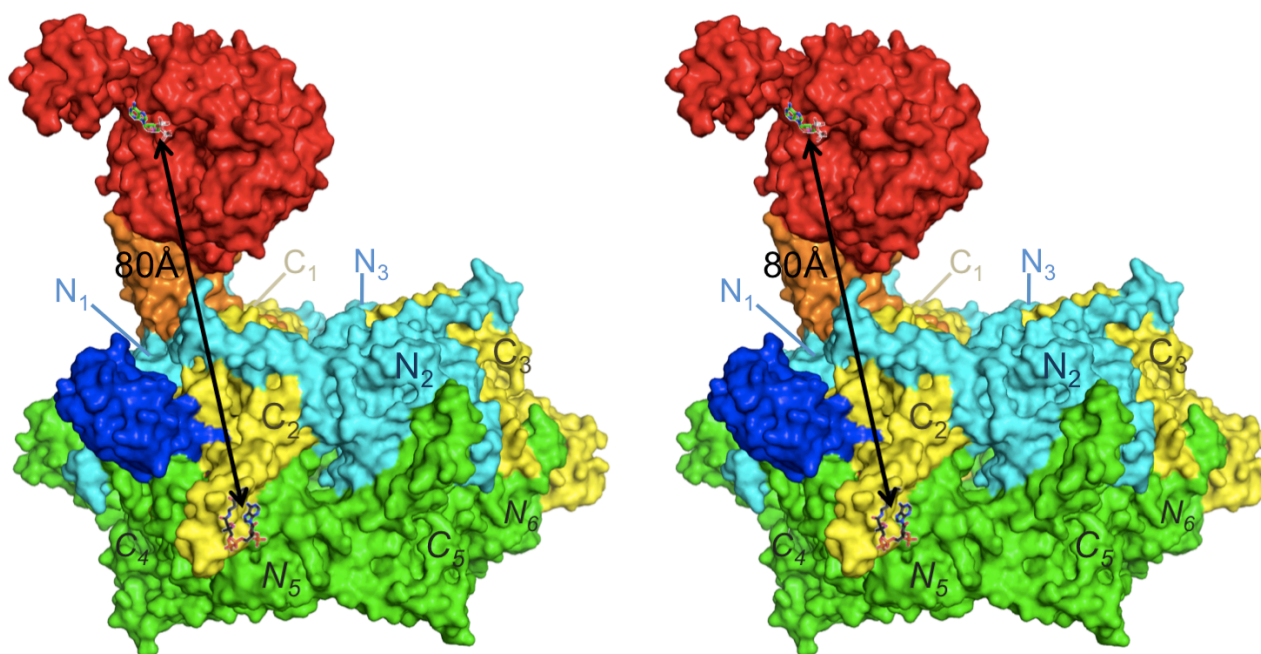

Figure 12. The BC and CT active sites of MCC. Stereo view of one α subunit and the β_6 hexamer. The BCCP domain (in blue) must translocate a considerable distance to access the two active sites. The hexamer is viewed from the side, in the same manner as Figure 6.

However, the effects of the active site swap on communication between the α and β subunits was not clear. In particular, it was not known how BCCP recognizes the CT active site in the context of a novel MCC architecture. A detailed look at the architecture of the CT active site and its interactions with BCCP is shown in Figure 13.
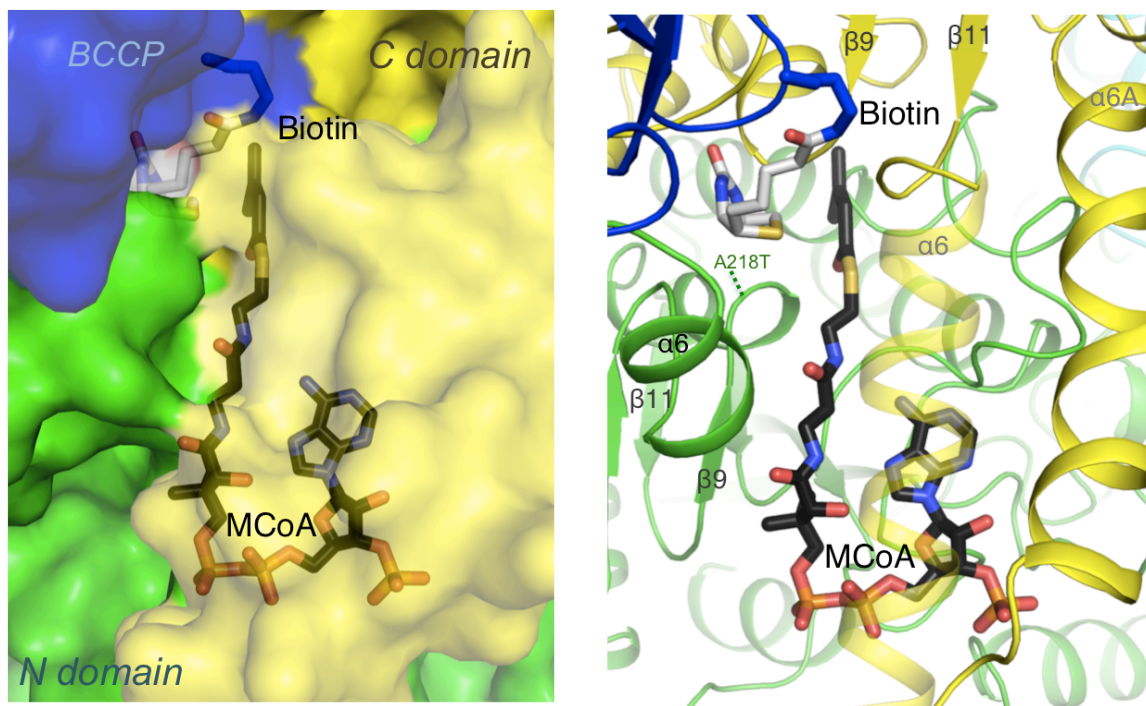

Figure 13. The CT active site. (left) The substrate-binding pocket is buried deep in the groove formed by the N and C domains of different β subunits. The overlaying portions of the C domain are rendered partially transparent to reveal the positions of biotin and 3-methylcrotonyl-CoA (MCoA). (right) Detailed view of the CT binding site. Helix α6 is rendered partially transparent to show the MCoA. Although CoA was observed in the MCC holoenzyme structure, the additional acyl groups were modeled using the binding mode of crotonyl-CoA in complex with GCDα [20].

Compared to PCC, the positions of biotin and 3-methylcrotonyl-CoA are buried much deeper within the CT active site of MCC. There is a shift in the positions of the α6 and α6A helices, such that they form a makeshift lid over the active site. In addition, several other conformational shifts are observed in the vicinity of 3-methylcrotonyl-CoA's acyl group, which is consistent with the hypothesis that a larger substrate necessitates a larger binding pocket. The

γ-carbon of 3-methylcrotonyl-CoA, which is the target of MCC carboxylation, is located approximately 6 Å away from the N1' atom of biotin. This distance is sufficient to place the γ-carbon within reach of carboxybiotin and allow for catalysis. The binding mode of biotin in the structure of PCC reveals that its biotin N1' atom is not buried as deeply within the active site, and therefore, PCC is unlikely to accommodate 3-methylcrotonyl-CoA as a substrate.

3.6   Effects of disease-causing mutations

The elucidation of the MCC holoenzyme structure provides a framework on which to study the molecular consequences of disease-associated gene mutations. Depending on the location of the mutations, their effects may range from reduced catalytic efficiency to disruption of the holoenzyme structure. There are approximately three dozen missense mutations in human MCC that have been identified and found to correlate with the genetic disease methylcrotonylglycinuria. These mutations have been mapped to the structure of PaMCC (Figure 14). For the most part, the residues that are implicated in humans are also conserved in *P. aeruginosa*, which may testify to their importance for proper MCC activity.
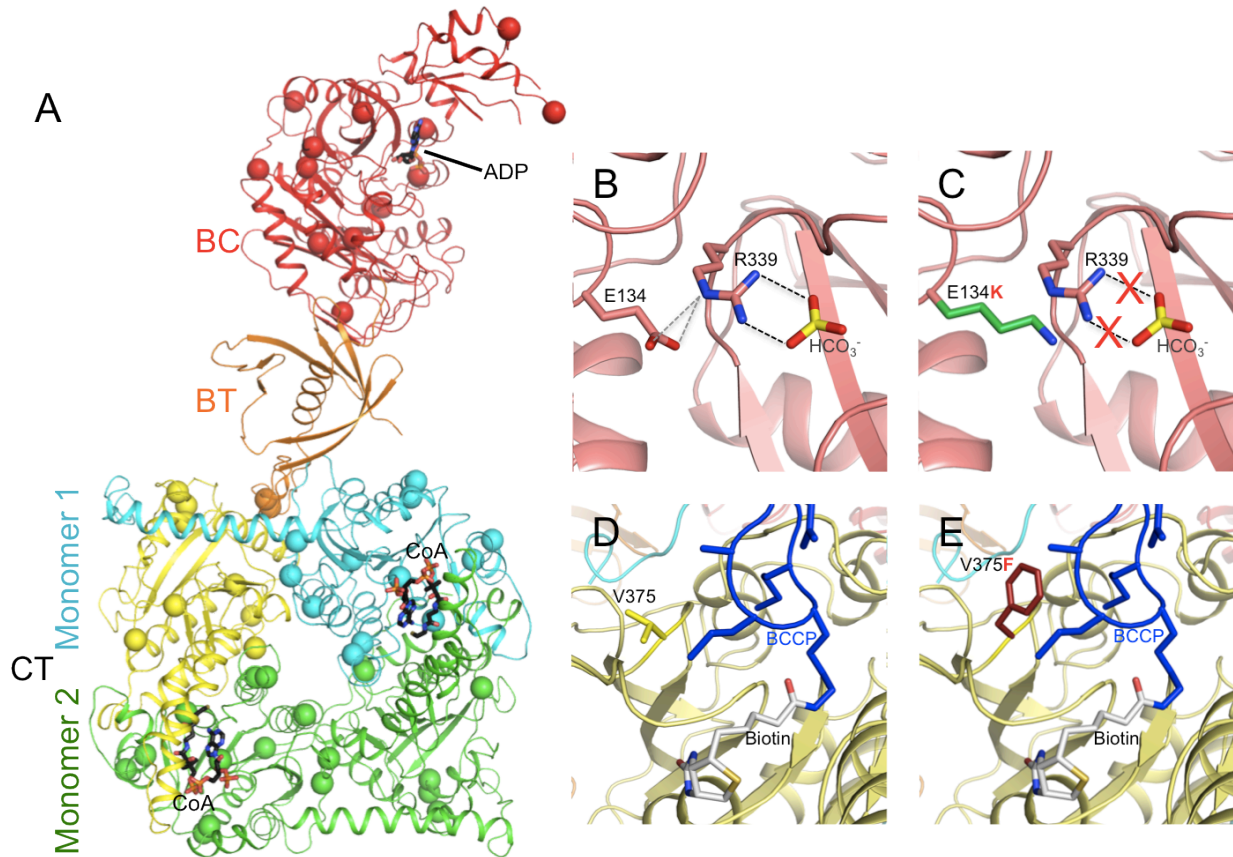
Figure 14. Locations of the BC and CT active sites and disease-associated gene mutations in the MCC holoenzyme. (A) Schematic representation of one α subunit and a β₂ dimer with the bound positions of ADP from *E. coli* ACC [26] and CoA. The locations of missense mutations associated with the human disease methylcrotonylglycinuria are indicated with spheres. Panels (B) and (C) depict the consequences of the E134K mutation in the BC domain, and (D) and (E) indicate likewise for the V375F mutation in the CT domain.

One example of a mutant potentially disrupting BC catalysis is E134K. Based on the structure of *E. coli* BC in complex with ADP, biotin, bicarbonate, and Mg^{2+} [26], a catalytic scheme for BC was proposed. In this mechanism, Arg292 was hypothesized to stabilize the bicarbonate ion (the source of CO_2 for the overall carboxylation reaction) prior to catalysis. Arg292, in turn, is held in a stable conformation by Glu87, and their proposed ion-pair interaction is 3 Å in length. Based on sequence and structural alignments, the corresponding residues in PaMCC are Arg339 and Glu134. Figures 14B and 14C illustrate the potential consequences of an E134K mutation. The replacement of Glu134 by a positively charged lysine

residue eliminates the ion-pairing that stabilizes Arg339, and by extension, bicarbonate. As a result, the bicarbonate ion loses a major stabilizing force in its pre-catalytic positioning, and the overall catalytic efficiency is likely reduced.

Within the CT domain, the V375F mutation (Figures 14D-E) does not disturb electrostatic interactions. Rather, the introduction of a bulky phenylalanine side chain is thought to introduce steric clashes with the side chains of BCCP. This may compromise the ability of BCCP-biotin to access the CT active site, thus affecting catalysis. Val375 is well conserved among the β subunits of various MCCs, and the V375F mutation has been found to correlate with methylcrotonylglycinuria in several patients. By engineering the V375F mutation into PaMCC, it is possible to observe whether catalysis is affected, and a structural model may reveal an alternative placement for BCCP if it cannot access the CT binding site. Additional discussion of this mutation is presented in the following section.

It is important to note that there is a wide spectrum of phenotypes associated with methylcrotonylglycinuria, even among patients with apparently identical disease mutations. As such, clinical data have not demonstrated a clear genotype-phenotype correlation for MCC deficiency [27, 28]. Nonetheless, the structures of MCC and related holoenzymes still provide a valuable foundation for studying the relationships between disease mutations and their resulting effects on enzymatic stability and/or function, and offer the possibility of designing therapeutic approaches to counter the effects of methylcrotonylglycinuria and other metabolic disorders.

3.7   Investigating BC-BCCP interactions

In order to fully understand the two-part mechanism and the basis of BCCP translocation in biotin-dependent carboxylases, it is necessary to study the interactions of BCCP-biotin with

both the BC and CT active sites. To date, the majority of studies have observed BCCP binding the CT domain. In addition to PCC and MCC, the interactions of BCCP-biotin with the CT active sites of human and *Rhizobium etli* pyruvate carboxylase have also been described [29].

In contrast, there are no documented reports of BCCP-biotin directly interacting with the BC active site. The current knowledge of BC catalysis stems from several crystal structures of the BC domain, either alone [30], in complex with ATP analogs [31], or in complex with biotin, bicarbonate, and Mg-ADP [26]. There have also been reports of BCCP interacting with the BC domain of *R. etli* PC [32] and *E. coli* ACC [33]. However, neither structure features BCCP bound within the BC active site. To address this lack of information regarding BC-BCCP interactions, we pursued a MCC mutation that would 'coax' the BCCP domain out of its current location in CT active site, and hopefully into the BC active site.

3.7.1   Preliminary results for a BCCP 'eviction mutant'

It is not known why BCCP possesses an apparent preference for the CT domain in the holoenzyme structures of PC, PCC, and MCC. After all, the mobile domain should exhibit similar affinities for the BC and CT active sites to promote efficient catalysis. Structural studies of the CT active site have identified a number of conserved non-covalent interactions that stabilize CT-BCCP binding. Mutations at these sites may destabilize BCCP from binding the CT domain – and upon its eviction from CT, BCCP may be favored to bind BC instead.

Based on the structure of the MCC holoenzyme, two disease-causing mutations in the CT active site were identified as possible stabilizers of CT-BCCP binding. The side chain of Arg218 (Figure 13) is located between 3-methylcrotonyl-CoA and the biotin group of BCCP, and the A218T mutant may prevent binding of one or both ligands. Val375 (Ile375 in PaMCC; Figure 14) is situated at the interface of the N domain of MCCβ and BCCP, and the V375F mutant may

introduce steric clashes to prevent BCCP-biotin from accessing the CT active site. To assess the effects of these mutations on MCC catalysis and integrity, several 'eviction mutants' were generated: A218T, V375F, and an A218T+V375F double mutant.
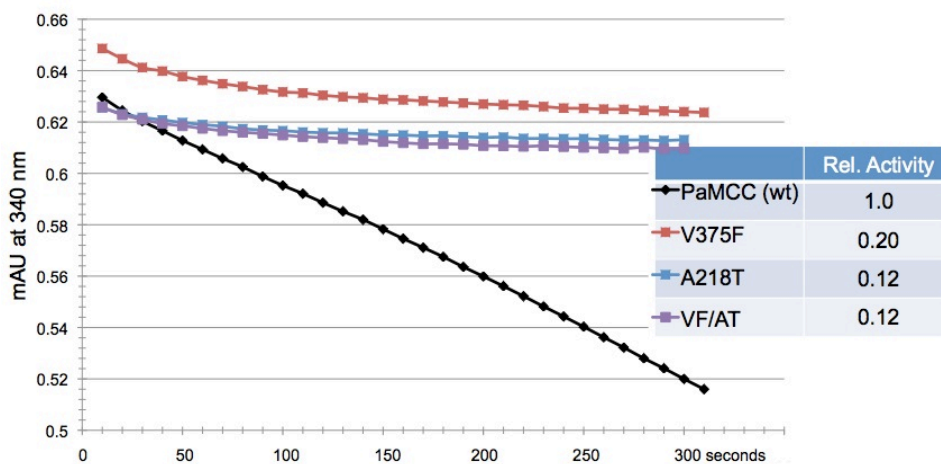

Figure 15. Kinetic assay of wild-type MCC and BCCP eviction mutants. An ATP hydrolysis assay was used to compare the catalytic activities of three MCCβ mutants against wild-type MCC. Each curve represents the average of three separate trials. The activity of wild-type MCC was arbitrarily set to 1.0, and the activities of the mutants are calculated in comparison to this value.

All three mutants were purified to homogeneity and their catalytic activities were surveyed using an ATP hydrolysis assay. Figure 15 shows that all three mutants exhibit significantly diminished catalysis compared to wild-type PaMCC. The A218T mutation proved more detrimental to MCC activity than the V375F mutation, and both A218T and the double mutant had equally low activities. With the reassurance that these mutations had significant effects on MCC catalysis, we decided to investigate the structural consequences of the mutations. In particular, we wanted to determine whether the reduced catalytic activities of the mutants were a result of impeded BCCP access to the CT active site.
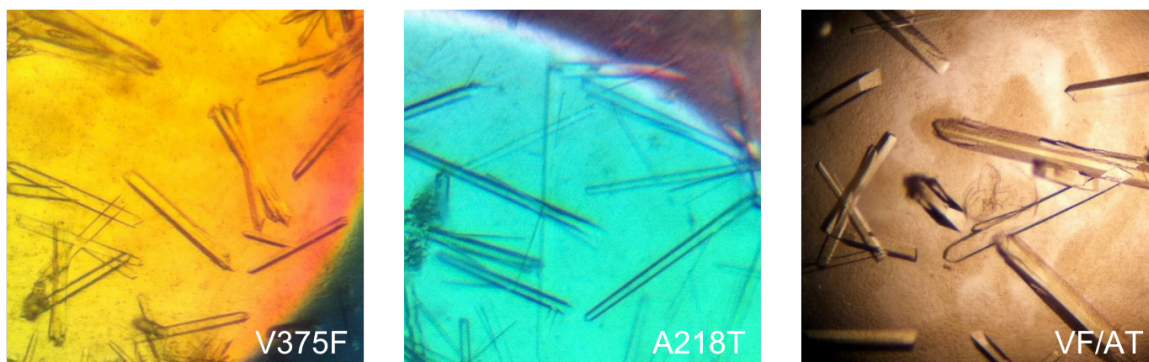
Figure 16. Crystals of BCCP eviction mutants from PaMCC. Mutations were introduced in the MCCβ subunit, with the intention of destabilizing BCCP-biotin interactions. Crystallization conditions are summarized in the Experimental Procedures.

Crystals of all three mutants were obtained using the same crystallization conditions as the wild-type MCC holoenzyme. The VF/AT double mutant crystals diffracted X-rays more strongly than the single mutant crystals. Currently, the best VF/AT crystal diffracts to approximately 5-Å resolution using a synchrotron radiation source, belongs to the $C222_1$ space group, and was indexed with approximate unit cell parameters of $a = 243$ Å, $b = 249$ Å, $c = 153$ Å, and $\alpha = \beta = \gamma = 90°$. Efforts are underway to improve the quality of these crystals.

3.7.2 Future perspectives

The primary goal for generating the VF/AT double mutant is that the BCCP domain will be destabilized from binding in the CT active site and will be evicted from this location. Ideally, the BC active site will also provide a series of non-covalent interactions to stabilize BCCP binding, and BCCP-biotin will be observed binding at the BC active site. Substrates of the BC reaction (Mg-ATP and bicarbonate) can also be added to the crystallization conditions to stabilize BCCP in the BC active site. Phosphonoacetate is a structural analog of carboxyphosphate (an intermediate of the BC reaction), and can also be used to capture BCCP-biotin in BC and prevent its translocation to the CT domain. Additional crystal optimization may

also be required; the binding of BC-BCCP may induce a global conformational change in the entire holoenzyme, thereby affecting crystal packing. If current efforts to improve the crystals' diffraction quality are not successful, then the purified VF/AT mutant will be re-tested against our collection of sparse-matrix and grid crystallization screens.

Another potential finding from the VF/AT structure is that BCCP is evicted from the CT domain, but does not enter the BC active site, and instead, settles elsewhere on the holoenzyme. This outcome has been observed previously with the structure of *S. aureus* pyruvate carboxylase (in which BCCP is binds an exo site) [29] and *R. etli* pyruvate carboxylase (in which BCCP binds BC, but not within the active site) [32].

By determining the structure of BCCP-biotin bound in the BC active site, we hope to understand the basis of BC catalysis in the context of the holoenzyme. The residues that govern BCCP and biotin binding are of particular interest, as their interactions must be specific enough to align all the reaction substrates in place for catalysis, but also transient in nature, to allow for BCCP-carboxybiotin translocation to the CT active site. In addition, the structure of BCCP-biotin bound to the BC active site will allow us to better understand the consequences of disease-associated gene mutations on the activity and architecture of the BC domain, in addition to understanding how BCCP translocation may be used in regulating the activity of the holoenzyme.

3.8   Implications of findings: two lineages of biotin-dependent acyl-CoA carboxylases

Our studies of the MCC represent the fourth reported crystal structure of a biotin-dependent carboxylase holoenzyme, and the third such structure from our laboratory. The structure of PaMCCβ revealed a surprising domain swap of the N and C domains compared to PCCβ, and this finding was not apparent from primary sequence analysis. The overall

architecture of the MCC holoenzyme is different from PCC as well, especially in the trimeric association of its BC domains, its modified BT domain, and swapping of the CT active sites. Studies to further investigate the CT active site and the interactions of BCCP in the BC domain are currently underway.

The structural knowledge garnered by the MCC and PCC holoenzymes suggest that there may be two distinct lineages of biotin-dependent acyl-CoA carboxylases (Figure 17). One lineage targets the α-carbon of saturated acids, and includes ACC and PCC. The other lineage carboxylates the γ-carbon of α-β unsaturated acids, and includes MCC, GCC (geranyl-CoA carboxylase), and GCD (glutaconyl-CoA decarboxylase). The CoA substrates of GCC and GCD feature substantially larger acyl groups, and it is expected that their corresponding binding sites in the enzymes must accommodate the increased bulk by an expansion and/or rearrangement of the active site architecture.
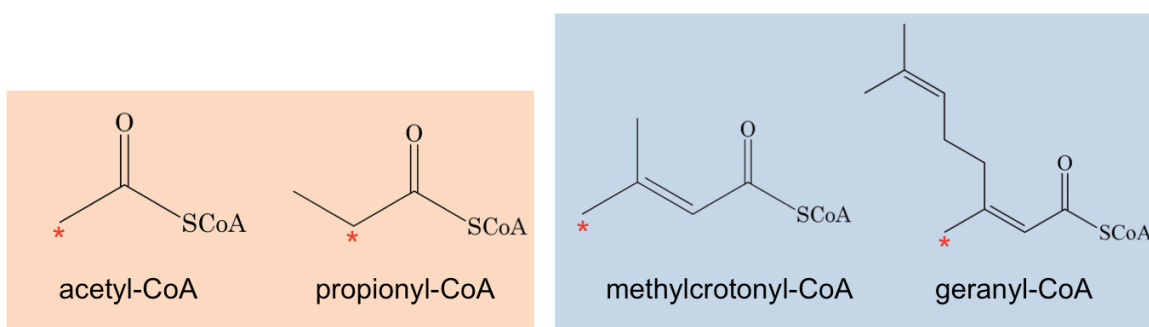

Figure 17. Two proposed lineages of acyl-CoA carboxylases. One lineage (orange) carboxylates the α-carbon of acyl-CoA substrates, while another targets the γ-carbon of the acyl-CoA. The sites of carboxylation are indicated with asterisks.

3.9   References

1.   Chu, C.-H. and Cheng, D. *Expression, purification, characterization of human 3-methylcrotonyl-CoA carboxylase (MCCC).* Protein Expression and Purification, 2007. **53**(2): p. 421-27.

2.   University of Florida, D.o.P., Division of Genetics and Metabolism.

3.   Moss, J. and Lane, M.D. *The biotin-dependent enzymes.* Adv Enzymol Relat Areas Mol Biol, 1971. **35**: p. 321-442.

4.   Höschle, B., Gnau, V. and Jendrossek, D. *Methylcrotonyl-CoA and geranyl-CoA carboxylases are involved in leucine/isovalerate utilization (Liu) and acyclic terpene utilization (Atu), and are encoded by liuB/liuD and atuC/atuF, in Pseudomonas aeruginosa.* Microbiology, 2005. **151**(11): p. 3649-56.

5.   Nikolau, B.J., Ohlrogge, J.B. and Wurtele, E.S. *Plant biotin-containing carboxylases.* Archives of biochemistry and biophysics, 2003. **414**(2): p. 211-22.

6.   Cowan, M., Packman, S., Wara, D., Ammann, A., Yoshino, M., Sweetman, L. and Nyhan, W. *Multiple biotin-dependent carboxylase deficiencies associated with defects in T-cell and B-cell immunity.* The Lancet, 1979. **314**(8134): p. 115-18.

7.   Friebel, D., Von Der Hagen, M., Baumgartner, E.R., Fowler, B., Hahn, G., Feyh, P., Heubner, G., Baumgartner, M.R., and Hoffmann, G.F. *The first case of 3-methylcrotonyl-CoA carboxylase (MCC) deficiency responsive to biotin.* Neuropediatrics, 2006. **37**(2): p. 72-78.

8.   Gallardo, M.E., Desviat, L.R., Rodr√≠guez, J.M., Esparza-Gordillo, J., P√©rez-Cerd√°, C., P√©rez, B.n., Rodr√≠guez-Pombo, P., Criado, O., Sanz, R., and Morton, D.H. *The molecular basis of 3-methylcrotonylglycinuria, a disorder of leucine catabolism.* The American Journal of Human Genetics, 2001. **68**(2): p. 334-46.

9.   Gompertz, D., Draffan, G.H., Watts, J.L. and Hull, D. *Biotin-responsive methylcrotonylglycinuria.* The Lancet, 1971. **298**(7714): p. 22-24.

10.   Huang, C.S., Sadre-Bazzaz, K., Shen, Y., Deng, B., Zhou, Z.H. and Tong, L. *Crystal structure of the alpha(6)beta(6) holoenzyme of propionyl-coenzyme A carboxylase.* Nature, 2010. **466**(7309): p. 1001-5.

11.   Wilson, K. *Preparation of genomic DNA from bacteria.* Current Protocols in Molecular Biology, 1987: p. 2.4. 1-2.4. 5.

12.   Blanchard, C.Z., Lee, Y.M., Frantom, P.A. and Waldrop, G.L. *Mutations at four active site residues of biotin carboxylase abolish substrate-induced synergism by biotin.* Biochemistry, 1999. **38**(11): p. 3393-400.

13. Otwinowski, Z. and Minor, W. *Processing of X-ray diffraction data.* Methods in Enzymology, 1997. **276**: p. 307-26.

14. McCoy, A.J., Grosse-Kunstleve, R.W., Adams, P.D., Winn, M.D., Storoni, L.C. and Read, R.J. *Phaser Crystallographic Software.* Journal of Applied Crystallography, 2007. **40**(4): p. 658-74.

15. Jones, T.A., Zou, J.Y., Cowan, S.W. and Kjeldgaard, M. *Improved methods for building protein models in electron density maps and the location of errors in these models.* Acta Crystallographica Section A: Foundations of Crystallography, 1991. **47**(2): p. 110-19.

16. Emsley, P. and Cowtan, K. *Coot: model-building tools for molecular graphics.* Acta Crystallographica Section D: Biological Crystallography, 2004. **60**(12): p. 2126-32.

17. Brunger, A.T., Adams, P.D., Clore, G.M., DeLano, W.L., Gros, P., Grosse-Kunstleve, R.W., Jiang, J.S., Kuszewski, J., Nilges, M., and Pannu, N.S. *Crystallography & NMR system: A new software suite for macromolecular structure determination.* Acta Crystallographica Section D: Biological Crystallography, 1998. **54**(5): p. 905-21.

18. Murshudov, G.N., Vagin, A.A. and Dodson, E.J. *Refinement of macromolecular structures by the maximum-likelihood method.* Acta Crystallographica Section D: Biological Crystallography, 1997. **53**(3): p. 240-55.

19. Hamed, R.B., Batchelar, E.T., Clifton, I.J. and Schofield, C.J. *Mechanisms and structures of crotonase superfamily enzymes: How nature controls enolate and oxyanion reactivity.* Cellular and Molecular Life Sciences, 2008. **65**(16): p. 2507-27.

20. Kress, D., Br√ºgel, D., Schall, I., Linder, D., Buckel, W. and Essen, L.-O. *An asymmetric model for Na+-translocating glutaconyl-CoA decarboxylases.* Journal of Biological Chemistry, 2009. **284**(41): p. 28401-09.

21. Hall, P.R., Wang, Y.-F., Rivera-Hainaj, R.E., Zheng, X., Pustai-Carey, M., Carey, P.R. and Yee, V.C. *Transcarboxylase 12S crystal structure: hexamer assembly and substrate binding to a multienzyme core.* The EMBO Journal, 2003. **22**(10): p. 2334-47.

22. Huang, C.S., Ge, P., Zhou, Z.H. and Tong, L. *An unanticipated architecture of the 750-kDa [agr] 6 [bgr] 6 holoenzyme of 3-methylcrotonyl-CoA carboxylase.* Nature, 2012: p. 219-23.

23. Schrodinger, LLC, *The PyMOL Molecular Graphics System, Version 1.3r1.* 2010.

24. Pettersen, E.F., Goddard, T.D., Huang, C.C., Couch, G.S., Greenblatt, D.M., Meng, E.C. and Ferrin, T.E. *UCSF Chimera, A visualization system for exploratory research and analysis.* Journal of Computational Chemistry, 2004. **25**(13): p. 1605-12.

25. Jogl, G., Tao, X., Xu, Y. and Tong, L. *COMO: a program for combined molecular replacement.* Acta Crystallographica Section D: Biological Crystallography, 2001. **57**(8): p. 1127-34.

26. Chou, C.Y., Yu, L.P. and Tong, L. *Crystal structure of biotin carboxylase in complex with substrates and implications for its catalytic mechanism.* J Biol Chem, 2009. **284**(17): p. 11690-7.

27. Dantas, M.F., Suormala, T., Randolph, A., Coelho, D., Fowler, B., Valle, D. and Baumgartner, M.R. *3-Methylcrotonyl-CoA carboxylase deficiency: Mutation analysis in 28 probands, 9 symptomatic and 19 detected by newborn screening.* Human Mutation, 2005. **26**(2): p. 164-64.

28. Grünert, S.C., Stucki, M., Morscher, R.J., Suormala, T., Bürer, C., Burda, P., Christensen, E., Ficicioglu, C., Herwig, J., and Kölker, S. *3-methylcrotonyl-CoA carboxylase deficiency: Clinical, biochemical, enzymatic and molecular studies in 88 individuals.* Orphanet J Rare Dis, 2012. **7**(1): p. 31.

29. Xiang, S. and Tong, L. *Crystal structures of human and Staphylococcus aureus pyruvate carboxylase and molecular insights into the carboxyltransfer reaction.* Nature Structural & Molecular Biology, 2008. **15**(3): p. 295-302.

30. Waldrop, G.L., Rayment, I. and Holden, H.M. *Three-dimensional structure of the biotin carboxylase subunit of acetyl-CoA carboxylase.* Biochemistry, 1994. **33**(34): p. 10249-56.

31. Mochalkin, I., Miller, J.R., Evdokimov, A., Lightle, S., Yan, C., Stover, C.K. and Waldrop, G.L. *Structural evidence for substrate-induced synergism and half-sites reactivity in biotin carboxylase.* Protein Science, 2008. **17**(10): p. 1706-18.

32. Lietzan, A.D., Menefee, A.L., Zeczycki, T.N., Kumar, S., Attwood, P.V., Wallace, J.C., Cleland, W.W. and St. Maurice, M. *Interaction between the biotin carboxyl carrier domain and the biotin carboxylase domain in pyruvate carboxylase from Rhizobium etli.* Biochemistry, 2011. **50**(45): p. 9708-23.

33. Broussard, T.C., Kobe, M.J., Pakhomova, S., Neau, D.B., Price, A.E., Champion, T.S. and Waldrop, G.L. *The Three-Dimensional Structure of the Biotin Carboxylase-Biotin Carboxyl Carrier Protein Complex of E. coli Acetyl-CoA Carboxylase.* Structure (Epub ahead of print), 2013.